Structural Engineering Report No. 133

Behaviour Of Fillet Welds As A Function Of The Angle Of Loading

by

Gregory S. Miazga

and

D. J. Laurie Kennedy

Department Of Civil Engineering

University Of Alberta

Edmonton, Alberta

March 1986

Abstract

Fillet welds subjected to longitudinal shear have been recognized as the weakest loading case for fillet welds as early as the 1930's. However, the lack of an analytical method relating the strength of fillet welds to the loading angle has led to a reluctance to utilize the increase in weld strength for loading cases other than longitudinal. Current methods, while predicting reasonable values for ultimate strength, do not correlate with fracture observations. This shortcoming, combined with the uncertainty of how loads are transferred through complex welded connections, has caused designers to adopt a lower bound strength approach, basing the strength of fillet welds on the strength of longitudinal fillets, regardless of the loading direction.

A rational analytical method for determining the ultimate strength of fillet welds loaded in shear is developed herein. The method gives new insights into how load is transferred through fillet welds and relates ultimate strengths to angles of fracture within the welds. The method is compared to the test results of a series of 42 fillet weld specimens presented herein. In addition, fillet weld ductility is examined. Weld deformations are seen to vary considerably with the loading direction, but weld ductility is concluded to be independent of the loading direction when gauge the lengths used to measure weld deformations are taken into consideration.

Acknowledgements

The thoughtful guidance offerred by Dr. D.J.L. Kennedy throughout this study is greatly appreciated.

Special thanks are extended to the Welding Research Department of Mineral Engineering at the University of Alberta for preparing the test specimens. Dr. B. Patchett provided valuable advice and C. Bicknell performed the welding.

The assistance of L. Burden and R. Helfrich of the I.F. Morrison Structural Laboratory in the experimental program is gratefully acknowledged.

Funding for this study was provided by the Central Research Fund of the University of Alberta. The author received personal funding from the Natural Sciences and Engineering Research Council of Canada and from the Alberta Region of the Canadian Institute of Steel Construction.

Table of Contents

List of Tables

List of Figures

Figure Page

1. Introduction

1.1 General

The ultimate strength of fillet welds loaded in shear is dependent upon the strength of the weld metal and the direction of loading. The weld may be loaded parallel to the direction of loading (longitudinal fillet), perpendicular to the direction of loading (transverse fillet), or loaded at an intermediate direction. Experimental studies have shown that fillets loaded longitudinally are the weakest and thus provide a lower bound to fillet weld strength. Because in complex connections it may be difficult to define the directions of loading on welds, the strength of the longitudinal fillet has been used to provide a basis for design recommendations in many design standards.

Clause 13 of CSA Standard CAN3-S16.1-M84 "Steel Structures for Buildings - Limit States Design" (CSA 1984) bases the resistance of fillet welds subject to shear on the strength of longitudinal fillets. In addition, it is stated that the vector sum of factored longitudinal and transverse shears shall not exceed factored resistances based on the strength of longitudinal fillets, but states that an ultimate strength analysis may be used instead. Such a method, however, is not given.

Clause 11 of CSA Standard W59-1982 "Welded Steel Construction (Metal Arc Welding)" (CSA 1982) also bases the resistance of fillet welds subject to shear on the strength

of longitudinal fillets and states that an ultimate strength analysis may be used instead, although a method of analysis is not given.

The purpose of this thesis is to develop a rational analytical method for predicting the ultimate strength of fillet welds loaded in shear that is consistent with both measured ultimate strengths and fracture observations.

1.2 Objectives

The objectives of this study are:

1. to develop an analytical method for determining the ultimate strength of fillet welds loaded in shear, as a function of the loading direction.
2. to substantiate the validity of this method by means of a suitable experimental program.
3. to compare the results of the experimental and analytical study with the results of others.

1.3 Scope

A series of 42 fillet weld specimens were tested. Seven loading angles and two weld sizes were examined with three specimens for each combination. Electrode and plate material grades were selected to represent the most common Canadian structural steelwork. The analytical method developed is compared with the results of the test series as well as with the test results of others.

2. Literature Review

2.1 General

This review of the behaviour of fillet welds subjected to shear loads covers experimental and theoretical research from the early 1930's to the present. A significant amount of research on fillet welds has been conducted, with the majority concerned only with fillet welds subjected to loads perpendicular to the weld axis, (transverse welds), or parallel to it, (longitudinal fillets).

The transverse and longitudinal load cases have been considered to define the upper and lower bounds on both strength and ductility. Few tests have been done on fillet welds loaded at intermediate angles. The most significant experimental studies involving the latter have been performed by Butler and Kulak (1971), Clark (1971), Holtz and Harre (1973, unpublished), Swannell and Skewes (1979), and Biggs et al (1981). As well, the theoretical study of fillet weld behaviour has generally been limited to the transverse and longitudinal loading cases. Neis (1985) and Marsh (1985) have attempted to establish theoretically ultimate fillet weld behaviour for any loading angle.

The review of the behaviour of fillet welds is considered in three sections. Section 2.2 presents tests and theories on fillet welds loaded longitudinally and transversely. Studies on welds loaded at intermediate angles are reviewed in Section 2.3, while some parameters which

affect fillet weld behaviour are discussed in Section 2.4.

2.2 Longitudinally and Transversely Loaded Fillet Welds

From a statistical analysis of 423 tests on transversely loaded welds and 416 tests on longitudinally loaded welds conducted by others, Spraragen and Claussen (1942) found that the maximum stress on the throat of longitudinal fillets at failure ranged from 60 to 100% of that of transverse fillets. They also concluded that both longitudinal and transverse welds were as strong in compression as in tension. The scatter of test data was seen to be greater for transverse fillets than for longitudinal fillets.

As part of a study on column brackets, Archer et al (1959) performed two longitudinal and two transverse fillet weld tests. Although details of the weld metal and plate material properties were not recorded, the transverse shear strength was calculated to be 1.59 times the longitudinal shear strength. The angle of the fracture plane in the weld approached the throat for longitudinal tests, but was less than 45° for transverse tests.

Experimental and theoretical investigations of the behaviour of transverse fillets were performed by Naka and Kato (1966). A total of 18 tests were conducted using three types of fillets, two kinds of electrodes, and three test specimens for each combination. Material properties, load, deformation and weld fracture angles were all measured. Five

different theories, more commonly used to predict yield loads, were used to predict ultimate loads of welds by substituting the ultimate tensile strength for the yield strength of the weld metal. All the theories underestimated the measured ultimate transverse weld strength, but the maximum shear stress developed was seen to be most closely related to the ultimate strength.

An additional failure theory was also investigated by Naka and Kato (1966), based on the general elastic solution developed by Timoshenko (1952) for calculating stresses in the uniformly loaded wedge shown in Fig 2.1. Naka and Kato differentiated Timoshenko's general expression for the shear stress to calculate the maximum shear stress and the corresponding plane defined by the angle θ. Naka and Kato then assumed the maximum shear stress to exist uniformly on a plane perpendicular to the plane determined from the differentiation process. This plane was taken to be the fracture plane as shown in Fig 2.2. However, when Timoshenko's true shear stress distribution is examined on the assumed fracture plane of Naka and Kato, it can be established, as shown in Fig 2.2, that the maximum shear stress predicted by Naka and Kato is actually the minimum shear stress that occurs on the fracture plane. Because weld failure was assumed to occur at a limiting value of shear stress and the elastic shear stress distribution was assumed to remain unchanged with increasing load, Naka and Kato predicted a higher transverse strength than would result

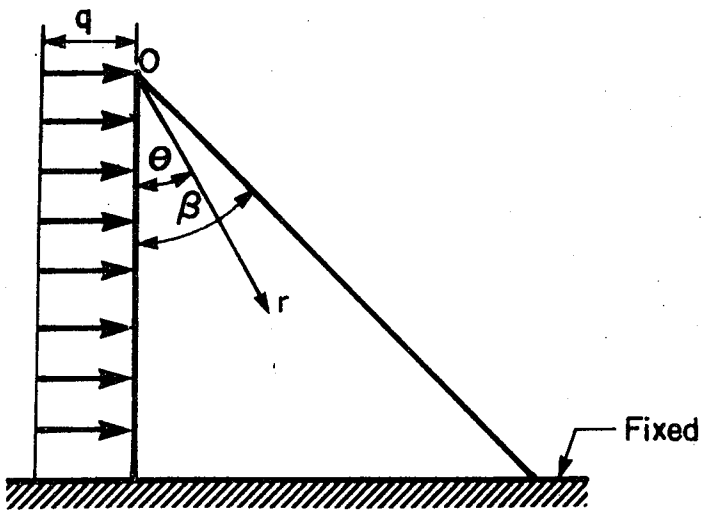

Figure 2.1 Uniformly Loaded Wedge, Timoshenko (1952)

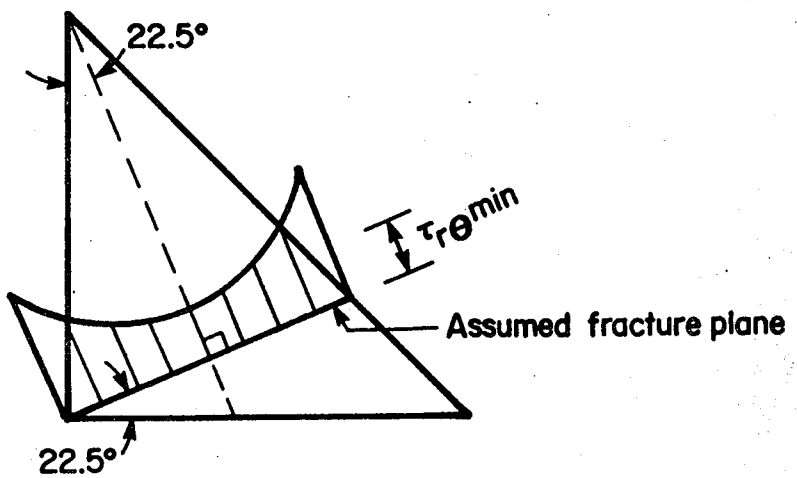

Figure 2.2 Shear Stress Distribution On 22.5° Plane

from a correct interpretation of Timoshenko's theory. Naka and Kato's theory also presupposes that the vertical face of the fillet weld is uniformly loaded. As discussed subsequently, this assumption is not considered valid. Naka and Kato's theory was later used by Kato and Morita (1969) and Kato and Morita (1974) as it predicted satisfactory ultimate strength results.

Ligtenburg (1968) reported on an international test series involving simple welded connections loaded in tension. Ten countries, including Canada, participated in the study. To ensure comparable test data, a specific format for testing was followed. As part of the study, each country performed separate tests on longitudinal and transverse fillets. The testing program covered acidic, basic and rutile electrodes with a weld tensile strength ranging from about 450 MPa to 580 MPa. It was determined statistically that the transverse weld strength was 1.59 times the longitudinal strength.

Higgins and Preece (1969) conducted a series of 168 tests on longitudinal and transverse fillets using a variety of electrode and base metal strengths. To evaluate observed strengths, recorded test loads were divided by measured failure surface areas. As details of the failure loads and fracture surface areas were not given, direct comparisons between longitudinal and transverse strengths cannot be made. However, based on proposed working stresses developed by them, the average transverse factor of safety was 1.41 to

1.57 times the average longitudinal factor of safety.

Kato and Morita (1974) studied the static strength and behaviour of transverse fillets both experimentally and theoretically. Failure loads and fracture angles from tests were compared with the maximum shear stress theory developed by Naka and Kato (1966).

The International Institute of Welding (IIW, 1980) presented data on load versus deformation curves of transverse and longitudinal fillet welds. The IIW recommended a transverse to longitudinal strength ratio of 1.22 and considered that higher observed ratios were due primarily to friction and supporting effects of plates. It was also concluded that longitudinal welds have about twice the deformation capacity of transverse welds.

The ultimate strength of longitudinal and transverse welds were investigated theoretically by Kamtekar (1982). Using the assumed force systems shown in Fig 2.3, weld strengths were determined as a function of weld geometry and the ultimate tensile strength of the weld metal. Kamtekar's solutions for the load carrying capacity of longitudinal and transverse welds satisfy Lay's (1982) requirements of a lower bound theorem as the internal and external forces and reactions are in equilibrium, and the internal forces assumed nowhere exceed the relevant force capacity, provided that the behaviour is ductile.

As discussed subsequently, the simple force systems assumed by Kamtekar do not appear to be an accurate

from a correct interpretation of Timoshenko's theory. Naka and Kato's theory also presupposes that the vertical face of the fillet weld is uniformly loaded. As discussed subsequently, this assumption is not considered valid. Naka and Kato's theory was later used by Kato and Morita (1969) and Kato and Morita (1974) as it predicted satisfactory ultimate strength results.

Ligtenburg (1968) reported on an international test series involving simple welded connections loaded in tension. Ten countries, including Canada, participated in the study. To ensure comparable test data, a specific format for testing was followed. As part of the study, each country performed separate tests on longitudinal and transverse fillets. The testing program covered acidic, basic and rutile electrodes with a weld tensile strength ranging from about 450 MPa to 580 MPa. It was determined statistically that the transverse weld strength was 1.59 times the longitudinal strength.

Higgins and Preece (1969) conducted a series of 168 tests on longitudinal and transverse fillets using a variety of electrode and base metal strengths. To evaluate observed strengths, recorded test loads were divided by measured failure surface areas. As details of the failure loads and fracture surface areas were not given, direct comparisons between longitudinal and transverse strengths cannot be made. However, based on proposed working stresses developed by them, the average transverse factor of safety was 1.41 to

1.57 times the average longitudinal factor of safety.

Kato and Morita (1974) studied the static strength and behaviour of transverse fillets both experimentally and theoretically. Failure loads and fracture angles from tests were compared with the maximum shear stress theory developed by Naka and Kato (1966).

The International Institute of Welding (IIW, 1980) presented data on load versus deformation curves of transverse and longitudinal fillet welds. The IIW recommended a transverse to longitudinal strength ratio of 1.22 and considered that higher observed ratios were due primarily to friction and supporting effects of plates. It was also concluded that longitudinal welds have about twice the deformation capacity of transverse welds.

The ultimate strength of longitudinal and transverse welds were investigated theoretically by Kamtekar (1982). Using the assumed force systems shown in Fig 2.3, weld strengths were determined as a function of weld geometry and the ultimate tensile strength of the weld metal. Kamtekar's solutions for the load carrying capacity of longitudinal and transverse welds satisfy Lay's (1982) requirements of a lower bound theorem as the internal and external forces and reactions are in equilibrium, and the internal forces assumed nowhere exceed the relevant force capacity, provided that the behaviour is ductile.

As discussed subsequently, the simple force systems assumed by Kamtekar do not appear to be an accurate

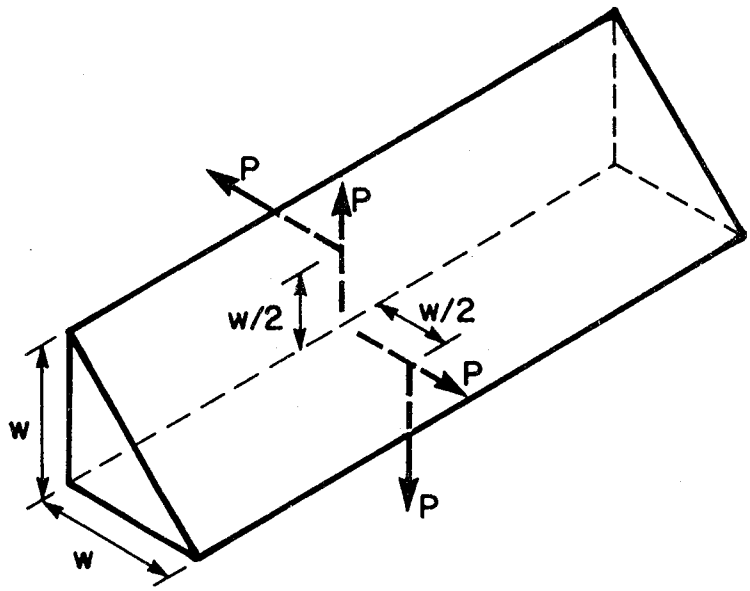

a) Transverse Weld Force System

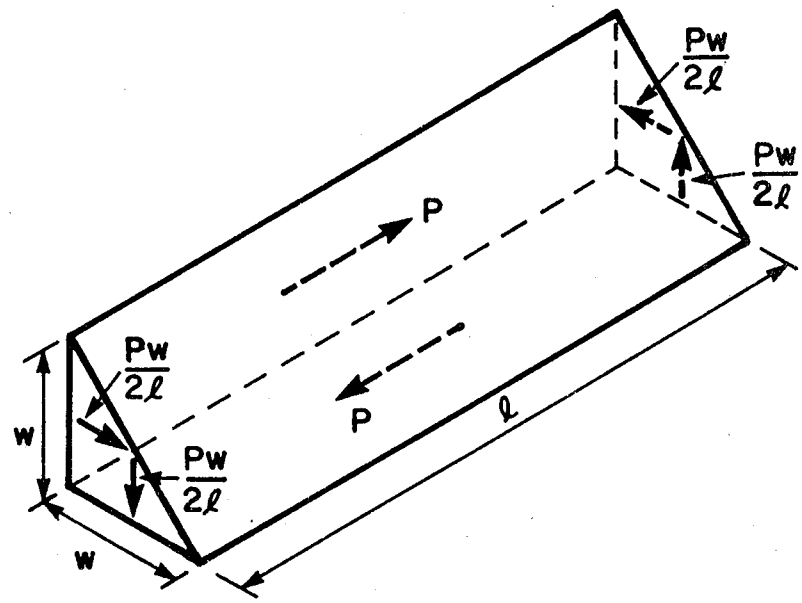

b) Longitudinal Weld Force System

Figure 2.3 Force Systems Acting On Welds, Kamtekar (1982)

representation of how loads are transferred by these welds. Kamtekar predicted a fracture surface at 0° to the horizontal weld leg for transverse welds. The experimental results of Naka and Kato (1966), and those reported here indicate that the failure surface of transverse welds does not coincide with the weld leg.

Krumpen and Jordan (1984) developed a procedure for sizing fillet welds in ship structures which allowed weld size reductions of up to 25% for steel and 37% for aluminum, by considering the increased strength of transverse fillet welds. They developed, based on test data from Butler and Kulak (1971), strength equations for basic loading conditions including longitudinal and transverse shear, assuming a transverse weld shear strength of 1.44 times the longitudinal shear strength. The procedure was examined over a wide range of material and electrode strengths.

2.3 Fillet Welds Loaded at Intermediate Angles

Early investigators such as Hankins (1934), Freeman (1932) and Vandeperre (1939) found that the maximum stress at fracture on the throat for fillets loaded at intermediate angles to be between longitudinal and transverse test results. This stress was simply computed as the maximum load divided by the throat area, even though the fracture plane may not have coincided with the throat. None of these investigators established a relationship for weld strength as a function of the loading angle.

As part of a larger study into the behaviour of eccentrically loaded welded connections, Butler and Kulak (1971) conducted a series of 23 tests to establish the effect of loading angle on load deformation relationships of fillet welds. The welds were 1/4" (6 mm) fillets made using AWS E60XX electrodes with CSA G40.21 steel plate having a specified minimum yield strength of 44 ksi (303 MPa) and a specified minimum tensile strength of 62 ksi (438 MPa). Angles of 0, 30, 60, and 90° between the load and the weld axis were examined. Empirical relationships describing both the ultimate strength and the maximum weld deformation as a function of the angle of loading were derived and used to develop the tables for eccentrically loaded welds given in the CISC Handbook of Steel Construction (CISC, 1984). The ultimate strength of the weld was seen to increase continuously from 0° to 90°, with the transverse strength 1.45 times the longitudinal strength. The longitudinal welds displayed much more deformation capacity than the transverse welds. No elastic weld behaviour was observed during any of the tests and it was concluded that fillet welds loaded in shear do not exhibit any well defined yield point.

Clark (1971) published load versus deformation curves on 8 mm fillets similar to those presented by Butler and Kulak (1971). Tests were carried out on welds loaded at 0, 30, 60, and 90° to the weld axis to obtain data beyond the ultimate weld strength. Theoretical stress models were reviewed and were found to underestimate the true weld

strength. Clark suggested that restraint resulting from the plates joined by the welds was an important factor in explaining the discrepancy between theoretical and observed strengths, although no details were given.

Fillet weld tests over a range of loading angles were performed by Holtz and Harre (1973, unpublished). A total of 59 tests were performed at loading angles of 0, 13, 30, 60, and 90°. The electrodes used were AWS E70XX and weld legs were 1/4" (6 mm). The results were considered by the authors to be in agreement with earlier tests done by Butler and Kulak (1971).

Swannell and Skewes (1979) reviewed elastic design methods and proposed an ultimate load method for the design of welded brackets. Recognizing that the strength of fillet welds is influenced by the direction of applied load, rules were incorporated in the Australian Standard AS1250 reflecting this criterion in 1975. These allowed increased strength for loading angles differing from longitudinal loading, with a 22.5% greater load for transverse fillets as compared to longitudinal fillets. As a basis for developing an ultimate load method, Swannell and Skewes determined experimentally load-deformation relationships for fillet welds representative of Australian welding practice. Tests were performed in compression and a minimum of six tests were conducted at each loading angle of 0, 30, 60, and 90°. However, as discussed subsequently, the test method tended to prescribe the angle of the fracture plane, and therefore,

to influence the ultimate strength. The results of transverse tension tests were also compared with transverse compression tests. Although ultimate loads were very similar, ultimate tensile deformations were less than ultimate compression deformations.

Biggs et al (1981) summarized the experimental results of both Crofts and Higgs on short fillet welds with equal leg lengths subject to static loads. The results showed that the angle of the failure plane within the weld varied with the loading direction. They proposed elliptical relationships relating the average tensile and shear stresses on the failure plane. Both Higgs and Crofts used beam-type loading arrangements which produced combinations of stresses in directions longitudinal and transverse to the fillet welds. However, the loading arrangement chosen appears to have introduced an unnecessary amount of scatter to the data; the loading angle was not constant throughout each test and it appears that the loading angle when the welds fractured could only have been estimated. In both cases no description of material properties was given. The experimental results of Higgs and Crofts are comparable, although limited in range.

Using a rate-dependent plasticity theory, Neis (1985) developed theoretical load deformation curves for fillet welds based on the mean stress distributions assumed by Kamtekar (1982) for the development of load transfer between the plates and the welds. A comparison between the curves

developed by Neis (1985) and the empirical curves of Butler and Kulak (1971) shows good agreement for loading angles of 0° and 90°, but the considerable discrepancy for other angles is probably related to the inaccurate initial premise for mean stress distributions. Therefore, this development must be questioned.

Marsh (1985) developed a theory relating the ultimate strength of fillet welds to the loading angle. His analysis is based on the two free-body diagrams shown in Fig 2.4, neither of which is in equilibrium. Also, all fillet welds, regardless of loading direction, were assumed to fail through the throat. This assumption is not consistent with test results.

Experimental data on the strength of fillet welds loaded in longitudinal and transverse shear have been reviewed by Kennedy and Kriviak (1985). Two possible interaction relationships were proposed for the design of fillet welds loaded simultaneously by longitudinal and transverse forces. They also suggested that the vector addition approach for considering simultaneous transverse and longitudinal forces was very conservative.

2.4 Parameters Inflencing Weld Behaviour

Other parameters that may influence the strength of fillet welds, in addition to the strength of the weld metal, the welding process used, and the direction of loading with respect to the weld axis, are presented in Sections 2.4.1 to

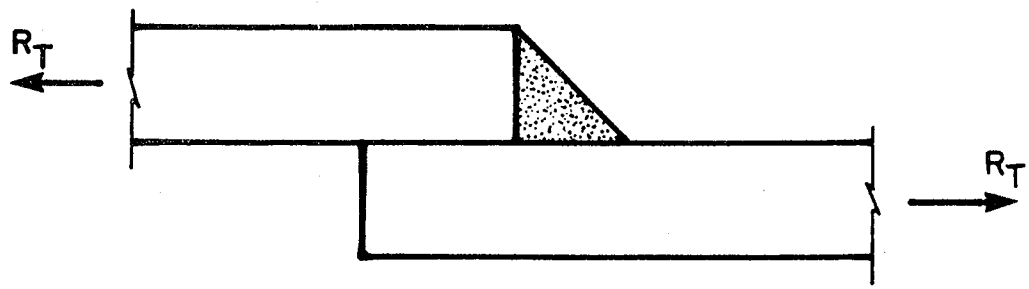

a) Transverse Fillet

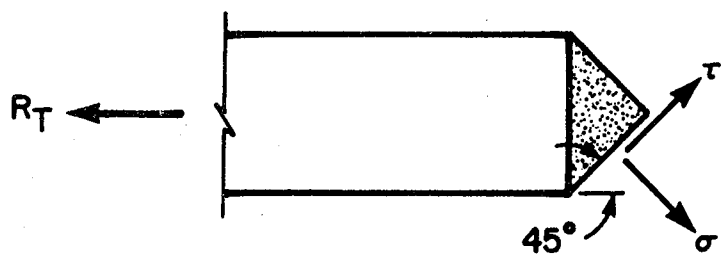

b) Top Plate

Figure 2.4 Equilibrium Of A Transverse Fillet, Marsh (1985)

2.4.3.

2.4.1 Throat Thickness

Due to metallurgical influences and differences in local deformation behavior, the strength of fillet welds is considered to decrease minimally with increasing throat thickness (IIW, 1980). Kato and Morita (1969), however, tested a range of throat thicknesses from 3.5 mm to 28.3 mm for transverse fillets and from 3.5 mm to 15.6 mm for longitudinal fillets and concluded that the average maximum stress of the fillet weld sizes tested was not affected by the throat size.

2.4.2 Strength of Base Metal

The effect of dilution between weld and base metal was examined by Higgins and Preece (1969) and Kato and Morita (1969), by welding various combinations of base and weld metal strengths. In the tests by Higgins and Preece (1969), dilution was seen to have a small effect. For example, 1/4" (6 mm) AWS E110XX fillet welds on steel with a tensile strength 36% less than that required were only 8% weaker than using the same electrode on A514 steel. Conversely, 1/4" (6 mm) AWS E70XX fillet welds on A514 steel having a tensile strength 65% stronger than that required for the electrodes, were only 2% stronger than those deposited on base metal having approximately the same mechanical properties as the electrodes. Similar results were obtained

by Kato and Morita (1969).

2.4.3 Weld Length

As the loading angle approaches the longitudinal case, longer weld lengths tend to exhibit lower strength per unit length of weld. In investigating the effect of weld length upon the strength of longitudinal welds, Swannell (1972) observed that longitudinal welds transmitted shear in a non-uniform manner along the weld length, with high shears occurring at the weld ends. From a theoretical investigation, Swannell concluded that for a given weld leg size, there exists a longitudinal weld length beyond which there is no significant gain in load carrying capacity. This length was, however, not stated.

3. Experimental Program

3.1 General

The objective of the experimental program was to examine the effect of loading angle on the behaviour of fillet welds. Seven loading angles, two weld sizes, and three specimens for each combination were tested. In addition, ancillary tests were performed on steel plate coupons and weld metal coupons.

3.2 Design of Test Specimens

The test specimens were proportioned for testing in the Materials Testing System (MTS) testing facilities at the I.F. Morrison Structural Laboratory of the University of Alberta. A typical test set-up is shown in Fig 3.1 and the dimensions of the test specimen are shown in Fig 3.2. The loading angles and weld sizes of the various specimens tested are shown in Figs 3.3 and 3.4.

Test specimens were initially designed as a tension member pinned at both ends. This design was subsequently modified such that the specimen was placed directly in hydraulic grips at one end. This modification reduced plate and machining costs, allowed thicker plate to be used in the test specimens, and facilitated testing. The pinned connection was made using a yoke and pin assembly. Self-aligning hydraulic grips were used at the other end as shown in Figure 3.1.

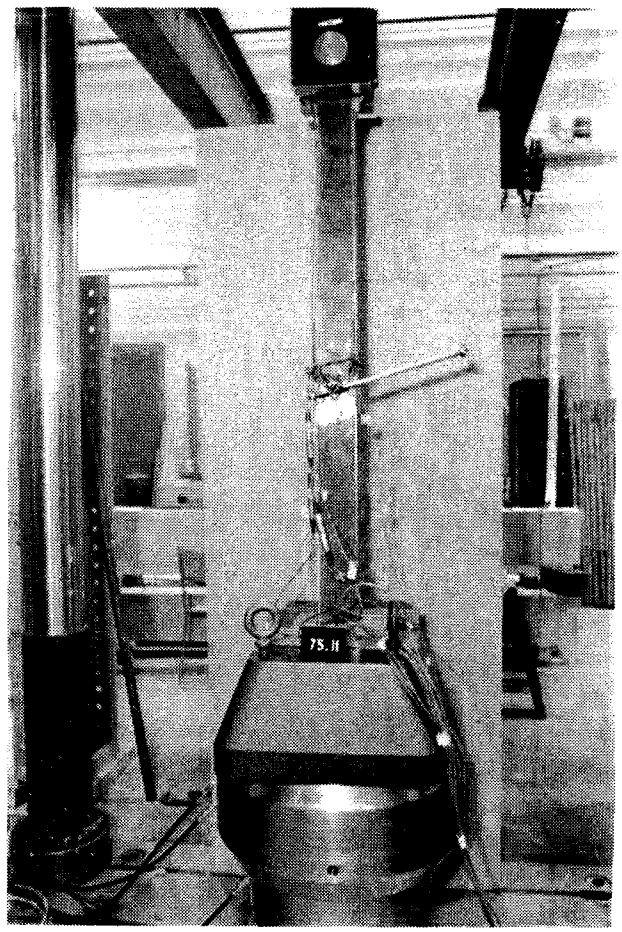

Figure 3.1 Typical Test Set-Up

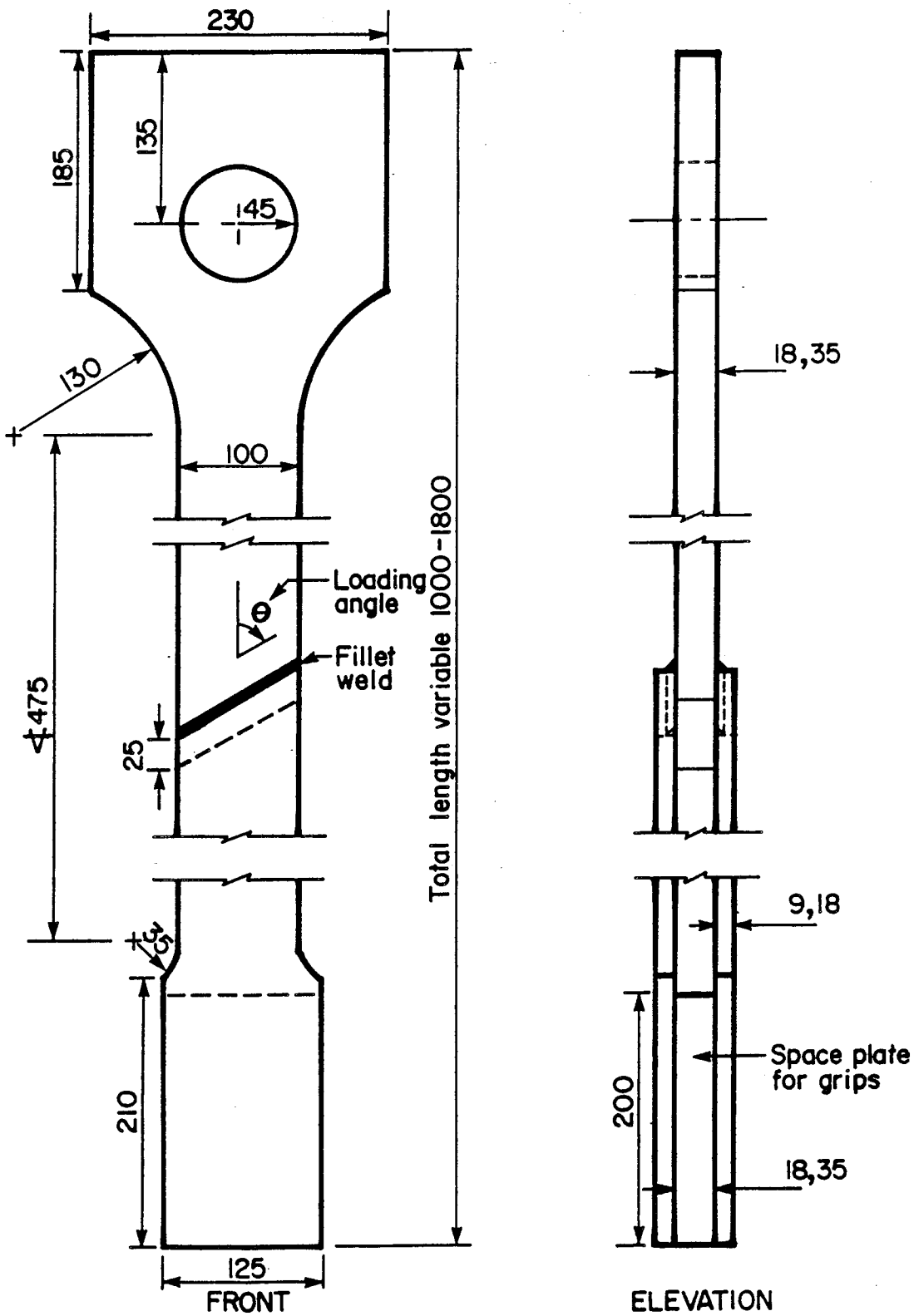

Figure 3.2 Test Specimen

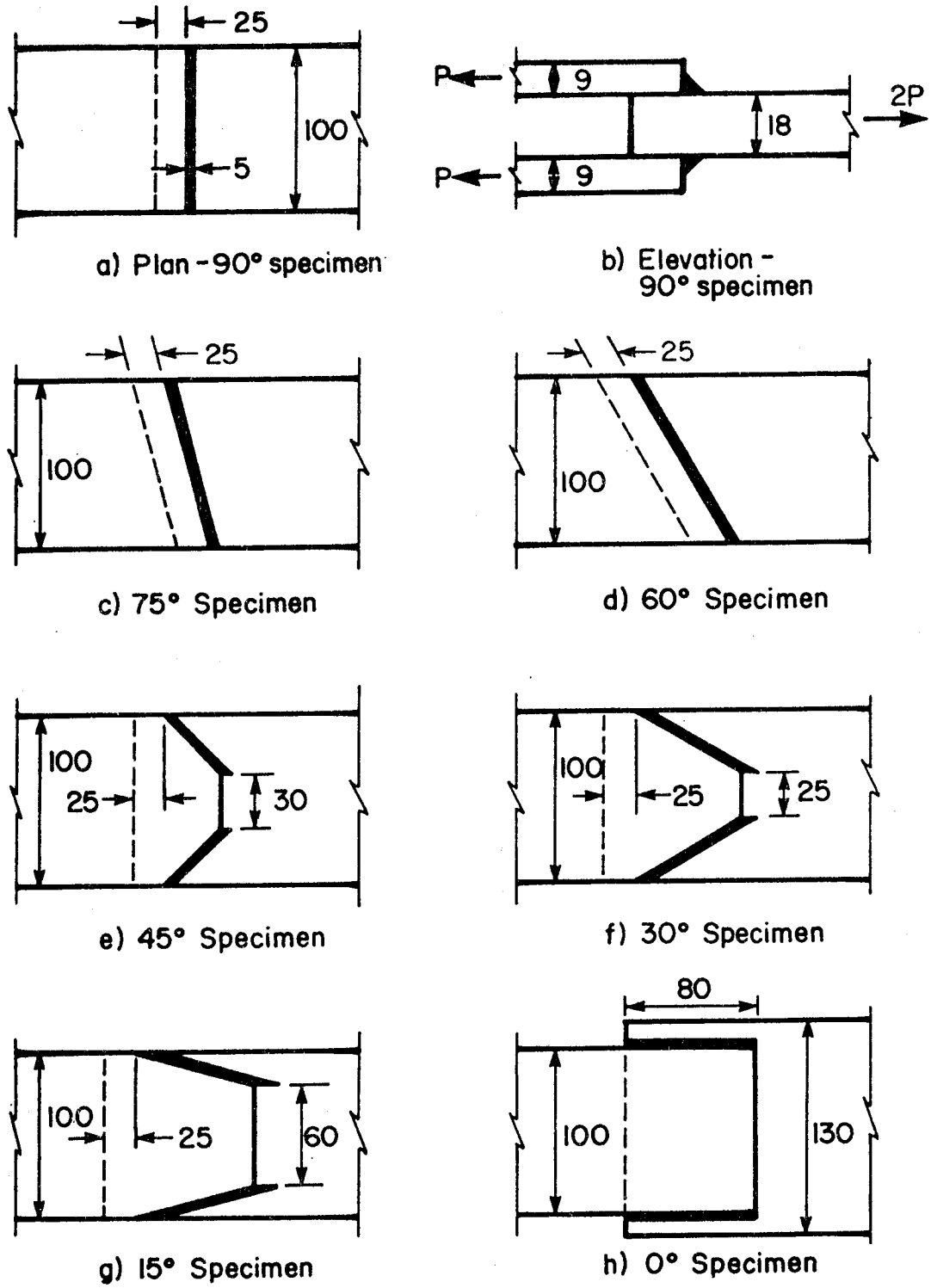

Figure 3.3 5 mm Fillet Weld Test Specimens

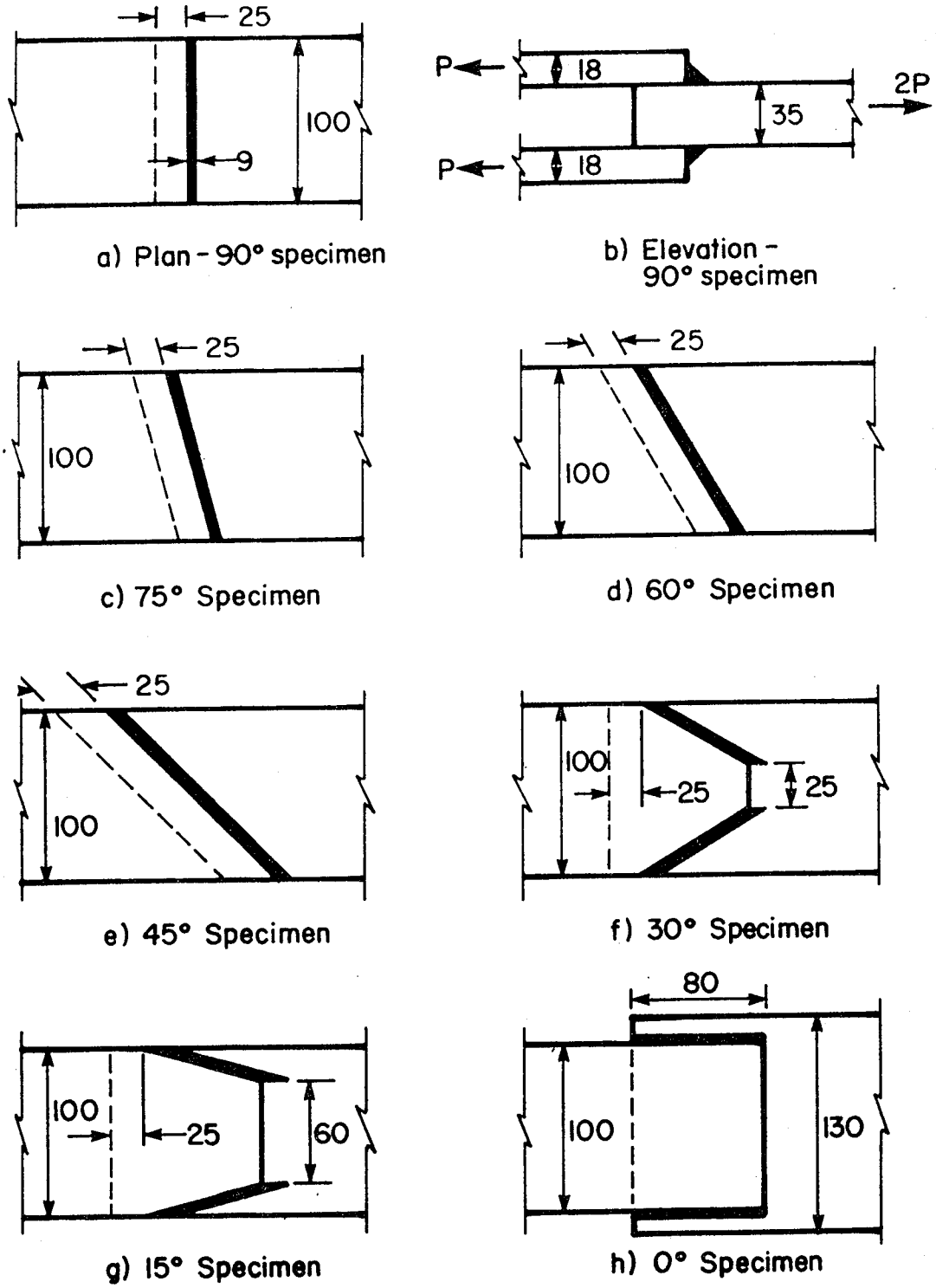

Figure 3.4 9 mm Fillet Weld Test Specimens

The pinned end of the test specimen was designed in accordance with Clause 12.4 of CSA Standard CAN3-S16.1-M84, "Steel Structures for Buildings - Limit States Design", (CSA, 1984). The 90 mm diameter pin had a rated load capacity of 2650 kN. Based on the available end distance behind the pin of 90 mm, the body width of the test specimens was limited to 100 mm. A finite element analysis was performed to determine the minimum distance along the specimen length from the pin hole at which the stresses across the specimen width were uniform. At a distance of 300 mm from the pin hole center, the variation in the elastic stress distribution was found not to exceed 1%. This was considered satisfactory.

The gripped ends of the test specimens were made in proportion to the gripped end of a tension coupon as given in ASTM A370-77, "Standard Methods and Definitions for Mechanical Testing of Steel Products", Part 1, (1977). The hydraulic grips of the MTS machine have a rated load capacity of 4000 kN.

As in other fillet weld tests, such as those performed by Butler and Kulak (1971), the test specimens were designed with fillet welds on both faces of the test specimens. This symmetric weld arrangement reduced the effect of bending moments caused by eccentric loading. Weld sizes and plate thicknesses were chosen to ensure that the welds ruptured before the connecting plates yielded. This allowed accurate weld deformation measurements to be made as the plate

deformations could be considered to be negligible as compared to weld deformations.

3.3 Steel Plate

Three thicknesses of CSA Standard CAN3-G40.21-M81, "Structural Quality Steels", (CSA, 1981), grade 300W steel - 9 mm, 18 mm, and 35 mm - were used. The plate was manufactured by Algoma Steel and was supplied by a local fabricator. Each plate thickness came from a single heat. The chemical composition, as given in the mill test reports, together with the requirements of CSA Standard CAN3-G40.21-M81 are given in Table 3.1. The composition of each heat is within the limits specified by CSA Standard CAN3-G40.21-M81.

3.4 Electrodes

CSA Standard W59, "Welded Steel Construction", (CSA, 1982), specifies E480XX electrodes as the matching electrode for grade 300W steel, and thus E48014 electrodes were selected. The electrodes, manufactured by Hobart Brothers of Canada, came from a single heat, No. G1244, and were 3.2 mm in diameter. The electrodes were manufactured to conform with CSA Standard W48.1-M80, "Mild Steel Covered Arc Welding Electrodes", (CSA, 1980).

CHEMICAL COMPOSITION						
Plate (mm)	Heat No.	C %	Mn %	S %	P %	Si %
9	8391M	0.17	1.11	0.012	0.017	0.22
18	8239M	0.17	1.11	0.012	0.012	0.25
35	6681J	0.18	1.22	0.019	0.013	0.21
Max or range specified in CSA G40.21-M81		0.22	0.50 to 1.50	0.05	0.04	0.40

Table 3.1 Plate Composition

3.5 Plate Preparation

Each plate for the test specimens was flame-cut individually from the pieces supplied, using an automatic machine to ensure uniformity. The machine was equipped with an optical scanner to trace the drawing. All pieces were cut with the longitudinal axis of the piece in the rolling direction of the plate. The pin-holes were roughed out by flame-cutting and then machined to a uniform diameter. Flame-cut edges were ground smooth and the ends to be welded were sawn square before welding. The plate edges for the longitudinal specimens were machined square before welding.

3.6 Welding Preparation

Trial tests were performed to establish welding parameters. The objective was to produce equal legged fillet welds with leg sizes of 5 mm and 9 mm, with sufficient root penetration, and a uniform weld profile. As well, the dimensional requirements for fillet welds as specified in CSA Standard W48.1-M80 (CSA, 1980) were to be met. The trial test pieces were welded, sectioned, and visually inspected for defects. Dye penetrant inspection, in accordance with ASTM E165-80, "Standard Practice for Liquid Penetrant Inspection Method", (1980), was used to check for cracking. Dimensions were examined using a Rank Scherr-Tumico Optical Comparator at a magnification of 10X. A computer program developed by The Welding Institute based on a carbon equivalent formula was used to establish pre-heat

temperatures. The parameters used to achieve the desired weld sizes are listed in Table 3.2.

The trial pieces were welded in a horizontal position using a semi-automatic welding procedure. In this procedure, the specimen to be welded moved at a constant speed on a bed driven by an electric motor and electrodes were hand fed. All welding was performed by one welder from the Welding Research Laboratory of the Department of Mineral Engineering at the University of Alberta. This same procedure was used throughout the test program.

3.7 Welding Procedure

Prior to welding, all mill scale near the area to be welded was removed by grinding and the weld area was brush-cleaned. As each test specimen was welded individually, a table with a jig arrangement was used for alignment. Run-on and run-off tabs were tack-welded to the test specimens so that stops or starts would not be present within the length of weld tested. Tack-welds were made as small as possible. The tack-welds for the 5 mm welds with 90, 75, 60, and 0° angles and for the 9 mm welds with 90, 75, 60, 45, and 0° angles, were located in 'dead' areas as shown in Fig 3.5. If a continuous weld bead was run across the entire test specimen width for the 5 mm welds with 45, 30 and 15° angles and the 9 mm welds with 30 and 15° angles, general plate yielding would have resulted before weld rupture. Therefore, two lesser weld lengths were deposited

WELDING PARAMETERS			
Leg Size (mm)	Weld Passes	Speed (mm/min)	Current (Amps)
5	1	250	125
9	3	205	125
Range specified in CSA W48.1-M80			110-160

Table 3.2 Welding Parameters

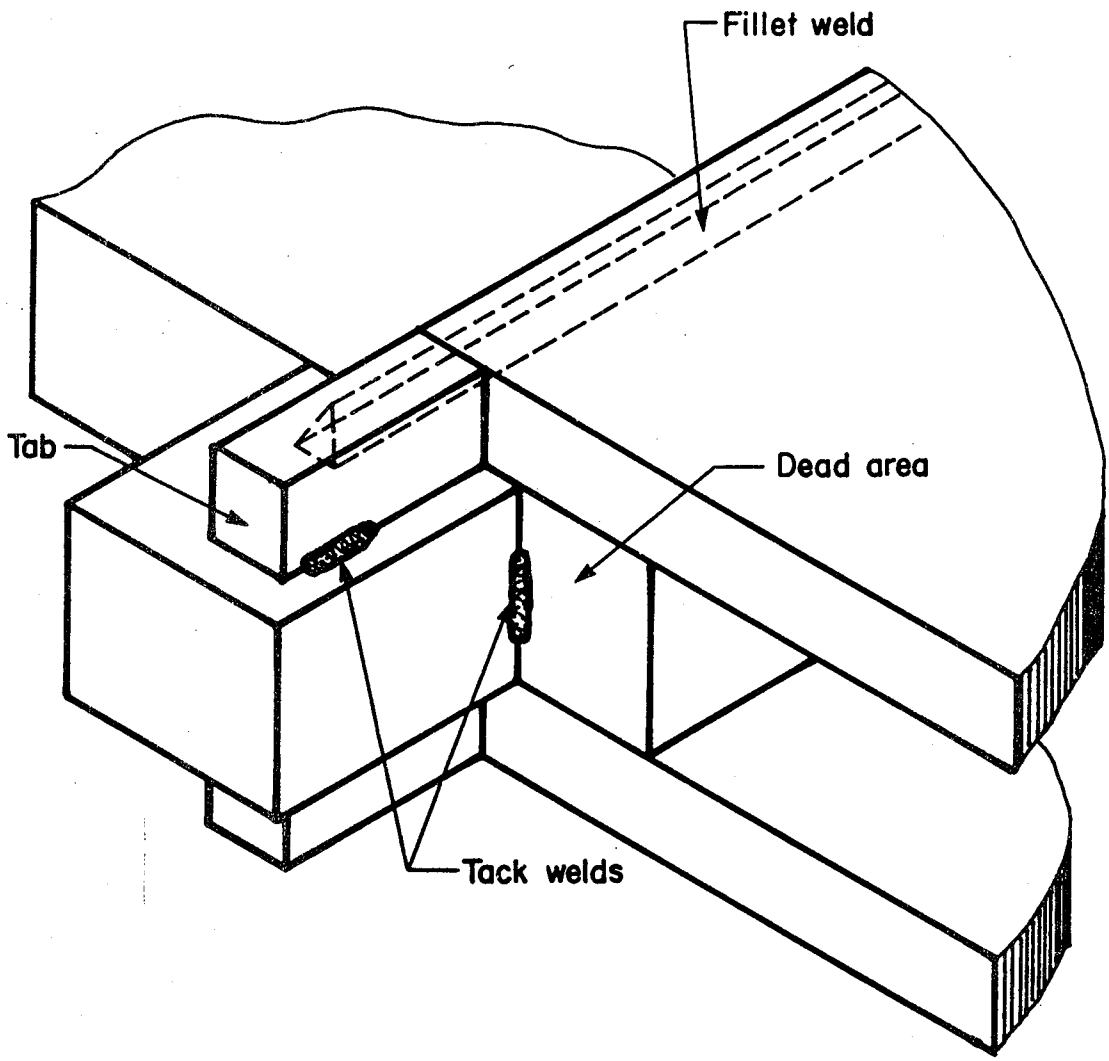

Figure 3.5 Run-Off Tabs Located On Specimen Edge

on each side of the test specimen. As shown in Fig 3.6, this required placing tabs on the test piece faces for these specimens.

With specimens placed on the welding bed, each weld bead was started on a run-on tab and continued without stopping to a run-off tab. The tabs were then removed by machining. Both ends of each weld test length were machined parallel to the direction of loading.

As the plates remained elastic throughout each test, it was possible to reuse plates in subsequent tests. The plates for the 90° weld tests were reused for the 60° tests and again for the 45° tests. Those for the 75° tests were reused for the tests at 30° and 15°. The 0° test specimens were only used once as re-use of these plates would have required excessive machining. After each testing stage, the failed area of the weld was sawn off and retained for further examination. The plates were then prepared for the next weld angle and re-welded following the established welding procedures.

3.8 Test Set-Up

The test set-up consisted of the MTS testing machine, the test specimen, electronic instrumentation including electronic resistance strain gauges and linear variable differential transformers (LVDTs), and a data acquisition system.

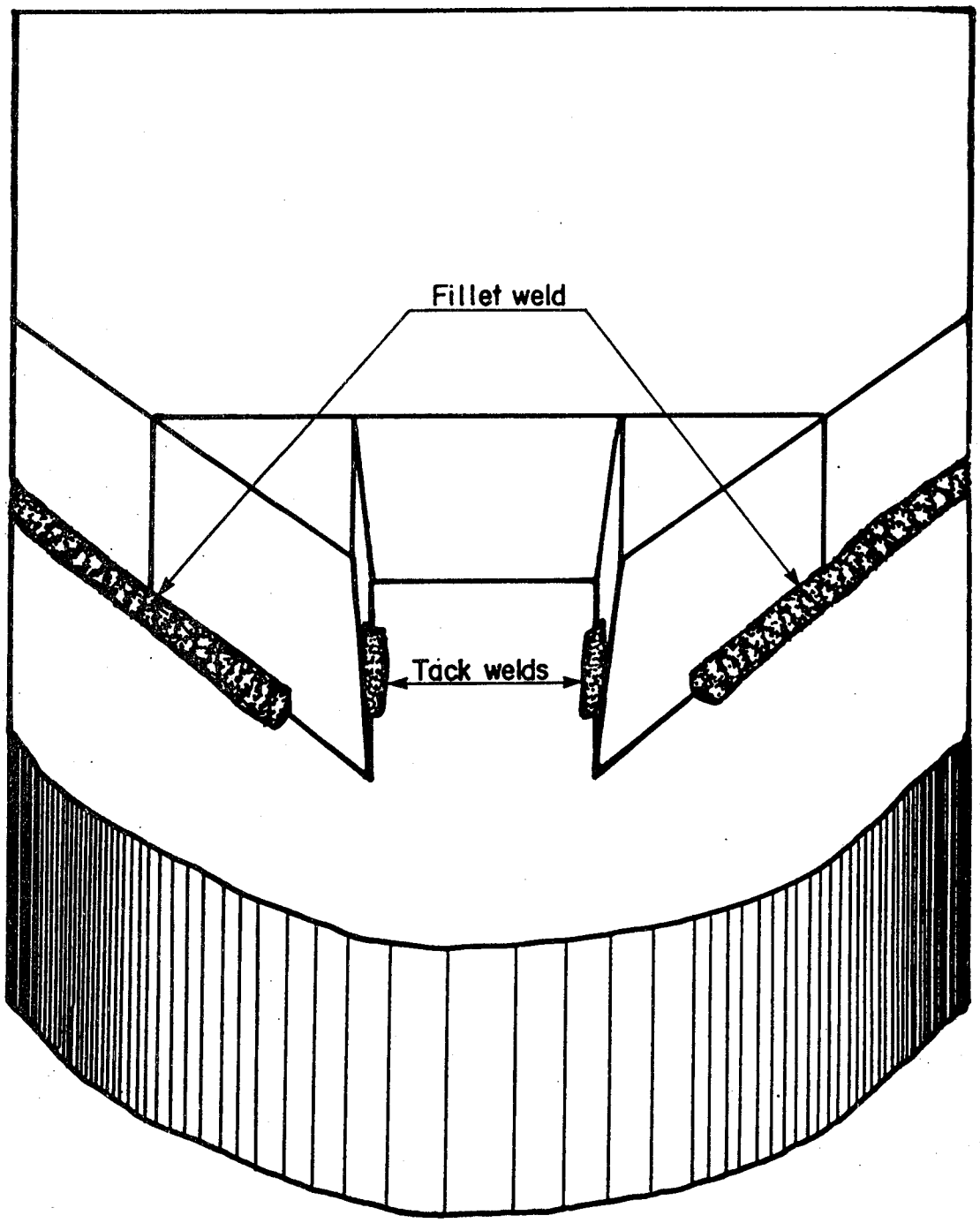

Figure 3.6 Run-Off Tabs Located On Specimen Face

The MTS testing machine loads hydraulically and is capable of operating either in stroke or load control. Load control in the 1300 kN load range was used for all tests as load readings obtained in load control were considered to be more precise than load readings obtained in stroke control for the loading range used.

All measurements were recorded electronically at discrete intervals using a data acquisition system. The data acquisition system consists of a remote terminal linked to a Data General S/120 system with 512 kilobytes of memory. A total of 256 channels were available for analog input. Load was measured internally by the MTS testing machine. This measurement was assigned a channel in the data acquisition system. Strain gauge readings were fed through a signal conditioner and each strain gauge was assigned a channel. Each LVDT output was assigned a channel. Power supplies for both the LVDTs and the strain gauges were assigned channels to monitor possible power fluctuations. Within the accuracy of monitoring equipment, power fluctuations did not occur during any of the tests. The total number of channels used for each test varied from 13 to 17, depending on the number of strain gauges used.

3.9 Instrumentation and Measurement

Showa electronic resistance strain gauges, with a resistance of 120 ohms, a gauge length of 5 mm and a gauge factor of 2.11, were used to measure strains in the plates.

This type of strain gauge was also used for strain measurements for the ancillary tests. Strain gauges were mounted on each specimen face at a minimum of three locations along the specimen length as shown in Fig 3.7. In some cases, additional gauges were located adjacent to the fillet welds to check for local plate yielding. This gauge arrangement allowed the specimen alignment to be monitored during testing, as eccentric loading would result in different strain readings on opposite specimen faces at a cross section. No significant eccentric loading occurred during the tests.

Four Hewlett Packard Model 24DCDT-100 LVDTs with a linear operating range of 5.0 mm were used to measure weld deformations during each test. Two LVDTs were located on each specimen face. Prior to testing, each LVDT was calibrated to establish its linear operating range. The LVDTs were supported on a rigid frame which in turn was clamped to the specimen. Two different frames were used, one for specimens with a continuous weld on each face, and the other for specimens with two weld lengths on each face.

The frame used on specimens with continuous welds shown in Fig 3.8 consists of two plates which were clamped to the specimen near the welds. The clamping force was provided through threaded rods at either end of the plates. Locking bolts on the threaded rods prevented rotational instability of the stand. The frame surfaces resting against the specimen were machined to a smooth, reduced area. Rigging to

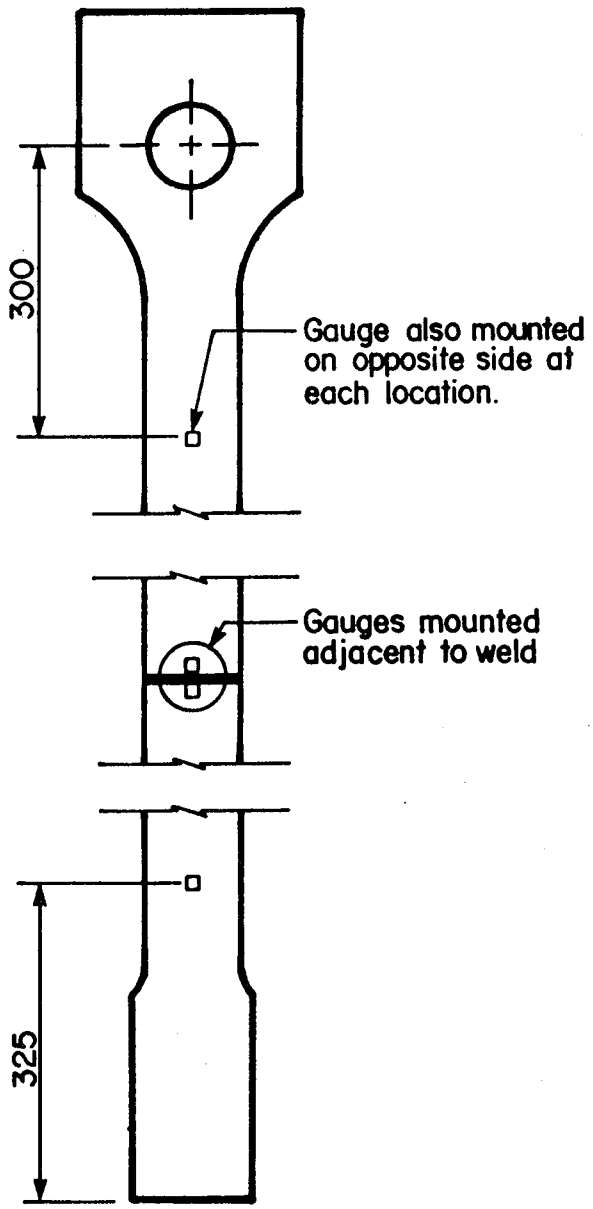

Figure 3.7 Strain Gauge Locations

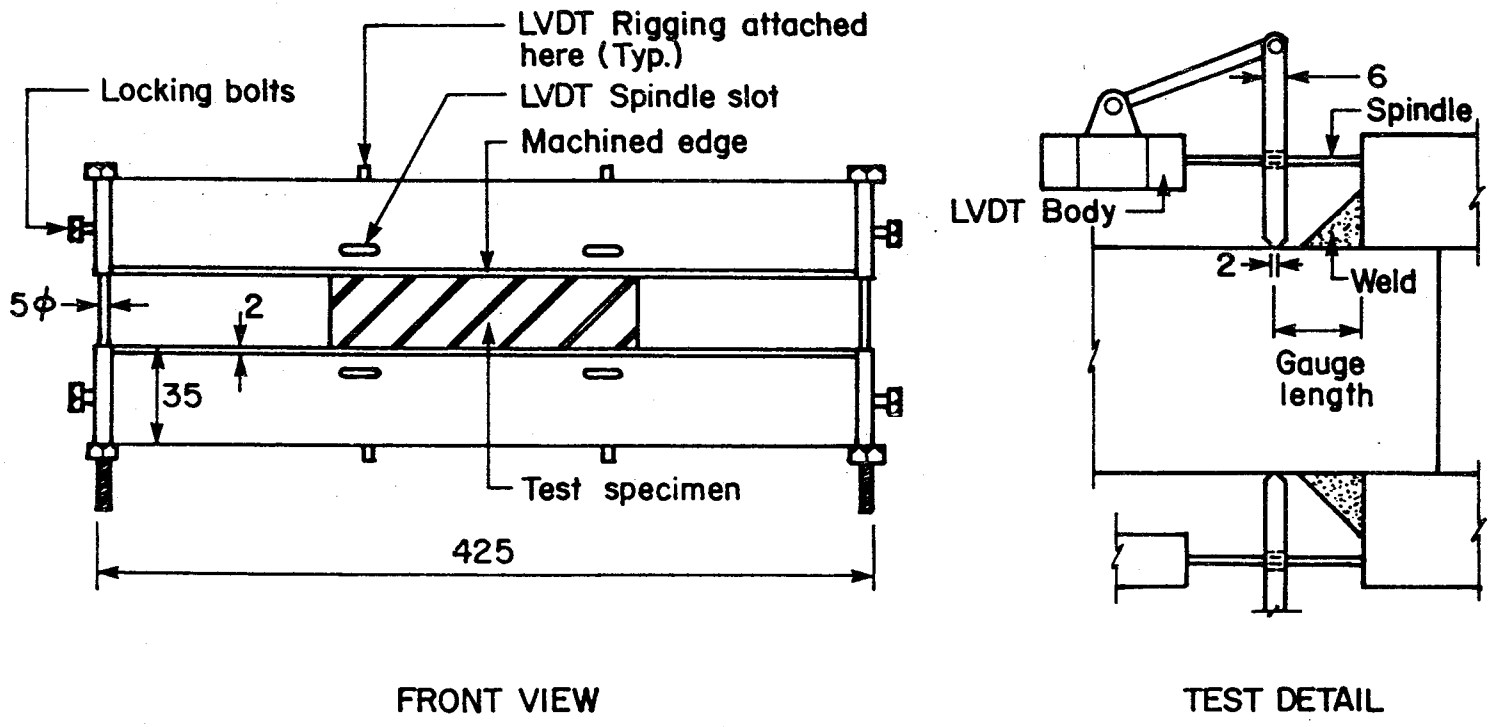

Figure 3.8 LVDT Frame For Continuous Welds On Each Specimen Face

support each LVDT was attached to the frame at the point where deformations were measured. Each LVDT spindle passed through a slot in the frame and butted against the plate edge.

The frame used on specimens with two welds on each specimen face is shown in Fig 3.9. One frame was clamped on each specimen face. This frame consists of plates attached to three legs with a hinge at the middle leg. Clamping force was applied through the outer legs with a C-clamp. As deformations were measured at each of the four outer legs, rigging to support the LVDTs was attached to each of these legs. The middle leg provided stability for the frame and the hinge allowed the frame to accomodate various loading angles. Each LVDT spindle passed directly adjacent to the frame leg between the test specimen surface and the bottom edge of the frame, to butt against the plate edge.

In all cases, deformations were measured parallel to the direction of loading. Thus, the gauge length over which deformations were measured varied with the angle of loading.

Because the test specimen plates were proportioned to remain elastic throughout each test, they were assumed to act as rigid bodies, with essentially all the deformation occurring across the welds. The rigid body movement of the plates allowed deformation differences between weld ends on each specimen face to be monitored, even though the LVDTs were connected to each other through the frame arrangement. Differences in deformations between welds on opposite faces

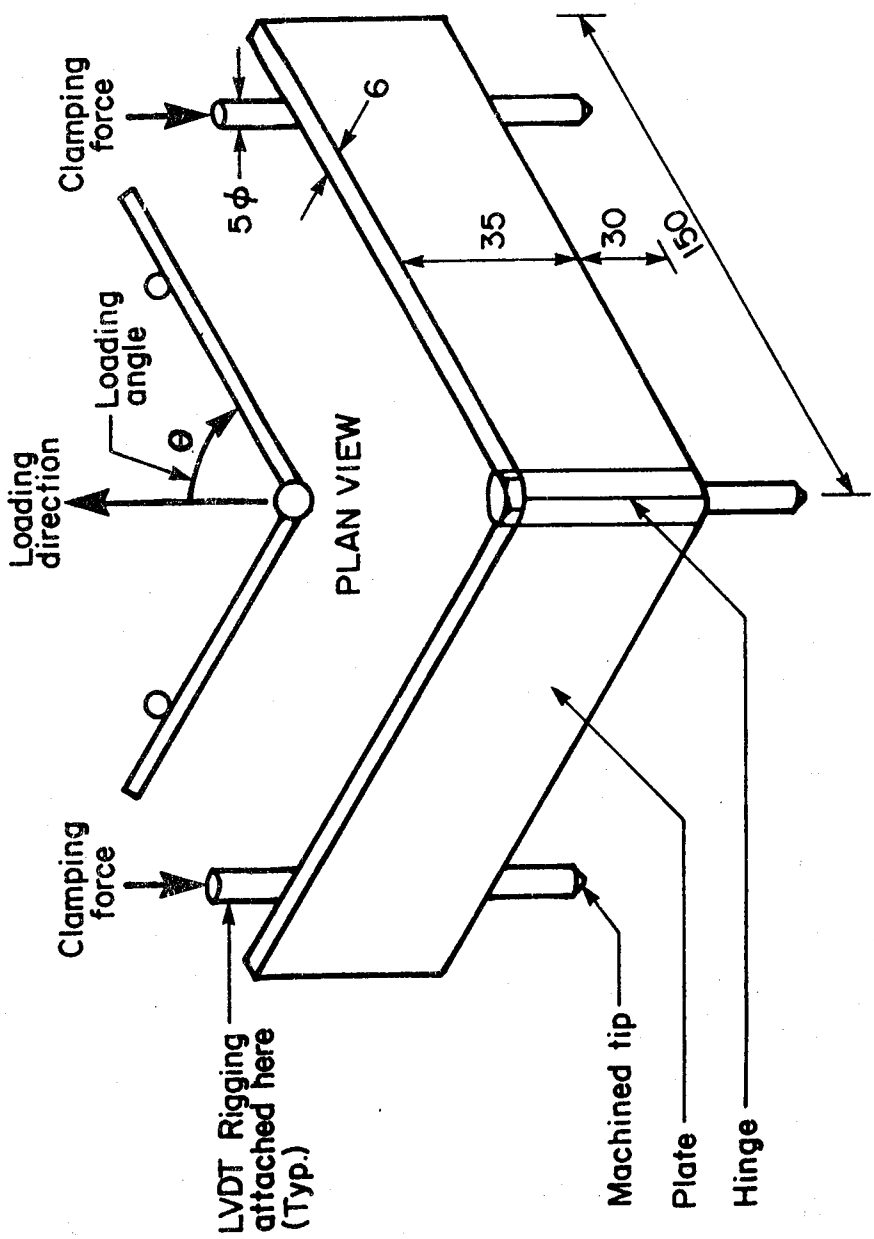

Figure 3.9 LVDT Frame For Specimen With Two Welds On Each Face

of the specimen resulted mainly from initial out-of-straightness of the specimen.

3.10 Test Procedure

For each test, the test specimen was first aligned vertically and then the bottom hydraulic grips clamped. A load of about one-tenth of the expected ultimate load was applied to the test specimen and the vertical alignment of the MTS machine was locked in place. After re-zeroing, load was applied in 20 kN increments for the 5 mm welds and in 40 kN increments for the 9 mm welds, using load control. As the ultimate weld strength was approached, these load increments were decreased. To achieve quasi-static readings during testing, the load was held stationary at the end of each load increment until the LVDT readings stabilized. A complete set of readings was then taken and loading continued. Load and deformation readings were continued beyond the ultimate strength of the weld metal until eventual weld fracture. Beyond the maximum load, load-deformation readings were obtained by decreasing the load in small decrements until the deformations stabilized for each decrement. After weld fracture, the pieces of the test specimen were carefully removed from the machine to prevent damage to the fracture surfaces. Photographs were taken and a written record maintained.

3.11 Fracture Observations

Failed weld areas were sawn off the test pieces and the location of the weld areas logged. The failed welds were then sectioned into a minimum of four pieces, as shown in Fig 3.10. An Optical Comparator with an accuracy of ±0.25° was used to measure the angle between the horizontal weld leg and the fracture surface. As the cracks are considered to have initiated at the weld root, the angle of the fracture surface was measured from there, as shown in Fig 3.11. Some weld cross sections were polished, etched and magnified up to 16X to observe fracture mechanisms. Fracture surfaces were also examined using a Scanning Electron Microscope (SEM) at magnifications up to 1800X. Photographs were taken of various fractures.

3.12 Ancillary Tests

3.12.1 Tension Coupons

Seven coupons, made in accordance with ASTM A370-77, Part 1 (1977), were taken from each of three plate thicknesses to determine the stress-strain characteristics of the plates. The coupons, of full plate thickness, were sawn parallel to the rolling direction and machined to the final dimensions. Cross-sectional dimensions were measured with a digital micrometer. A strain gauge was mounted on each face of a coupon to determine strains. These gauges were wired to form a full bridge system allowing the average

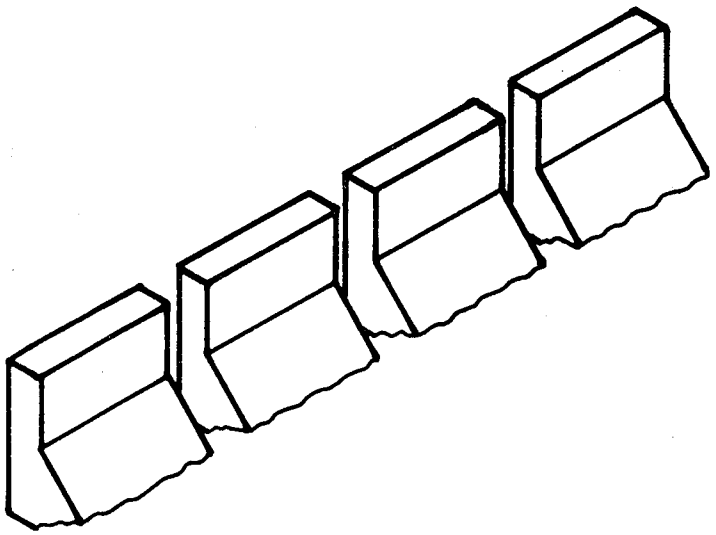

Figure 3.10 Weld Sections

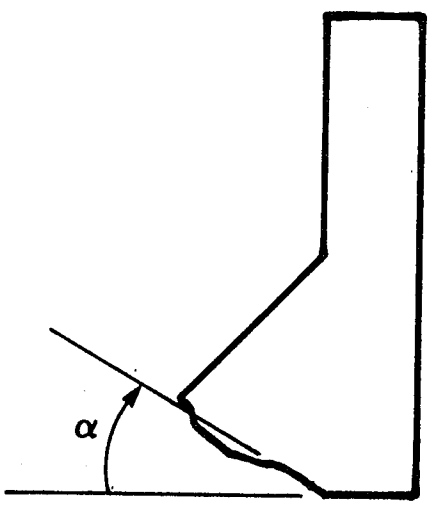

Figure 3.11 Fracture Surface Orientation

strain to be measured with double the sensitivity of a single gauge. Large strains were found by measuring deformations over a 200 mm gauge length with calipers. The 9 mm and 18 mm thick coupons were tested in a Baldwin testing machine with a 880 kN tensile capacity and the 35 mm thick coupons were tested in the MTS system of the I.F. Morrison Structural Laboratory. All coupons were tested in accordance with ASTM A370-77, Part 1 (1977).

3.12.2 All-Weld Metal Coupons

Three all-weld metal coupons with a 50 mm gauge length were made in accordance with CSA Standard W48.1-M80 (CSA, 1980). The electrodes used were from the same lot as those used in the fillet weld tests. The 300W plate used for backing pieces was the same as the plate used in the test specimens. The coupons were made by the same welder who welded the fillet weld specimens. Prior to final machining, the coupons were tested for cracking using dye penetrant inspection according to ASTM E165-80 (1980). Cross-sectional dimensions were measured using a digital micrometer. As with the tension coupons, strain gauges were mounted on opposite sides of a weld coupon to form a full bridge system. The coupons were tested in an MTS testing system with a 225 kN tensile capacity in the Department of Mineral Engineering at the University of Alberta. The coupons were tested in accordance with CSA Standard W48.1-M80, (CSA, 1980). Load and deformation measurements were taken.

4. Test Results

4.1 Ancilliary Test Results

4.1.1 Tension Tests On Plates

Typical stress versus strain curves for each plate thickness are shown in Fig 4.1. Tables 4.1 to 4.3 give values of significant parameters. The modulus of elasticity, (E), was determined using the method of least squares, as given in ASTM E111-61 (1961), based on strain gauge readings. The static yield stress was determined by decreasing the strain rate to zero. Calipers were used to measure deformations beyond the typical failure strain of 1.5% of the strain gauges.

Minimum strength and elongation requirements as specified in CSA Standard CAN3-G40.21-M81 (1981) were satisfied for all three plate thicknesses.

4.1.2 All-Weld Metal Tension Coupons

A typical stress versus strain curve for the all-weld metal tension coupon test is shown in Fig 4.2. Significant parameters for the weld metal, determined on the same basis as for the plate coupons, are listed in Table 4.4.

The minimum strength and elongation requirements as specified in CSA Standard W48.1-M80 (CSA, 1980) were met for all three coupons.

9MM PLATE TENSION COUPON DATA						
Coupon No.	E X10E3 (MPa)	Yield Strain X10E-6 (mm/mm)	Yield Stress (MPa)	Ult. Strain (mm/mm)	Ult. Stress (MPa)	Final Elong (%)
1	220.1	1750	363	0.15	520	24
2	215.2	1850	367	0.14	521	21
3	225.8	1710	358	0.15	520	24
4	225.1	1730	377	0.16	522	24
5	218.8	1760	365	0.15	521	23
6	209.2	1840	358	0.15	524	24
7	215.9	1830	361	0.15	525	22
Mean	218.6	1780	364	0.15	522	23
Min.or range requirements from CSA G40.21-M81.			300		450-620	20

Table 4.1 Standard Tensile Data On 9 mm Plate

18MM PLATE TENSION COUPON DATA						
Coupon No.	E X10E3 (MPa)	Yield Strain X10E-6 (mm/mm)	Yield Stress (MPa)	Ult. Strain (mm/mm)	Ult. Stress (MPa)	Final Elong (%)
8	221.1	1720	338	0.15	506	27
9	221.1	1700	342	0.16	506	26
10	214.3	1700	332	0.16	502	28
11	222.6	1660	350	0.15	523	28
12	213.1	1780	351	0.16	518	26
13	212.9	1760	353	0.15	519	26
14	217.5	1670	353	0.16	520	27
Mean	217.5	1710	346	0.16	513	27
Min.or range requirements from CSA G40.21-M81.			300		450-620	20

Table 4.2 Standard Tensile Data On 18 mm Plate

35MM PLATE TENSION COUPON DATA						
Coupon No.	E X10E3 (MPa)	Yield Strain X10E-6 (mm/mm)	Yield Stress (MPa)	Ult. Strain (mm/mm)	Ult. Stress (MPa)	Final Elong (%)
15 *	207.6	1740	339	-	-	-
16	205.3	1690	326	0.17	492	32
17	208.3	1690	321	0.16	500	32
18	201.0	1740	326	0.17	492	33
19	200.8	1770	324	0.17	493	31
20	206.4	1690	311	0.17	490	32
21	201.9	1740	324	0.16	491	32
Mean	204.5	1720	324	0.17	493	32
Min. or range requirements from CSA G40.21-M81.			300		450-620	20

Note: * coupon tested in Baldwin testing machine. This machine had insufficient capacity to fail coupon.

Table 4.3 Standard Tensile Data On 35 mm Plate

ALL WELD METAL TENSION COUPON DATA						
Coupon No.	E X10E3 (MPa)	Yield Strain X10E-6 (mm/mm)	Yield Stress (MPa)	Ult. Strain (mm/mm)	Ult. Stress (MPa)	Final Elong (%)
1	208.3	2380	469	0.17	543	25
2	206.9	2440	460	0.17	529	28
3 *	-	-	466	0.17	541	23
Mean	207.6	2410	465	0.17	538	25
Min. requirements of CSA W48.1-M80.			410		500	17

Note: * inaccurate initial strain readings.

Table 4.4 Standard Tensile Test Data On Weld Metal

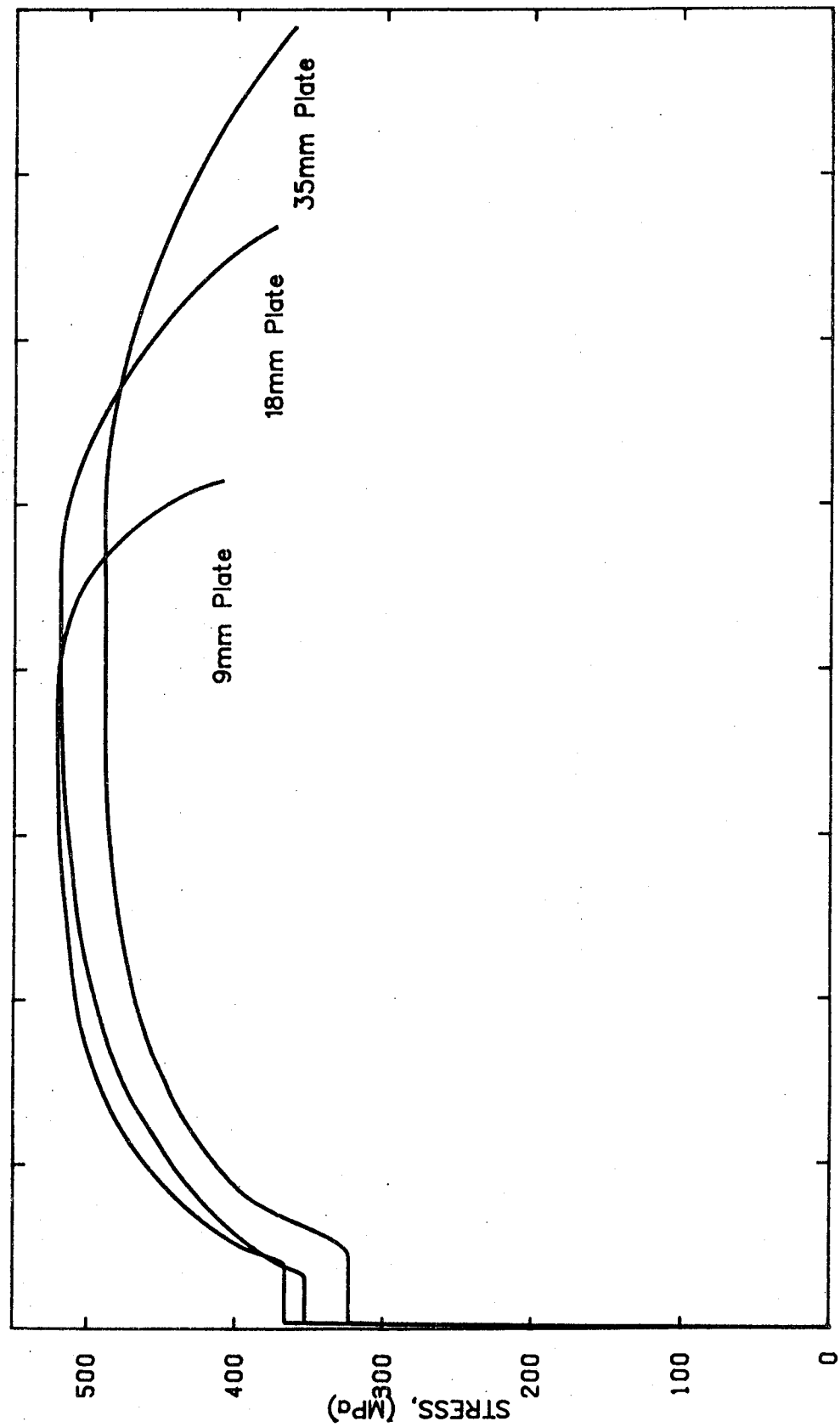

Figure 4.1 Stress-Strain Curves From Plate Tension Coupons

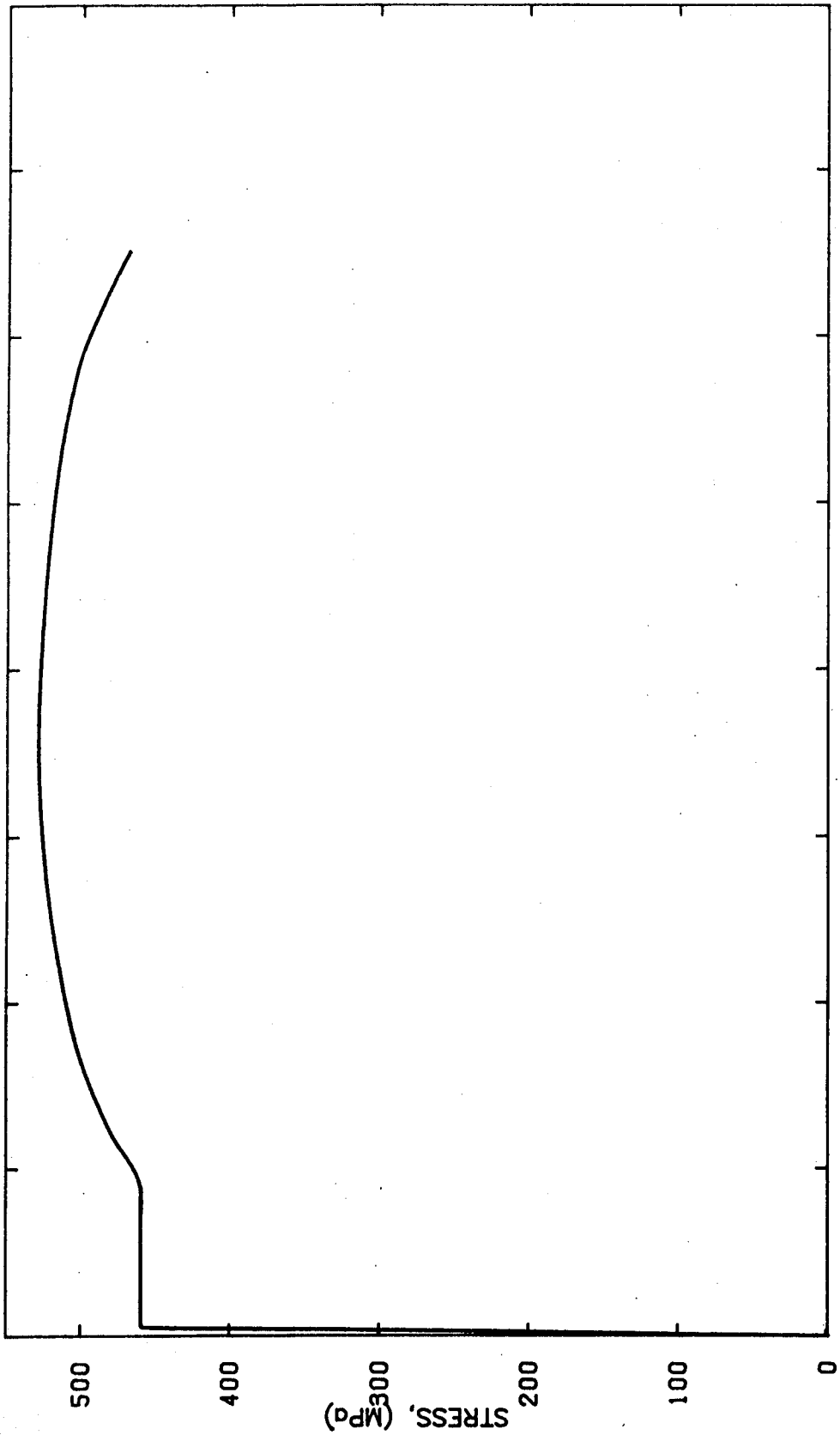

Figure 4.2 Stress-Strain Curve From All-Weld Metal Tension Coupon

4.2 Fillet Weld Test Results

4.2.1 General

In none of the tests were the plates strained beyond the yield strain. Therefore, in comparison to the significant deformation of the welds, the total deformation of the plates within the gauge length of the LVDTs can be considered negligible.

All test specimens failed in the welds. With one exception, the welds on both sides of all specimens appeared to fail simultaneously.

The first two digits of each test specimen number, as shown in Tables 4.5 and 4.6, give the angle of loading in degrees. The last digit identifies the order of testing.

4.2.2 Weld Dimensions

To normalize the test data, the leg size and length of each weld were measured using a digital micrometer with an accuracy of ±0.005 mm. The mean leg size for each test specimen was computed from a minimum of 44 readings. Average dimensions for the 5 mm and 9 mm weld series are given in Tables 4.5 and 4.6, respectively. A summary of the weld dimensions is given in Table 4.7.

4.2.3 Fracture Surface Observations

Weld fractures did not occur on well defined planes, but rather, on uneven surfaces, as has been observed by Naka

DIMENSIONS OF 5MM WELDS						
Test	Leg Size					Length
	n	Mean (mm)	σ (mm)	V (%)	Mean/Nominal	(mm)
90.1	44	5.25	0.31	5.8	1.05	200
90.2	44	5.33	0.34	6.4	1.07	200
90.3	44	5.29	0.39	7.2	1.06	201
75.1	44	5.14	0.36	7.0	1.03	215
75.2	44	5.01	0.35	7.1	1.00	211
75.3	44	5.12	0.29	6.0	1.02	210
60.1	48	5.12	0.33	6.4	1.02	230
60.2	48	5.06	0.32	6.3	1.01	231
60.3	48	5.03	0.37	7.2	1.01	226
45.1	48	5.37	0.52	9.9	1.07	204
45.2	48	5.10	0.52	10.1	1.02	200
45.3	48	5.12	0.37	7.1	1.02	196
30.1	64	5.31	0.40	7.5	1.06	294
30.2	62	5.50	0.39	7.1	1.10	302
30.3	60	5.27	0.34	6.5	1.05	296
15.1	58	5.19	0.50	9.9	1.04	306
15.2	58	5.14	0.37	7.2	1.03	313
15.3	59	5.09	0.45	8.9	1.02	311
00.1	72	4.94	0.40	8.1	0.99	316
00.2	72	5.22	0.39	7.5	1.04	309
00.3	72	5.16	0.32	6.2	1.03	315

Table 4.5 Dimensions Of 5 mm Welds

DIMENSIONS OF 9MM WELDS						
Test	Leg Size					Length
	n	Mean (mm)	σ (mm)	V (%)	Mean/Nominal	(mm)
90.11	44	9.10	0.49	5.4	1.01	197
90.12	44	9.26	0.39	4.3	1.03	200
90.13	44	9.16	0.54	5.8	1.02	200
75.11	44	9.18	0.58	6.4	1.02	211
75.12	44	9.08	0.53	5.8	1.01	207
75.13	44	9.24	0.42	4.5	1.03	209
60.11	48	9.42	0.38	4.1	1.05	226
60.12	48	9.65	0.35	3.6	1.07	229
60.13	48	9.88	0.41	4.2	1.10	228
45.11	56	9.43	0.50	5.4	1.05	272
45.12	56	9.46	0.48	5.0	1.05	279
45.13	58	9.18	0.50	5.6	1.02	279
30.11	64	9.41	0.36	3.8	1.05	296
30.12	60	9.16	0.40	4.3	1.02	296
30.13	58	9.74	0.40	4.1	1.08	294
15.11	54	8.79	0.34	8.8	0.98	300
15.12	52	9.23	0.40	4.4	1.03	294
15.13	54	9.06	0.38	4.2	1.01	294
00.11	64	9.50	0.35	3.7	1.06	300
00.12	72	9.10	0.44	4.9	1.01	321
00.13	72	9.20	0.34	3.7	1.02	316

Table 4.6 Dimensions of 9 mm Welds

SUMMARY OF WELD DIMENSIONS		
	Weld Size	
	5mm	9mm
Mean (mm)	5.18	9.30
σ (mm)	0.13	0.25
V (%)	2.6	2.7
Mean of $\frac{\text{Mean}}{\text{Nominal}}$	1.04	1.03
σ	0.03	0.03
V (%)	2.6	2.7

Table 4.7 Summary Of Weld Dimensions

and Kato (1966). Average values of the fracture surface angles measured are given in Tables 4.8 and 4.9.

For tests on 9 mm welds, made with three passes, for loading angles of 30° to 90°, it was evident that after initial cracking, crack extension tended to follow heat affected zones between weld passes as shown in Figure 4.3. For the 15° and 0° tests in the 9 mm series, failure near the weld throat region governed and, as seen in Fig 4.4, cracks in these tests propagated across the weld pass interfaces. The 5 mm welds were deposited in a single pass and the phenomenon of crack propogation along interfaces between weld passes does not apply.

A Scanning Electron Microscope, (SEM), was used to examine appearances of fracture surfaces of transversely and longitudinally loaded fillet welds. The fracture surface of the transversely loaded fillet weld exhibited a transition from brittle fracture at the weld root, shown in Fig 4.5(a), to ductile fracture where the crack terminated, as shown in Fig 4.5(c). The middle of the fracture surface, shown in Fig 4.5(b), shows 'islands' of brittle fracture interspersed with ductile fracture. Conversely, the fracture surface of the longitudinally loaded fillet weld did not show a transition between brittle and ductile fracture as shown in Fig 4.6. The entire fracture surface, including the weld root area, consisted predominantly of ductile fracture, with 'islands' of brittle fracture randomly dispersed.

5MM WELD FRACTURE OBSERVATIONS		
Test	n	Average Angle (degrees)
90.1	3	10.0
90.2	3	13.0
90.3	6	9.5
75.1	6	12.0
75.2	3	11.0
75.3	6	12.0
60.1	6	18.5
60.2	6	18.5
60.3	6	18.0
45.1	8	33.5
45.2	8	23.0
45.3	8	25.0
30.1	8	27.5
30.2	8	19.5
30.3	8	21.5
15.1	8	42.0
15.2	8	42.0
15.3	8	42.5
00.1	8	50.5
00.2	8	49.0
00.3	8	50.5

Table 4.8 Fracture Surface Angles Of 5 mm Welds

9MM WELD FRACTURE OBSERVATIONS		
Test	n	Average Angle (degrees)
90.11	6	15.5
90.12	6	20.5
90.13	6	19.5
75.11	6	18.0
75.12	6	18.5
75.13	6	20.0
60.11	6	17.5
60.12	6	15.5
60.13	6	16.5
45.11	6	19.0
45.12	6	24.5
45.13	6	19.0
30.11	8	18.5
30.12	8	17.0
30.13	8	15.0
15.11	7	25.5
15.12	4	36.5
15.13	5	24.5
00.11	8	48.5
00.12	7	48.0
00.13	6	49.0

Table 4.9 Fracture Surface Angles Of 9 mm Welds

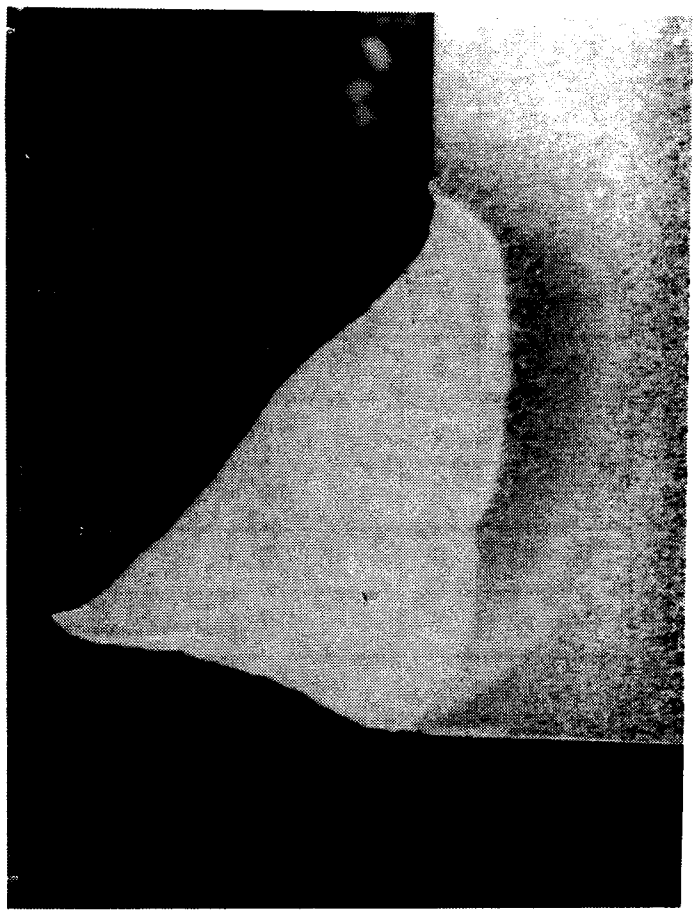

Figure 4.3 Crack Propagation Along Weld Pass Interface
(6.4X Mag.)

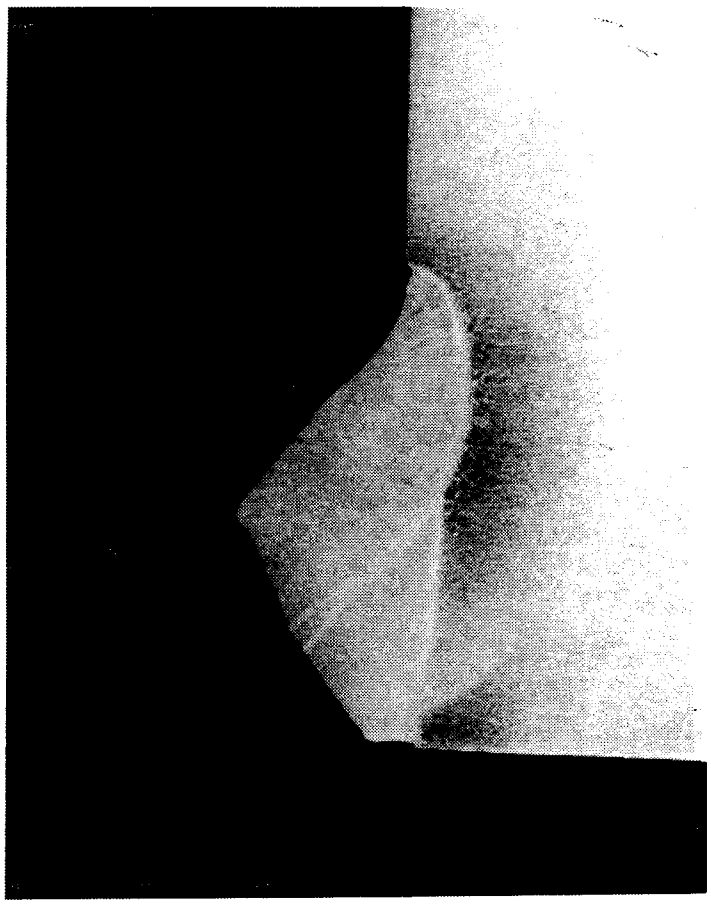

Figure 4.4 Crack Propagation Through Weld Pass Interfaces
(6.4X Mag.)

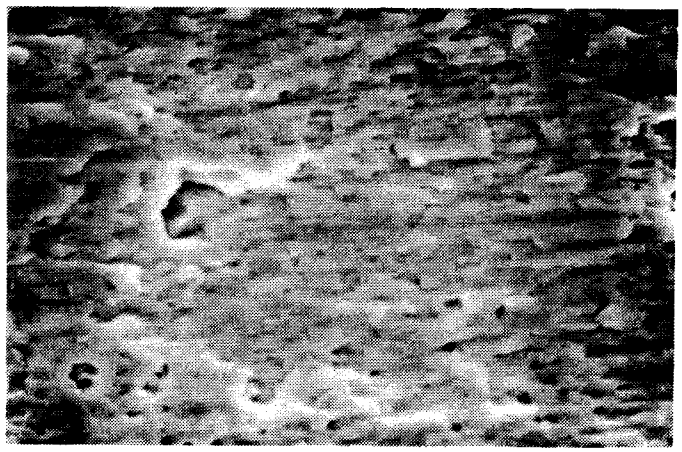

a) Near Weld Root

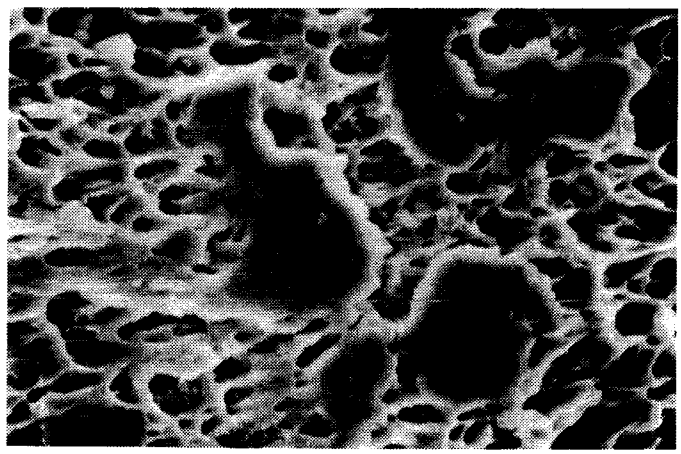

b) Middle of Fracture Surface

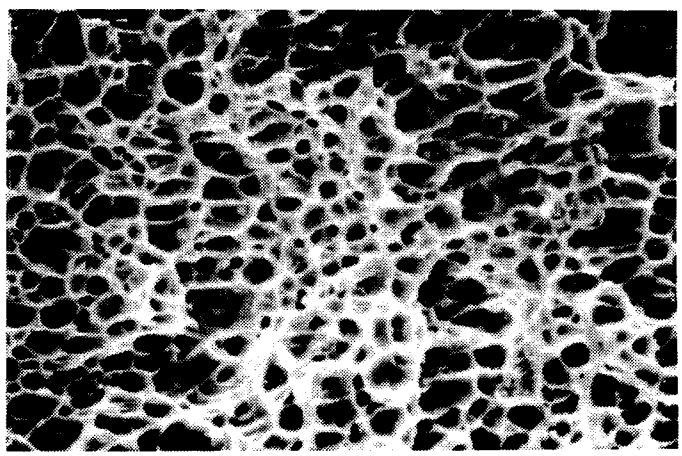

c) Near Edge of Fracture Surface

Figure 4.5 Fracture Surface Of Transverse Fillet (1800X Mag.)

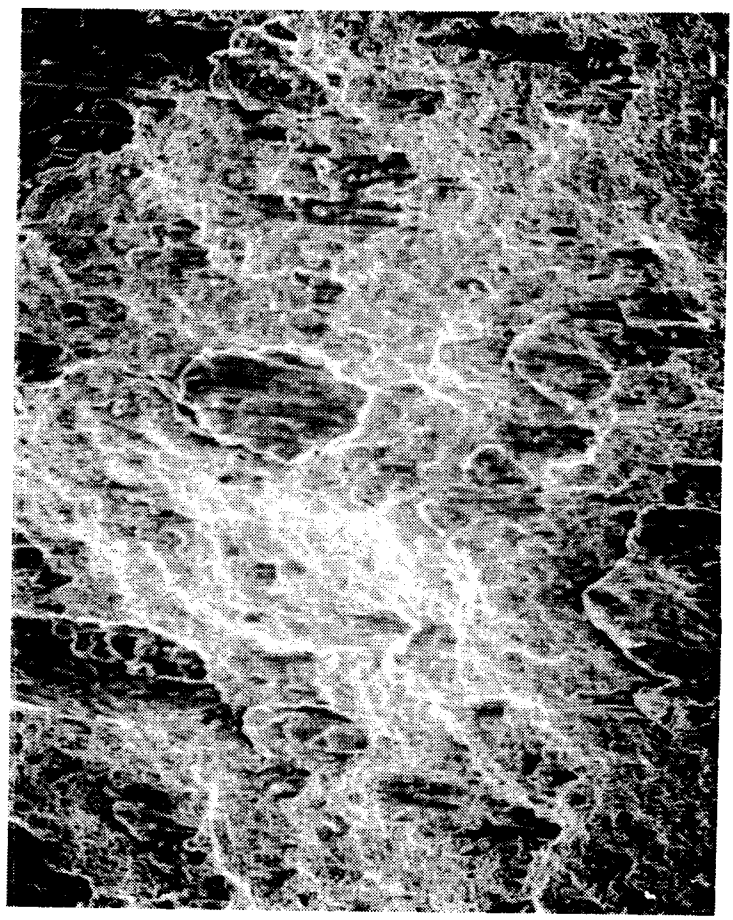

Figure 4.6 Fracture Surface Of Longitudinal Fillet
(110X Mag.)

4.2.4 Ultimate Weld Strength

Ultimate loads per millimeter of weld length, normalized by dividing the measured ultimate load by the ratio of the actual average leg size to the specified leg size, are given in Tables 4.10 and 4.11 for the 5 mm and 9 mm welds, respectively.

4.2.5 Weld Deformations and Weld Strains

Weld deformations at both the ultimate load and at weld fracture are given in Tables 4.12 to 4.25. The deformations have been normalized two ways.

In the first normalization method, (A), the deformations are divided by the ratio of the actual average leg to the specified leg size.

In the second method, (B), deformations are divided by the ratio of the gauge length used to measure the weld deformation to the specified leg size. Any deformation of the plate within the gauge length was neglected.

Average weld strains at the ultimate load and at weld fracture have been computed by dividing measured deformations by the gauge lengths used to obtain the deformations, and are shown in Fig 4.7 to 4.10.

Various gauge lengths were used to measure deformations in the longitudinally loaded specimens. As the deformations were observed to be independent of the gauge length used to obtain the deformations, it was concluded that the plates moved essentially as rigid bodies with respect to one

ULTIMATE STRENGTH OF 5MM WELDS		
Test	Failure Load (kN)	Normalized Ultimate Strength (kN/mm of weld)
90.1	421.3	2.000
90.2	431.4	2.020
90.3	407.3	1.915
75.1	465.9	2.110
75.2	451.3	2.140
75.3	471.1	2.185
60.1	568.2	2.415
60.2	566.3	2.420
60.3	558.5	2.450
45.1	446.7	2.040
45.2	433.0	2.130
45.3	419.0	2.095
30.1	613.9	1.970
30.2	626.4	1.885
30.3	609.9	1.960
15.1	484.2	1.525
15.2	477.0	1.480
15.3	481.9	1.520
00.1	512.5	1.640
00.2	486.8	1.510
00.3	482.5	1.485

Table 4.10 Ultimate Strength Of 5 mm Welds

ULTIMATE STRENGTH OF 9MM WELDS		
Test	Failure Load (kN)	Normalized Ultimate Strength (kN/mm of weld)
90.11	789.2	3.970
90.12	807.4	3.915
90.13	790.5	3.890
75.11	821.8	3.825
75.12	810.4	3.885
75.13	804.5	3.755
60.11	895.4	3.780
60.12	891.5	3.635
60.13	894.1	3.570
45.11	842.0	2.955
45.12	858.3	2.930
45.13	860.5	3.030
30.11	980.4	3.165
30.12	968.4	3.220
30.13	988.6	3.105
15.11	772.9	2.640
15.12	723.7	2.400
15.13	814.6	2.750
00.11	752.3	2.375
00.12	824.7	2.540
00.13	786.9	2.440

Table 4.11 Ultimate Strength of 9 mm Welds

DEFORMATIONS OF 5MM WELDS						
Test	Deformation At Ultimate Load (mm)	Normalized By Method (A) (mm)	Normalized By Method (B) (mm)	Deformation At Fracture (mm)	Normalized By Method (A) (mm)	Normalized By Method (B) (mm)
00.1	0.876	0.887	-	1.561	1.580	-
	0.939	0.950	-	2.276	2.304	-
	0.943	0.955	-	1.519	1.537	-
	0.988	1.000	-	1.898	1.921	-
00.2	1.062	1.017	-	1.720	1.648	-
	0.946	0.906	-	1.688	1.616	-
	1.095	1.049	-	1.915	1.834	-
	0.967	0.926	-	1.917	1.836	-
00.3	0.933	0.904	-	1.510	1.463	-
	0.990	0.959	-	1.468	1.423	-
	1.009	0.978	-	1.948	1.888	-
	0.995	0.964	-	1.619	1.569	-

Table 4.12 Deformations Of 5 mm Welds Loaded At 0°

DEFORMATIONS OF 5MM WELDS						
Test	Deformation At Ultimate Load (mm)	Normalized By Method (A) (mm)	Normalized By Method (B) (mm)	Deformation At Fracture (mm)	Normalized By Method (A) (mm)	Normalized By Method (B) (mm)
15.1	0.566	0.545	0.141	0.686	0.661	0.171
	0.572	0.551	0.143	0.732	0.705	0.183
	0.551	0.531	0.137	0.663	0.639	0.165
	0.562	0.541	0.140	0.695	0.667	0.173
15.2	0.500	0.486	0.126	0.608	0.591	0.153
	0.483	0.470	0.122	0.560	0.545	0.141
	0.512	0.498	0.129	0.660	0.642	0.166
	0.494	0.480	0.124	0.581	0.565	0.146
15.3	0.594	0.584	0.151	1.150	1.129	0.292
	0.492	0.483	0.125	0.676	0.664	0.172
	0.484	0.475	0.123	0.790	0.776	0.201
	0.380	0.373	0.097	0.492	0.483	0.125

Table 4.13 Deformations Of 5 mm Welds Loaded At 15°

DEFORMATIONS OF 5MM WELDS						
Test	Deformation At Ultimate Load (mm)	Normalized By Method (A) (mm)	Normalized By Method (B) (mm)	Deformation At Fracture (mm)	Normalized By Method (A) (mm)	Normalized By Method (B) (mm)
30.1	0.404	0.380	0.190	0.547	0.515	0.258
	0.451	0.425	0.212	0.584	0.550	0.275
	0.440	0.414	0.207	0.639	0.602	0.301
	0.419	0.395	0.197	0.553	0.521	0.260
30.2	0.364	0.331	0.166	0.575	0.523	0.261
	-	-	-	-	-	-
	0.400	0.364	0.182	0.656	0.596	0.298
	-	-	-	-	-	-
30.3	0.428	0.406	0.203	0.647	0.614	0.307
	-	-	-	-	-	-
	0.381	0.362	0.181	0.567	0.540	0.270
	-	-	-	-	-	-

Table 4.14 Deformations Of 5 mm Welds Loaded At 30°

DEFORMATIONS OF 5MM WELDS						
Test	Deformation At Ultimate Load (mm)	Normalized By Method (A) (mm)	Normalized By Method (B) (mm)	Deformation At Fracture (mm)	Normalized By Method (A) (mm)	Normalized By Method (B) (mm)
45.1	0.324	0.302	0.213	0.547	0.509	0.360
	0.323	0.301	0.213	0.543	0.506	0.358
	0.271	0.252	0.178	0.385	0.359	0.254
	0.313	0.291	0.206	0.433	0.403	0.285
45.2	0.307	0.301	0.213	0.525	0.515	0.364
	0.327	0.321	0.227	0.650	0.637	0.451
	0.273	0.268	0.189	0.447	0.438	0.310
	0.305	0.299	0.211	0.572	0.561	0.396
45.3	0.337	0.329	0.233	0.453	0.442	0.313
	0.381	0.372	0.263	0.600	0.586	0.414
	0.300	0.293	0.207	0.365	0.356	0.252
	0.344	0.336	0.238	0.458	0.447	0.316

Table 4.15 Deformations Of 5 mm Welds Loaded At 45°

DEFORMATIONS OF 5MM WELDS						
Test	Deformation At Ultimate Load (mm)	Normalized By Method (A) (mm)	Normalized By Method (B) (mm)	Deformation At Fracture (mm)	Normalized By Method (A) (mm)	Normalized By Method (B) (mm)
60.1	0.380	0.371	0.321	0.484	0.473	0.409
	0.319	0.312	0.270	0.341	0.333	0.288
	0.363	0.355	0.307	0.461	0.450	0.390
	0.271	0.265	0.229	0.294	0.287	0.249
60.2	0.324	0.320	0.277	0.400	0.395	0.342
	0.315	0.311	0.270	0.371	0.367	0.318
	0.301	0.297	0.258	0.382	0.378	0.327
	0.345	0.341	0.295	0.405	0.400	0.347
60.3	0.332	0.330	0.286	0.400	0.398	0.344
	0.386	0.384	0.332	0.476	0.473	0.410
	0.298	0.296	0.256	0.360	0.358	0.310
	0.352	0.350	0.303	0.424	0.422	0.365

Table 4.16 Deformations Of 5 mm Welds Loaded At 60°

DEFORMATIONS OF 5MM WELDS						
Test	Deformation At Ultimate Load (mm)	Normalized By Method (A) (mm)	Normalized By Method (B) (mm)	Deformation At Fracture (mm)	Normalized By Method (A) (mm)	Normalized By Method (B) (mm)
75.1	0.275	0.268	0.258	0.275	0.268	0.258
	0.174	0.169	0.164	0.174	0.169	0.164
	0.309	0.301	0.290	0.309	0.301	0.290
	0.193	0.188	0.181	0.192	0.188	0.181
75.2	0.111	0.111	0.107	0.111	0.111	0.107
	0.233	0.233	0.225	0.233	0.233	0.225
	0.310	0.309	0.299	0.310	0.309	0.299
	0.441	0.440	0.425	0.441	0.440	0.425
75.3	0.285	0.278	0.269	0.323	0.315	0.305
	0.163	0.159	0.154	0.173	0.169	0.163
	-	-	-	-	-	-
	0.200	0.195	0.189	0.229	0.224	0.216

Table 4.17 Deformations Of 5 mm Welds Loaded At 75°

DEFORMATIONS OF 5MM WELDS						
Test	Deformation At Ultimate Load (mm)	Normalized By Method (A) (mm)	Normalized By Method (B) (mm)	Deformation At Fracture (mm)	Normalized By Method (A) (mm)	Normalized By Method (B) (mm)
90.1	0.398	0.379	0.379	0.398	0.379	0.379
	0.205	0.195	0.195	0.205	0.195	0.195
	0.416	0.396	0.396	0.416	0.396	0.396
	0.228	0.217	0.217	0.228	0.217	0.217
90.2	0.165	0.155	0.155	0.165	0.155	0.155
	0.128	0.120	0.120	0.128	0.120	0.120
	0.306	0.287	0.287	0.306	0.287	0.287
	0.214	0.201	0.201	0.214	0.201	0.201
90.3	0.368	0.348	0.348	0.368	0.348	0.348
	0.226	0.214	0.214	0.226	0.214	0.214
	0.503	0.475	0.475	0.503	0.475	0.475
	0.313	0.296	0.296	0.313	0.296	0.296

Table 4.18 Deformations Of 5 mm Welds Loaded At 90°

DEFORMATIONS OF 9MM WELDS						
Test	Deformation At Ultimate Load (mm)	Normalized By Method (A) (mm)	Normalized By Method (B) (mm)	Deformation At Fracture (mm)	Normalized By Method (A) (mm)	Normalized By Method (B) (mm)
00.11	1.282	1.215	-	2.518	2.386	-
	1.385	1.312	-	3.225	3.055	-
	1.258	1.192	-	2.892	2.739	-
	1.463	1.386	-	3.263	3.091	-
00.12	0.914	0.904	-	2.625	2.596	-
	1.032	1.021	-	2.965	2.932	-
	0.924	0.914	-	2.944	2.912	-
	1.061	1.049	-	3.187	3.152	-
00.13	1.422	1.391	-	2.357	2.306	-
	1.650	1.614	-	3.049	2.983	-
	1.486	1.454	-	2.394	2.342	-
	1.616	1.581	-	2.897	2.834	-

Table 4.19 Deformations Of 9 mm Welds Loaded At 0°

DEFORMATIONS OF 9MM WELDS						
Test	Deformation At Ultimate Load (mm)	Normalized By Method (A) (mm)	Normalized By Method (B) (mm)	Deformation At Fracture (mm)	Normalized By Method (A) (mm)	Normalized By Method (B) (mm)
15.11	0.647	0.663	0.172	1.472	1.507	0.390
	0.589	0.603	0.156	1.136	1.163	0.301
	0.799	0.818	0.212	2.742	2.808	0.727
	0.732	0.750	0.194	2.083	2.133	0.552
15.12	0.659	0.643	0.166	1.058	1.032	0.267
	0.758	0.739	0.191	1.405	1.370	0.355
	0.800	0.780	0.202	1.362	1.328	0.343
	0.876	0.854	0.221	1.603	1.563	0.405
15.13	0.680	0.676	0.175	1.120	1.113	0.288
	0.808	0.803	0.208	1.446	1.436	0.372
	0.625	0.621	0.161	0.938	0.932	0.241
	0.723	0.718	0.186	1.175	1.167	0.302

Table 4.20 Deformations Of 9 mm Welds Loaded At 15°

DEFORMATIONS OF 9MM WELDS						
Test	Deformation At Ultimate Load (mm)	Normalized By Method (A) (mm)	Normalized By Method (B) (mm)	Deformation At Fracture (mm)	Normalized By Method (A) (mm)	Normalized By Method (B) (mm)
30.11	0.516	0.494	0.247	0.669	0.640	0.320
	0.670	0.641	0.320	0.894	0.855	0.428
	0.562	0.538	0.269	0.707	0.676	0.338
	0.661	0.632	0.316	0.860	0.823	0.411
30.12	0.334	0.328	0.164	0.483	0.475	0.237
	0.435	0.427	0.214	0.794	0.780	0.390
	0.474	0.465	0.233	0.686	0.674	0.337
	0.562	0.552	0.276	1.037	1.019	0.509
30.13	0.629	0.581	0.291	0.994	0.919	0.459
	0.707	0.653	0.327	1.155	1.067	0.534
	0.600	0.554	0.277	0.964	0.891	0.445
	0.719	0.664	0.332	1.125	1.040	0.520

Table 4.21 Deformations Of 9 mm Welds Loaded At 30°

DEFORMATIONS OF 9MM WELDS						
Test	Deformation At Ultimate Load (mm)	Normalized By Method (A) (mm)	Normalized By Method (B) (mm)	Deformation At Fracture (mm)	Normalized By Method (A) (mm)	Normalized By Method (B) (mm)
45.11	0.538	0.514	0.363	0.920	0.878	0.621
	0.759	0.724	0.512	1.385	1.322	0.935
	0.491	0.469	0.331	0.880	0.840	0.594
	0.665	0.635	0.449	1.292	1.233	0.872
45.12	0.444	0.422	0.299	1.124	1.069	0.756
	0.585	0.557	0.394	1.052	1.001	0.708
	0.439	0.418	0.295	1.111	1.057	0.747
	0.556	0.529	0.374	1.083	1.030	0.729
45.13	0.681	0.668	0.472	1.028	1.008	0.713
	0.850	0.833	0.589	1.424	1.396	0.987
	0.676	0.663	0.469	1.038	1.018	0.720
	0.747	0.732	0.518	1.227	1.203	0.851

Table 4.22 Deformations Of 9 mm Welds Loaded At 45°

DEFORMATIONS OF 9MM WELDS						
Test	Deformation At Ultimate Load (mm)	Normalized By Method (A) (mm)	Normalized By Method (B) (mm)	Deformation At Fracture (mm)	Normalized By Method (A) (mm)	Normalized By Method (B) (mm)
60.11	0.401	0.383	0.332	0.465	0.444	0.385
	0.556	0.531	0.460	0.729	0.696	0.603
	0.468	0.447	0.387	0.550	0.525	0.455
	0.626	0.598	0.518	0.800	0.764	0.662
60.12	0.362	0.338	0.292	0.509	0.475	0.411
	0.426	0.397	0.344	0.777	0.725	0.628
	0.356	0.332	0.288	0.491	0.458	0.397
	0.415	0.387	0.335	0.700	0.653	0.565
60.13	0.486	0.443	0.383	0.592	0.539	0.467
	0.575	0.524	0.454	0.832	0.758	0.656
	0.382	0.348	0.301	0.469	0.427	0.370
	0.481	0.438	0.379	0.694	0.632	0.547

Table 4.23 Deformations Of 9 mm Welds Loaded At 60°

DEFORMATIONS OF 9MM WELDS						
Test	Deformation At Ultimate Load (mm)	Normalized By Method (A) (mm)	Normalized By Method (B) (mm)	Deformation At Fracture (mm)	Normalized By Method (A) (mm)	Normalized By Method (B) (mm)
75.11	0.432	0.424	0.409	0.522	0.512	0.494
	0.410	0.402	0.388	0.508	0.498	0.481
	0.404	0.396	0.383	0.484	0.475	0.458
	0.471	0.462	0.446	0.564	0.553	0.534
75.12	0.398	0.394	0.381	0.458	0.454	0.438
	0.446	0.442	0.427	0.557	0.552	0.533
	0.464	0.460	0.444	0.525	0.520	0.503
	0.452	0.448	0.433	0.545	0.540	0.522
75.13	0.486	0.473	0.457	0.586	0.571	0.551
	0.294	0.286	0.277	0.330	0.321	0.310
	0.310	0.302	0.292	0.375	0.365	0.353
	0.214	0.208	0.201	0.230	0.224	0.216

Table 4.24 Deformations Of 9 mm Welds Loaded At 75°

DEFORMATIONS OF 9MM WELDS						
Test	Deformation At Ultimate Load (mm)	Normalized By Method (A) (mm)	Normalized By Method (B) (mm)	Deformation At Fracture (mm)	Normalized By Method (A) (mm)	Normalized By Method (B) (mm)
90.11	0.337	0.333	0.333	0.394	0.390	0.390
	0.500	0.495	0.495	0.598	0.591	0.591
	0.430	0.425	0.425	0.495	0.490	0.490
	0.523	0.517	0.517	0.622	0.615	0.615
90.12	0.416	0.404	0.404	0.455	0.442	0.442
	0.508	0.494	0.494	0.558	0.542	0.542
	0.379	0.368	0.368	0.410	0.398	0.398
	0.441	0.429	0.429	0.485	0.471	0.471
90.13	0.331	0.325	0.325	0.427	0.420	0.420
	0.424	0.417	0.417	0.575	0.565	0.565
	0.345	0.339	0.339	0.448	0.440	0.440
	0.421	0.414	0.414	0.583	0.573	0.573

Table 4.25 Deformations Of 9 mm Welds Loaded At 90°

another. Therefore, deformations of longitudinal welds were not normalized by method (B), and weld strains of longitudinal fillets are not shown in Fig 4.7 to 4.10.

4.2.6 Weld Stress-Strain Curves

Normalized ultimate loads were converted to stresses by dividing by the specified leg size. Typical stress-strain curves are shown in Fig 4.11 to 4.12.

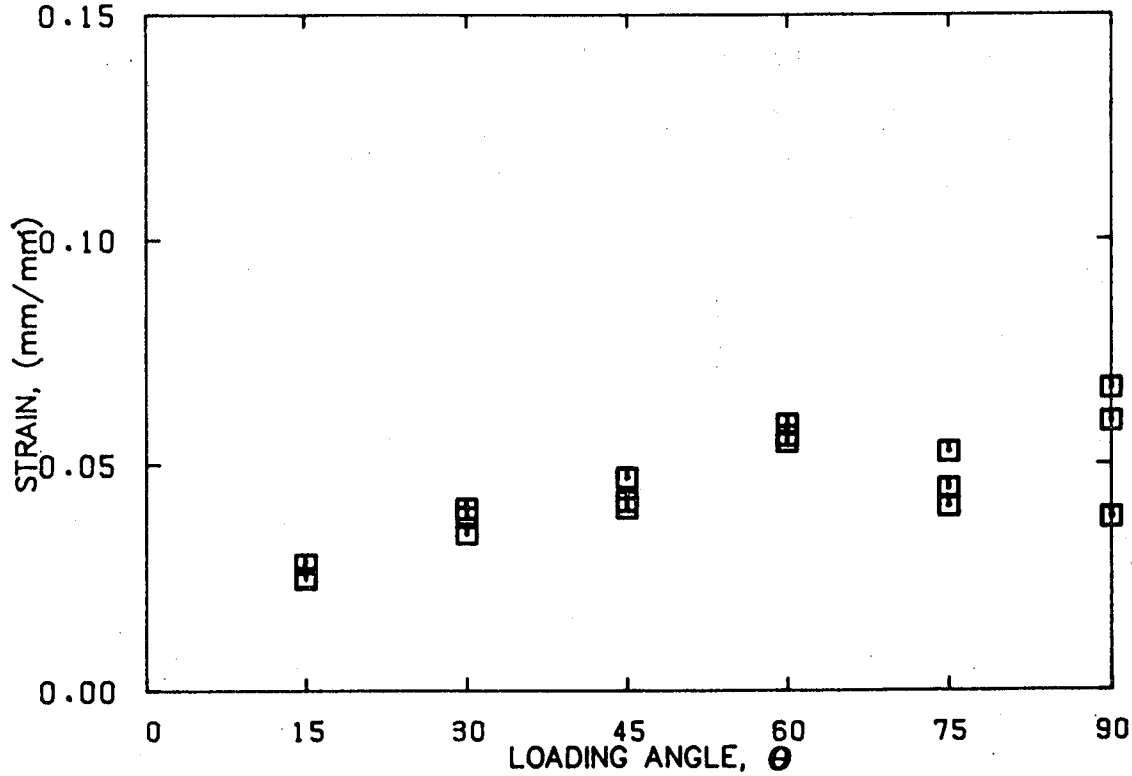

Figure 4.7 5 mm Weld Strains At Ultimate Load

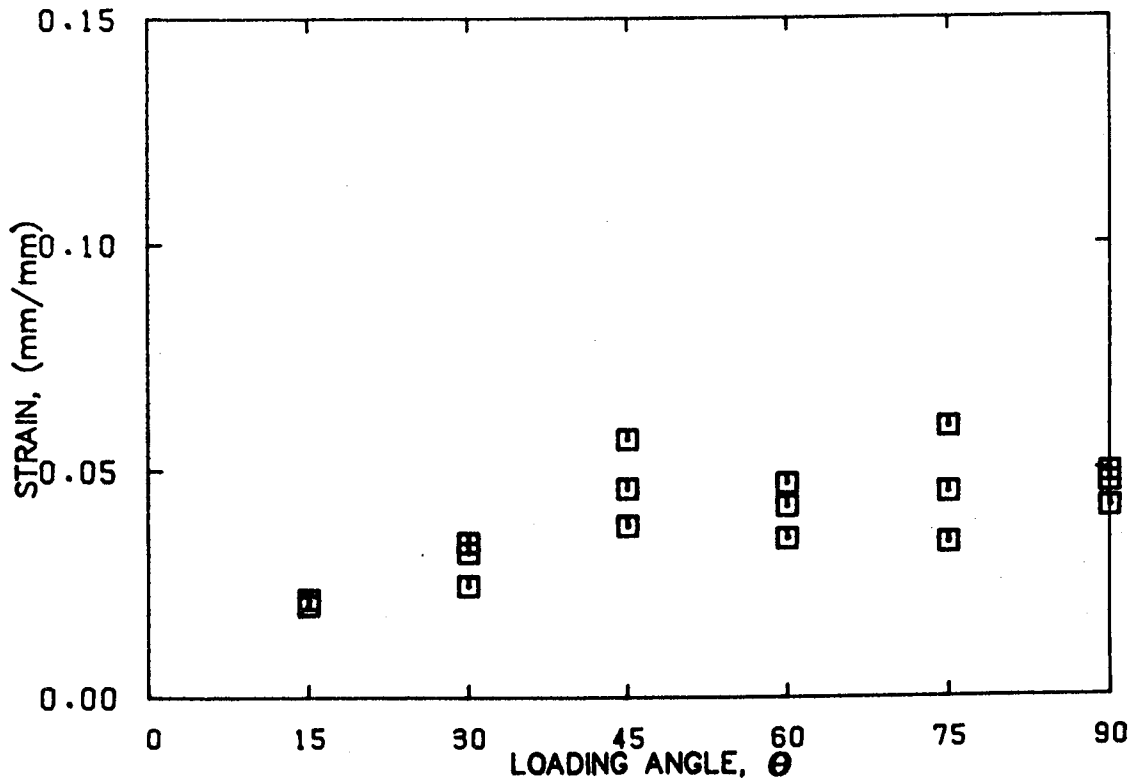

Figure 4.8 9 mm Weld Strains At Ultimate Load

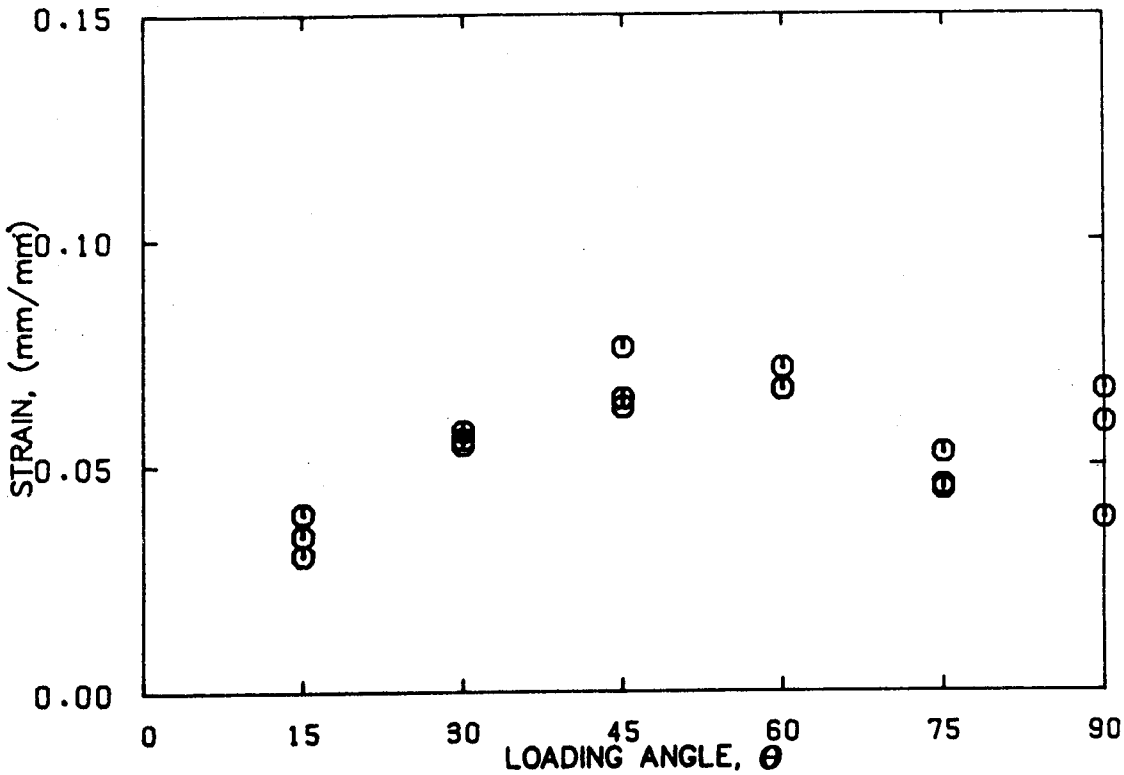

Figure 4.9 5 mm Weld Strains At Fracture

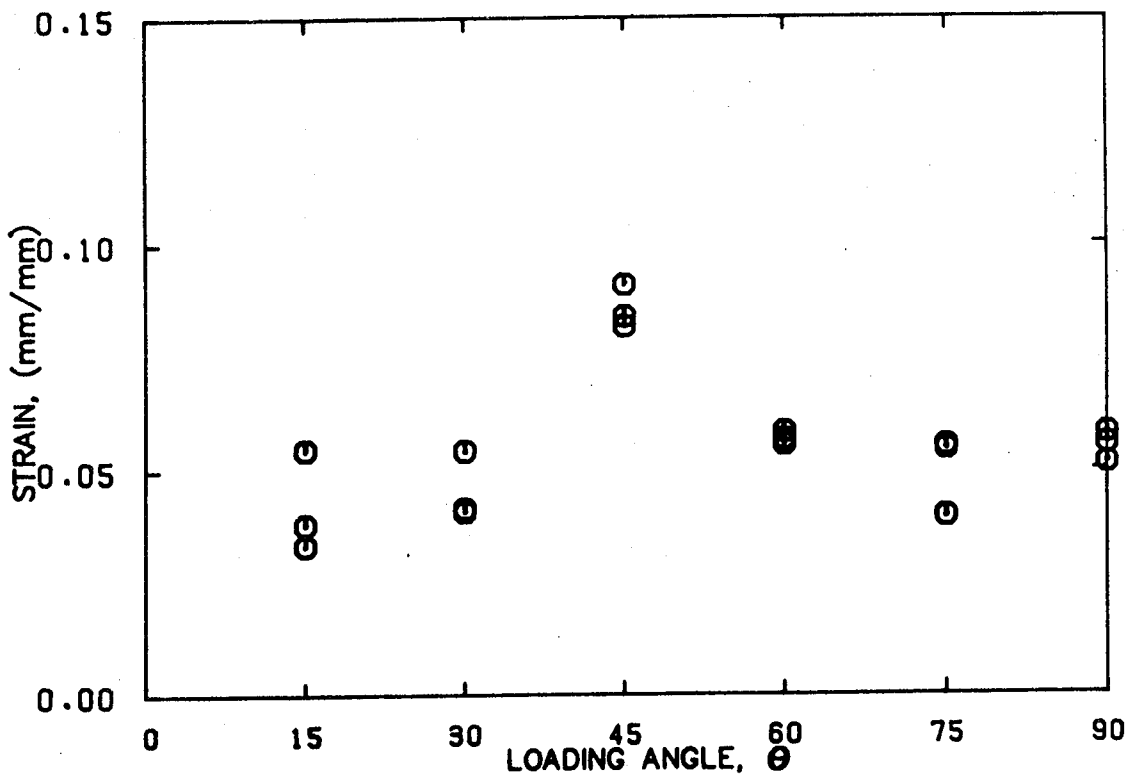

Figure 4.10 9 mm Weld Strains At Fracture

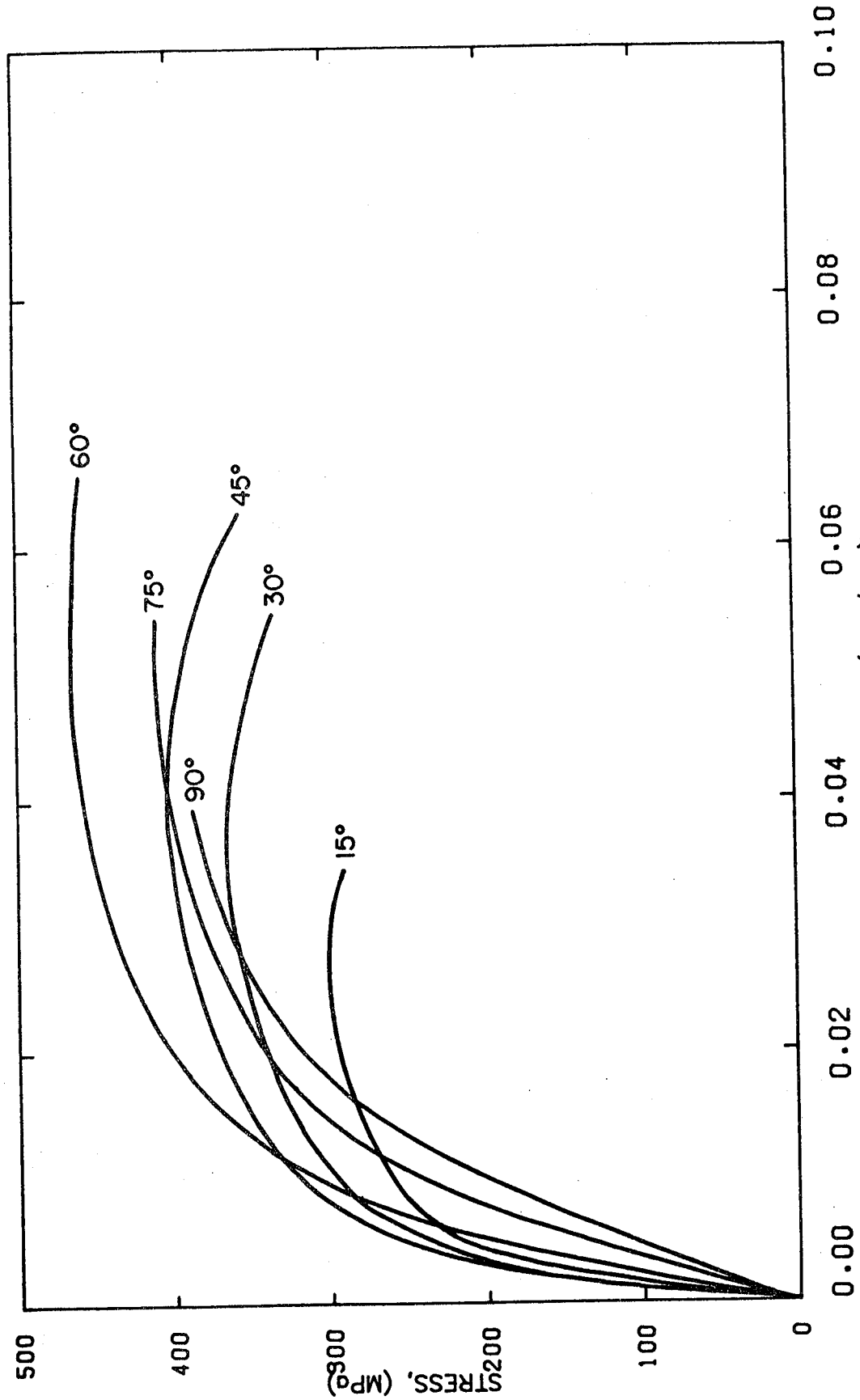

Figure 4.11 Stress-Strain Curves For 5 mm Welds

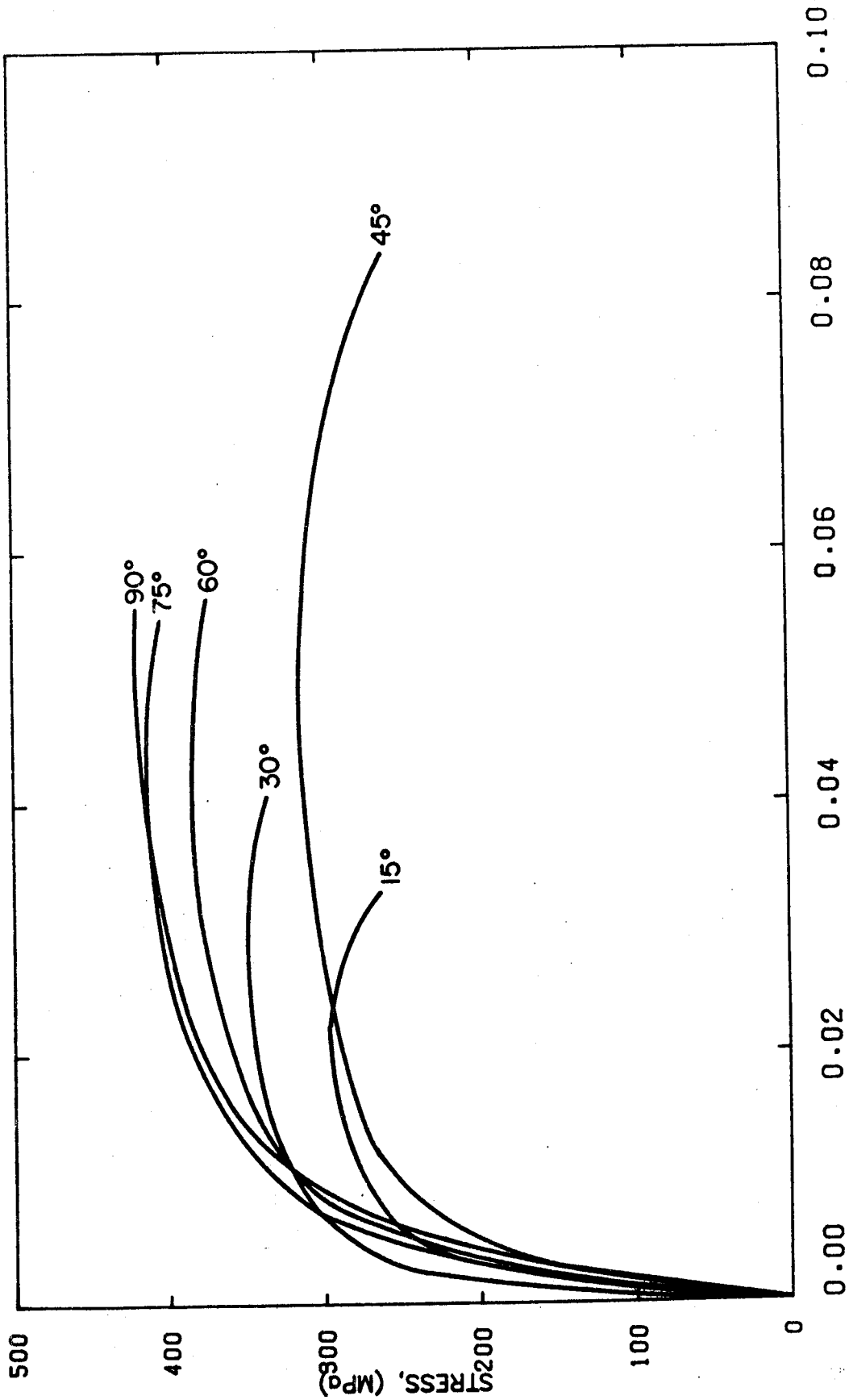

Figure 4.12 Stress-Strain Curves For 9 mm Welds

5. Analysis and Discussion of Test Results

5.1 Weld Equilibrium

The objective of the weld equilibrium analysis is to derive general expressions for the mean shear and normal stresses on an assumed fracture surface within the fillet weld. Forces acting on the fracture surface are assumed to act at the middle of the fracture surface. The fillet weld is assumed to be equal legged and the fracture surface planar, as shown in Fig 5.1.

The force P, acting on a fillet weld at a general loading angle, θ, has components $P\cos\theta$ and $P\sin\theta$ as shown in Fig 5.2. Consider the equilibrium of the weld segment shown in Fig 5.3 where the portion of the weld from the fracture surface to the vertical fusion face is considered as a free body. The fracture surface area is

$$[5.1] \quad A_\theta = \frac{wl(\sin(\pi/4))}{(\sin(\pi/4 + \alpha))}$$

The force components $P\sin\theta$ and $P\cos\theta$ on the fracture surface are opposed by equal and opposite forces on the vertical face. As shown in Section A-A of Fig 5.3(c), the equal and opposite forces $P\cos\theta$ are not colinear and the equal and opposite forces $P\sin\theta$ need not be colinear. To balance the couple generated by the forces $P\sin\theta$ about the z axis,

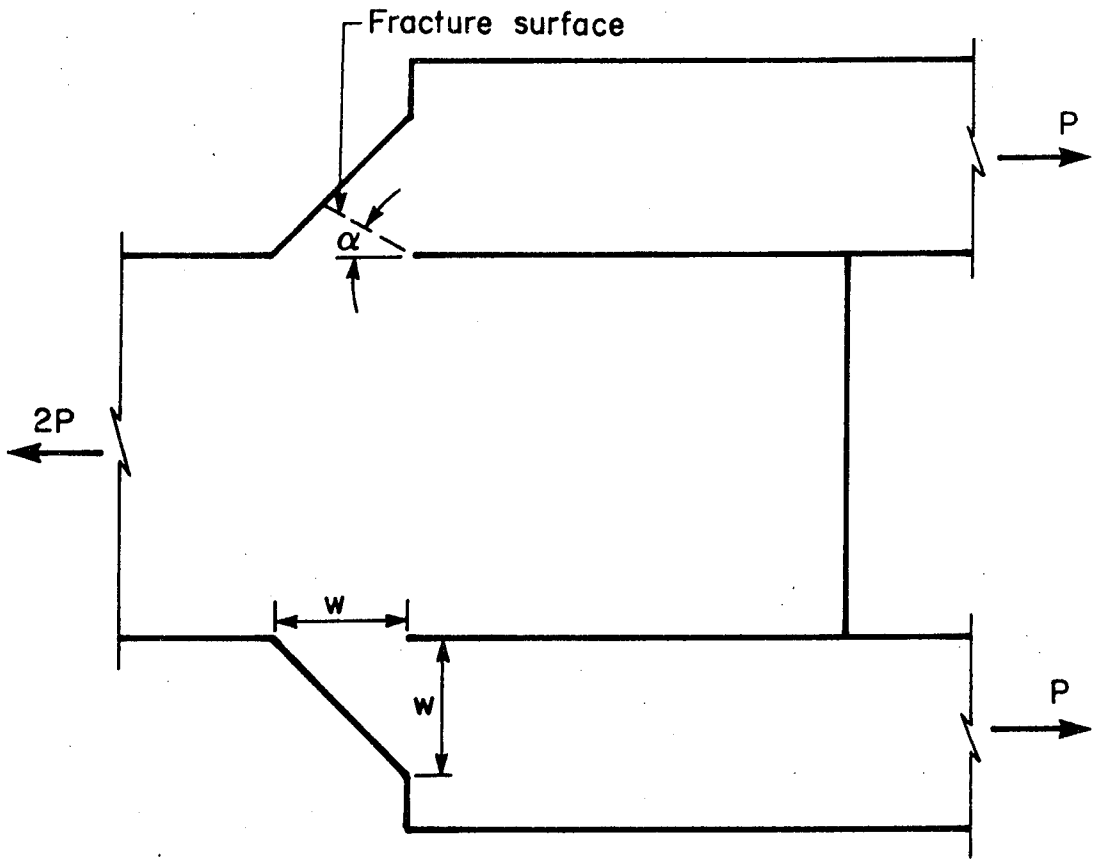

Figure 5.1 Elevation Of Fillet Weld Specimen

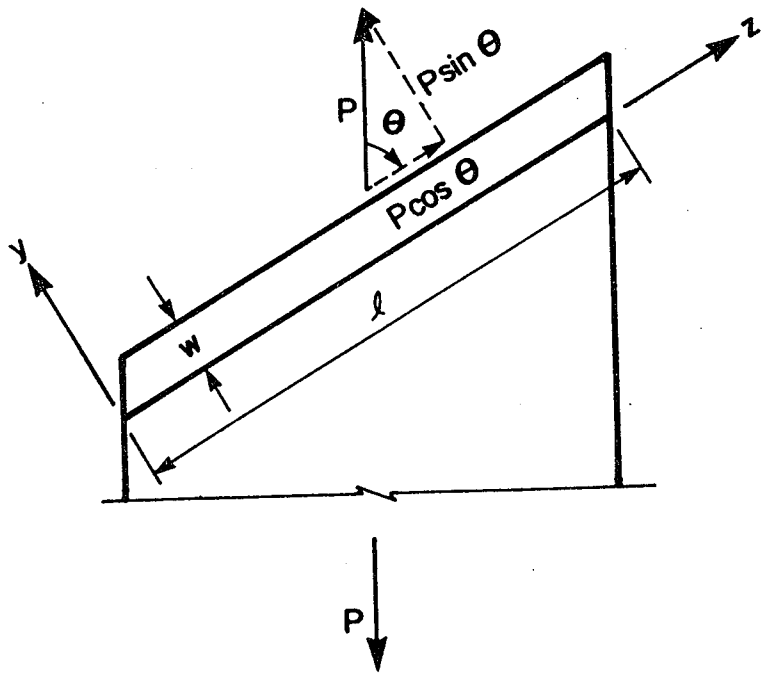

Figure 5.2 Plan Of Fillet Weld Loaded At A General Angle

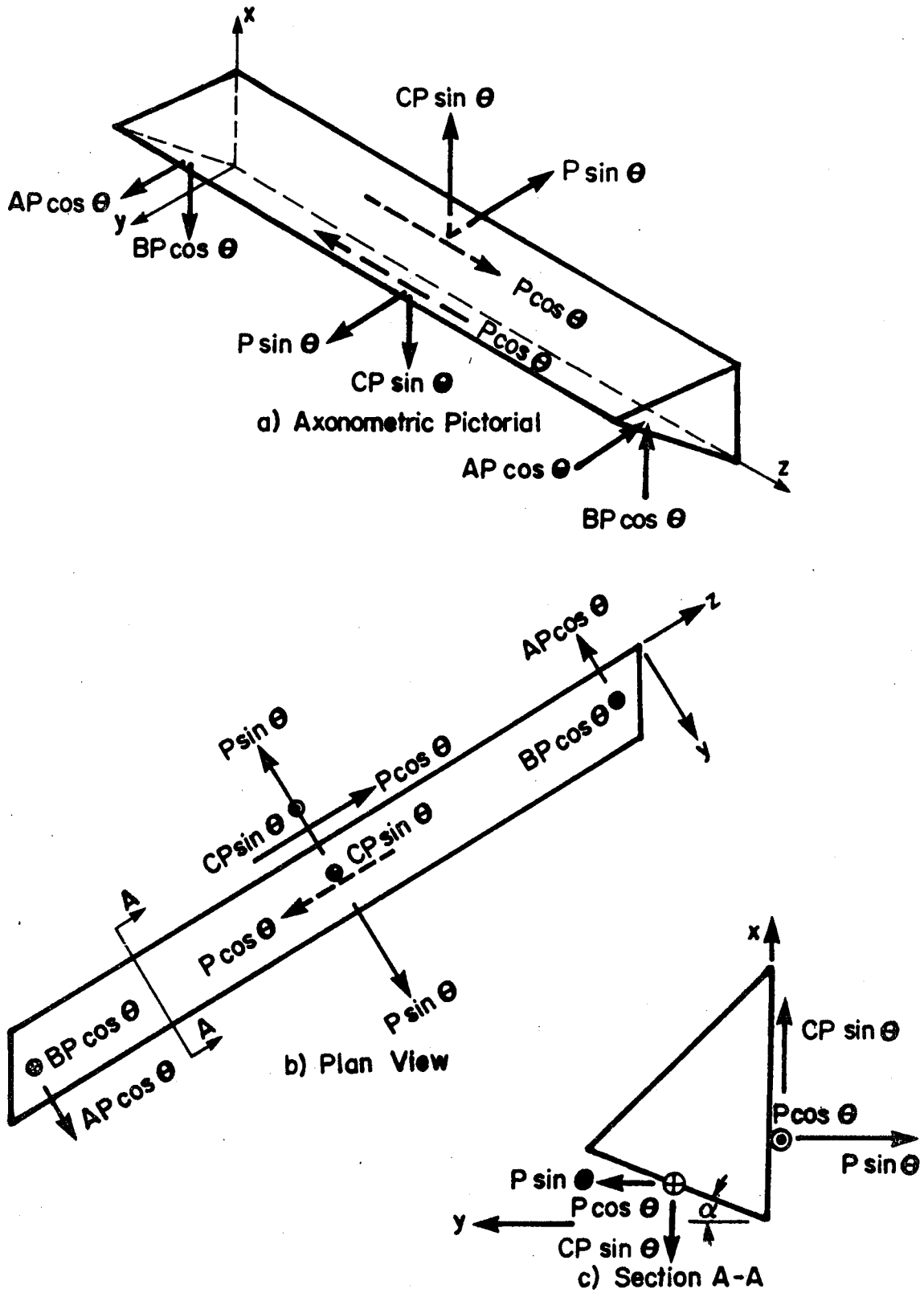

Figure 5.3 Equilibrium Of A Fillet Weld

stress resultants (forces) $CP\sin\theta$, where C is a numerical coefficient, are postulated to exist. To balance the couple generated by the forces $P\cos\theta$ about the x and y axes respectively, the couples of the stress resultants $AP\cos\theta$ and $BP\cos\theta$ are postulated to exist.

If the stress resultants $AP\cos\theta$ and $BP\cos\theta$ are neglected, the average shear stress acting on the fracture surface is

$$[5.2] \quad \tau = \frac{P}{A_\theta}[((\sin\theta)(\cos\alpha) - C(\sin\theta)(\sin\alpha))^2 + (\cos\theta)^2]^{1/2}$$

and the average normal stress is

$$[5.3] \quad \sigma = \frac{P}{A_\theta}[((\sin\theta)(\sin\alpha) + C(\sin\theta)(\cos\alpha)]$$

It is assumed that $AP\cos\theta$ and $BP\cos\theta$ can be neglected because:

i) with lever arms approaching the length of the weld, which is large (even for minimum weld lengths as specified in CSA Standard W59-82) compared to the weld leg size, their magnitude relative to the other

forces is small.

ii) fracture observations showed that for small values of θ, for which these forces would have the greatest effect, fracture angles at opposite ends were not significantly different, which would be the case if they were significant.

5.2 Failure Theories

Three different failure theories are used to predict the ultimate behaviour of fillet welds, based on using [5.2] and [5.3], with the value of the coefficient C initially set equal to zero. The effect of the variation of C is discussed subsequently.

5.2.1 Maximum Shear Stress Theory

Differentiating [5.2], which gives the average shear stress on the fracture surface, with respect to the fracture angle, α, yields

$$[5.4] \quad \frac{\partial \tau}{\partial \alpha} = \frac{P}{wl(\sin(\pi/4))} [((\sin\theta)(\cos\alpha) - C(\sin\theta)(\sin\alpha))^2 + (\cos\theta)^2]^{-1/2}$$

$$* [\cos(\pi/4 + \alpha)[((\sin\theta)(\cos\alpha) - C(\sin\theta)(\sin\alpha))^2 + (\cos\theta)^2] + \frac{\sin(\pi/4 + \alpha)}{2} [2C(\sin\theta)^2$$

$$*(2(\sin\alpha)^2 - 1) + (2(\sin\theta)^2(\cos\alpha)(\sin\alpha))(C^2 - 1)]]$$

from which the maximum shear stress and corresponding value of α for any value of θ can be determined by setting the derivative equal to zero. Values of α with C=0 are shown in Fig 5.4, where average fracture angles for each loading angle also are plotted. Ultimate loads, as a function of θ, can also be derived by substituting values of α from Fig 5.4 into [5.2] and assuming a maximum value for the shear stress, τ_u. These ultimate loads, P_θ, can be normalized by dividing by the ultimate load for θ=0°, P_1, yielding

$$[5.5] \quad P_\theta / P_1 = \tau_u A_\theta / [\tau_u A_1[((\sin\theta)(\cos\alpha) - C(\sin\theta)(\sin\alpha))^2 + (\cos\theta)^2]^{1/2}]$$

which reduces to

$$[5.6] \quad P_\theta / P_1 = A_\theta / A_1[[((\sin\theta)(\cos\alpha) - C(\sin\theta)(\sin\alpha))^2 + (\cos\theta)^2]^{1/2}]$$

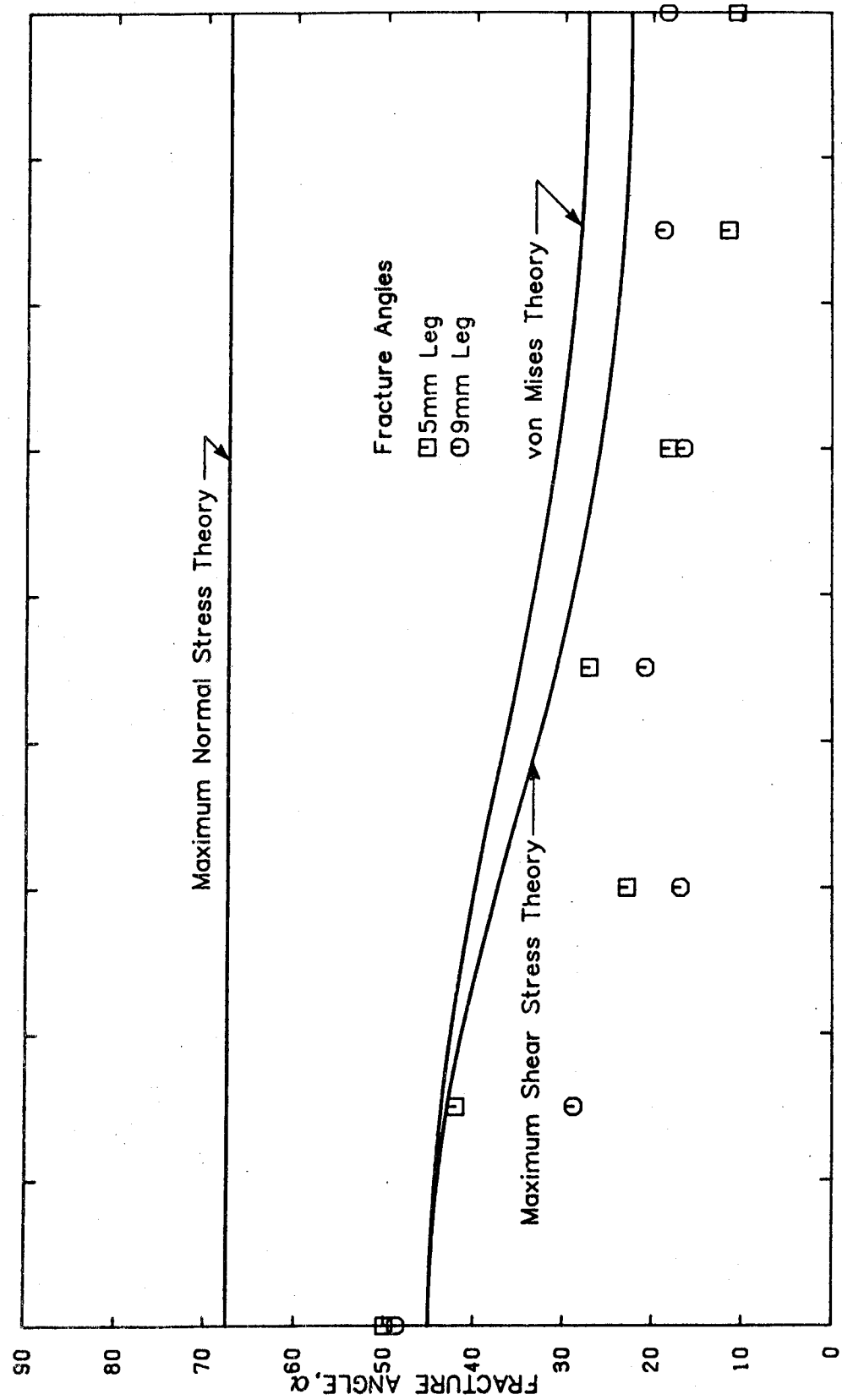

Figure 5.4 Predicted Fracture Angles And Test Results For C=0

where A_l is the area of the fracture surface of a longitudinal fillet. The variation of ultimate loads with loading angle, θ, normalized thus with C=0 are shown in Fig 5.5, where P_t represents the ultimate transverse load. The ultimate loads for the 5 mm and 9 mm weld specimens are also shown in Fig 5.5, normalized by dividing by their respective average longitudinal ultimate loads.

5.2.2 Maximum Normal Stress Theory

Differentiating [5.3], which gives the average normal stress on the fracture surface, with respect to the fracture angle, α, yields

$$[5.7] \quad \frac{\partial \sigma}{\partial \alpha} = \frac{P}{wl(\sin(\pi/4))} [(\cos(\pi/4 + \alpha))[(\sin\theta)(\sin\alpha) + C(\sin\theta)(\cos\alpha)] + (\sin(\pi/4 + \alpha))[(\sin\theta)(\cos\alpha) - C(\sin\theta)(\sin\alpha)]]$$

from which the maximum normal stress and corresponding value of α for any value of θ can be determined by setting the derivative equal to zero. For this failure theory, the value of α is independent of the value of θ, as shown in Fig 5.4. Because the normal stress is zero for the case where θ=0°, it is not possible to show ultimate loads for the maximum

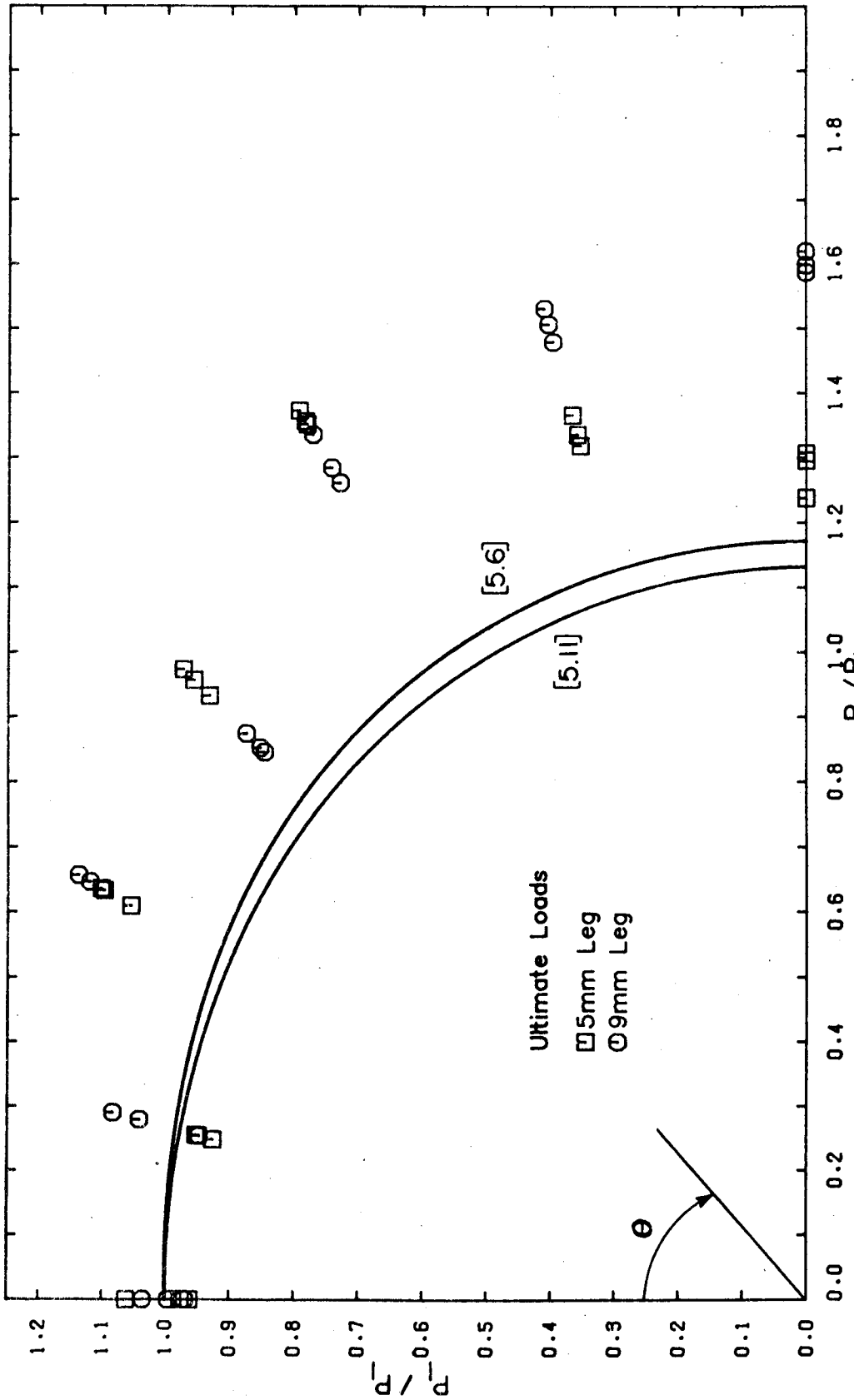

Figure 5.5 Ultimate Load Interaction Diagram For C=0

normal stress theory in Fig 5.5.

5.2.3 Elastic Strain Energy of Distortion Theory

A failure theory based on the von Mises theory of elastic strain energy of distortion can be examined at ultimate conditions. The failure theory is given by

$$[5.8] \quad \sigma_g = [\sigma^2 + 3\tau^2]^{1/2}$$

where σ and τ are obtained from [5.3] and [5.2], respectively. Differentiating the resulting expression [5.8] with respect to the fracture angle, α, yields,

$$\begin{aligned}[5.9] \quad \frac{\partial \sigma g}{\partial \alpha} = \frac{P}{2wl(\sin(\pi/4))}&[((\sin(\pi/4 + \alpha))[(\sin\theta)(\sin\alpha) \\ &+ C(\sin\theta)(\cos\alpha)])^2 + 3(\sin(\pi/4 + \alpha))[((\sin\theta)(\cos\alpha) \\ &- C(\sin\theta)(\sin\alpha))^2 + (\cos\theta)^2]^{1/2})^2]^{-1/2} \\ &* [2(\sin(\pi/4 + \alpha))(\cos(\pi/4 + \alpha))[(\sin\theta)^2(1 + C^2 \\ &+ 2C^2(\sin\alpha)^2 - 4C(\sin\alpha)(\cos\alpha) + 2(\cos\alpha)^2 + 3(\cos\theta)^2] \\ &+ 4(\sin\theta)^2(\sin(\pi/4 + \alpha))^2[(\sin\alpha)(\cos\alpha)(C^2 - 1)\end{aligned}$$

$$+ C(1 - 2(\cos\alpha)^2)]]$$

from which the maximum comparative stress, σ_g, and corresponding value of α for any value of θ can be determined by setting the derivative equal to zero. Values of α, determined thus with C=0 are shown in Fig 5.4. Ultimate loads, as a function of θ, can also be derived by substituting values of α from Fig 5.4 into [5.7] and assuming a maximum value for the comparative stress, σ_{gu}. These ultimate loads can be normalized by dividing by the ultimate load for θ=0° yielding

$$[5.10] \quad P_\theta / P_1 = \sigma_{gu}A_\theta(3)^{1/2} / [\sigma_{gu}A_1[[(\sin\theta)(\sin\alpha) + C(\sin\theta)(\cos\alpha)]^2 + 3[((\sin\theta)(\cos\alpha) - C(\sin\theta)(\sin\alpha))^2 + (\cos\theta)^2]]^{1/2}]$$

which reduces to

$$[5.11] \quad P_\theta / P_1 = A_\theta(3)^{1/2} / A_1[[[(\sin\theta)(\sin\alpha) + C(\sin\theta)(\cos\alpha)]^2 + 3[((\sin\theta)(\cos\alpha)$$

$$- C(\sin\theta)(\sin\alpha))^2 + (\cos\theta)^2]]^{1/2}]$$

The variation of ultimate loads with loading angle, θ, determined thus with C=0 are shown in Fig 5.5.

5.2.4 Summary

The failure theory based on a maximum normal stress on the fracture surface does not correlate well with test results and is therefore rejected. The von Mises shear energy of distortion theory and the maximum shear stress theory are in reasonable agreement with the test results as seen in Figs 5.4 and 5.5, with the maximum shear stress theory in somewhat better correspondence in both cases.

5.2.5 Value of the Coefficient C

Figure 5.6 shows the equilibrium of a transverse fillet weld cross section with the coefficient C equal to zero. The two tensile forces, P, are colinear. Figure 5.7 shows the equilibrium of a transverse weld cross-section with the coefficient C set equal to 1.0. For equilibrium, the force P on the vertical leg must act at w/2 (mid-height) from the weld root, irrespective of the fracture angle, α. This further implies that the normal stresses on the vertical face are uniformly distributed, as discussed subsequently. A value of 1.0 for C is considered to be an upper bound.

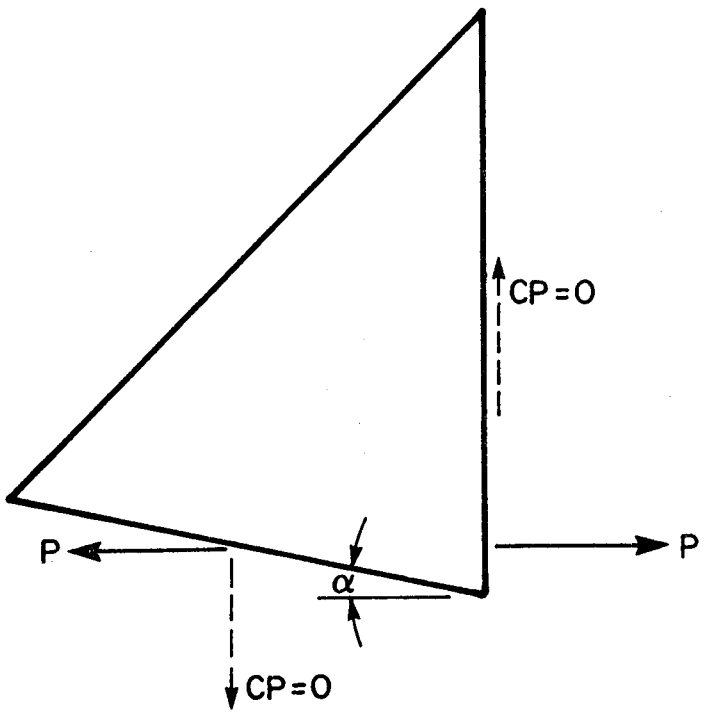

Figure 5.6 Equilibrium Of Fillet Weld With C=0

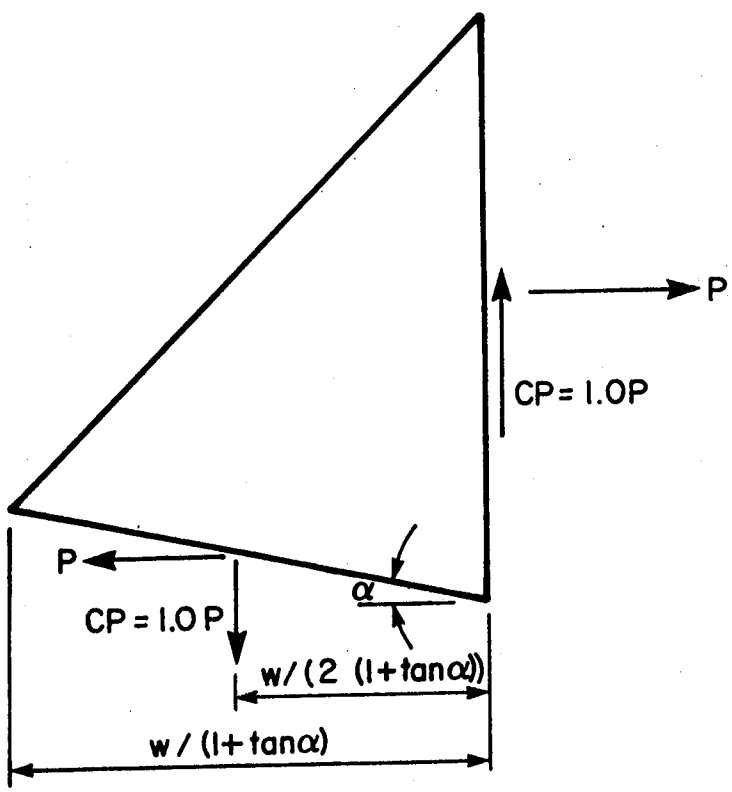

Figure 5.7 Equilibrium Of Fillet Weld With C=1.0

The effect of introducing different values of C into [5.2] and [5.8] on the fracture angle, α, is seen in Figs 5.8 and 5.9 for the maximum shear stress theory and for the von Mises theory, respectively.

The stress resultant $CP\sin\theta$ must exist for equilibrium, that is, $0 < C \leq 1.0$. Except for longitudinal welds ($\theta=0°$), or for low values of θ combined with large values of C, (ie. approaching 1.0), the presence of the stress resultant $CP\sin\theta$ tends to reduce the fracture angle considerably, and to have a greater reduction in general for the maximum shear stress theory than for the von Mises theory. Kamtekar's (1982) solution, in which a value of C of 1.0 was assumed, gives a fracture angle of 0° for the transverse weld. This fracture angle is not corroborated by tests.

5.3 Material Capacity and Restraint

A value of C=1.0 implies, as shown in Fig 5.7, that the normal force on the vertical leg acts at mid-height, that is, the normal stresses are uniformly distributed. Conversely, a small value of C implies that the resultant stress on the vertical leg acts near the weld root and that the normal stresses are not uniformly distributed. In Fig 5.10, the tensile stresses at fracture are assumed to act uniformly over a height of 2e. Such a uniform stress block is often taken as the idealized case in plastic analysis of structural elements.

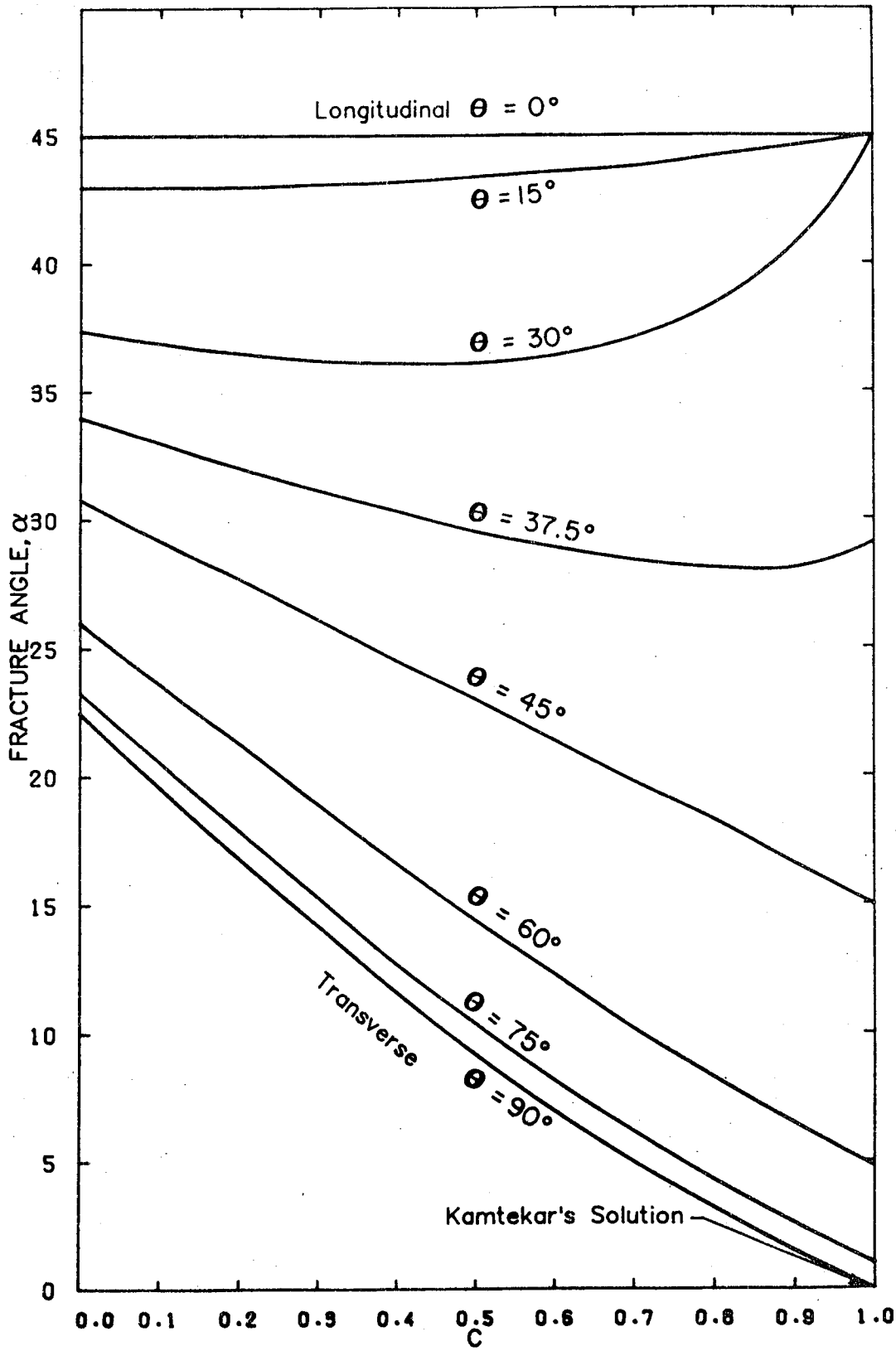

Figure 5.8 Influence Of The Value Of C On Fracture Angles Predicted By The Maximum Shear Stress Theory

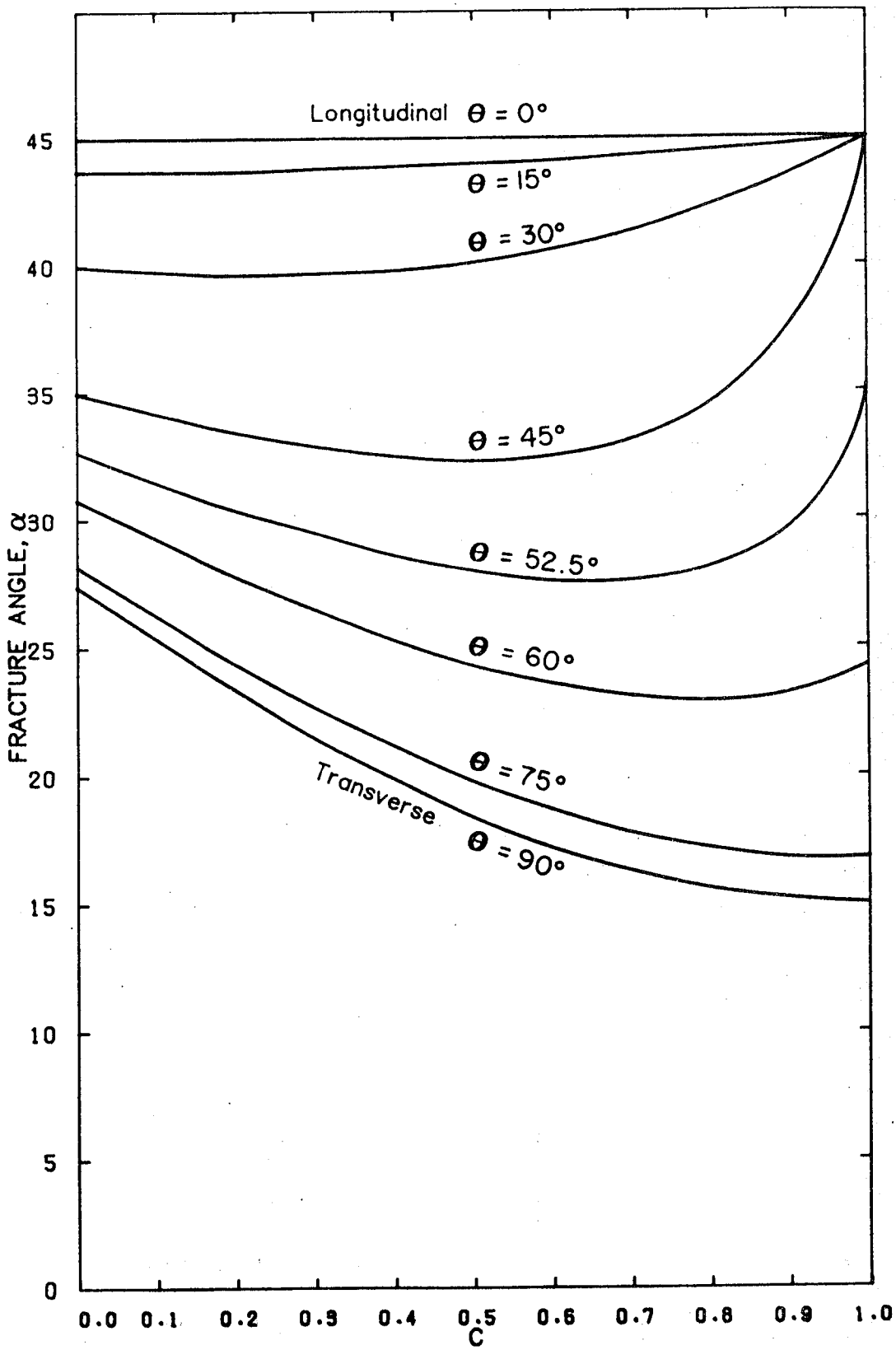

Figure 5.9 Influence Of The Value Of C On Fracture Angles Predicted By The von Mises Theory

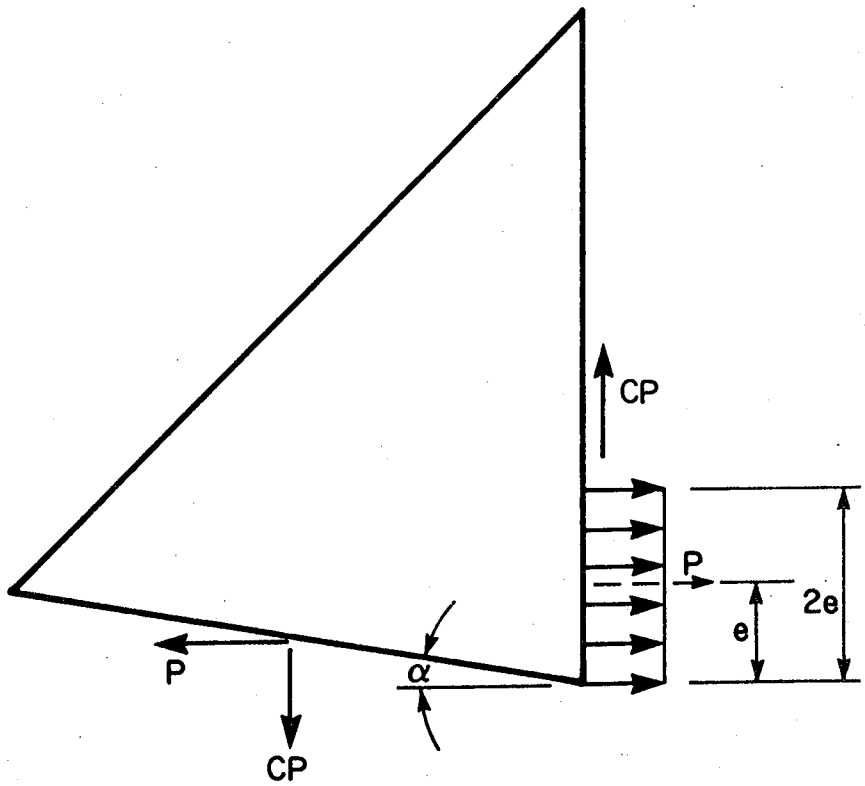

Figure 5.10 Tensile Stress Distribution On Vertical Weld Leg

The average ultimate tensile strength for the weld metal, that is, the maximum load divided by the initial area for the all-weld metal tensile tests, was found to be 538 MPa, as given in Table 4.4. Timoshenko (1955) and Davis et al (1982), among others, have shown that the ultimate tensile strength can be significantly increased by restraining deformations transverse to the direction of applied load.

Timoshenko (1955) reported on a series of tests on plain and notched tensile specimens made from carbon and nickel-chrome steels. Standard tension tests on normal cylindrical specimens with a 0.5 in. (12 mm) diameter showed a proportional limit of 56.0 ksi (385 MPa), a yield point of 64.5 ksi (445 MPa), and an ultimate strength of 102.0 ksi (700 MPa) for the carbon steel and corresponding values of 80.0 ksi (550 MPa), 85.0 ksi (585 MPa), and 108.0 ksi (745 MPa) for the nickel-chrome steel. The dimensions of the notched specimens are shown in Fig 5.11. As shown in Table 5.1, the ultimate loads of the notched specimens were up to 1.6 and 1.8 times the ultimate loads for plain carbon and nickel-chrome steel specimens, respectively.

A series of tests done on tension coupons in the early 1900's was reported by Davis et al (1982). These were tension tests on carbon steel with various gauge lengths, as shown in Fig 5.12. The ultimate loads of specimens with a gauge length approaching zero were found to be about 1.75 times the ultimate loads of standard tensile specimens. It

a (in.)	Carbon Steel		
	Ult Load (kips)	Ult Strength (ksi)	Normalized Ultimate Strength
1/32	32.0	163	1.60
1/16	32.2	164	1.61
1/8	28.1	143	1.40
Normal Specimen	20.0	102	1.00
a	Nickel-Chrome Steel		
1/32	37.9	193	1.79
1/16	36.1	184	1.70
1/8	30.2	154	1.43
Normal Specimen	21.2	108	1.00

Table 5.1 Test Data For Notched Specimens

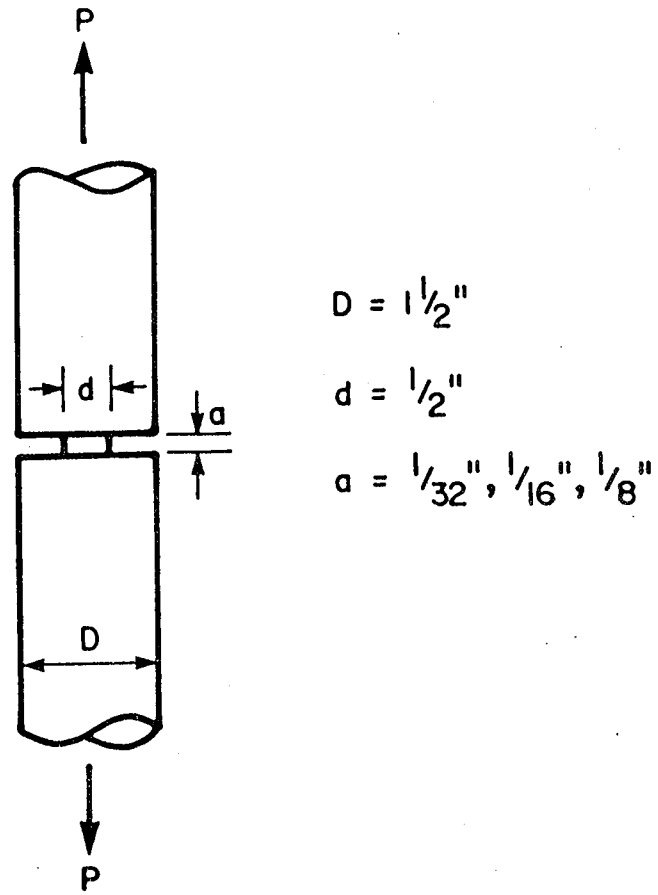

Figure 5.11 Cylindrical Notched Test Specimens,

Timoshenko (1955)

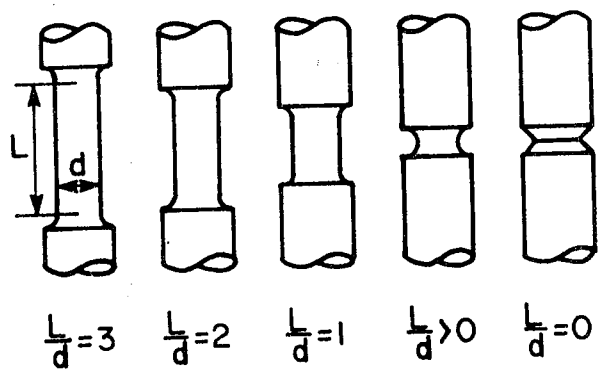

Figure 5.12 Test Specimens With Various Gauge Lengths,

Davis et al (1982)

was concluded that the effect of notching was to suppress necking at the reduced section, thus increasing the ultimate tensile strength.

Figure 5.13(a) shows a transversely loaded fillet weld with coordinate axes x,y and z. A possible tensile stress flow pattern is sketched in Fig 5.13(b). The tensile stresses on the plane a-a will not be uniformly distributed and will be highest at the weld root, (location A), where the tensile stress is concentrated. The weld will attempt to contract laterally here, ie. in the z direction, but will be restrained by the unstressed adjoining plate below A. Moreover, as the weld cross-sectional area is less than that of the plates, particularly if the plate thickness exceeds the weld size as shown in Fig 5.13, the plates will be less heavily stressed than the weld and will tend to prevent contraction of the weld in the x direction.

The plates were observed to remain elastic in the tests, and thus, a condition approaching full restraint in both the x and z directions exists at the weld root. The brittle nature of the fracture surface at the weld root of transverse fillets as shown in Fig 4.5(a) confirms that yielding did not occur here and that significant triaxial tensions, consistent with heavily restrained conditions, existed at the weld root. Therefore, it is postulated that the tensile strength of the weld metal at the root could be substantially higher than that obtained using the unrestrained all-weld metal tensile coupon.

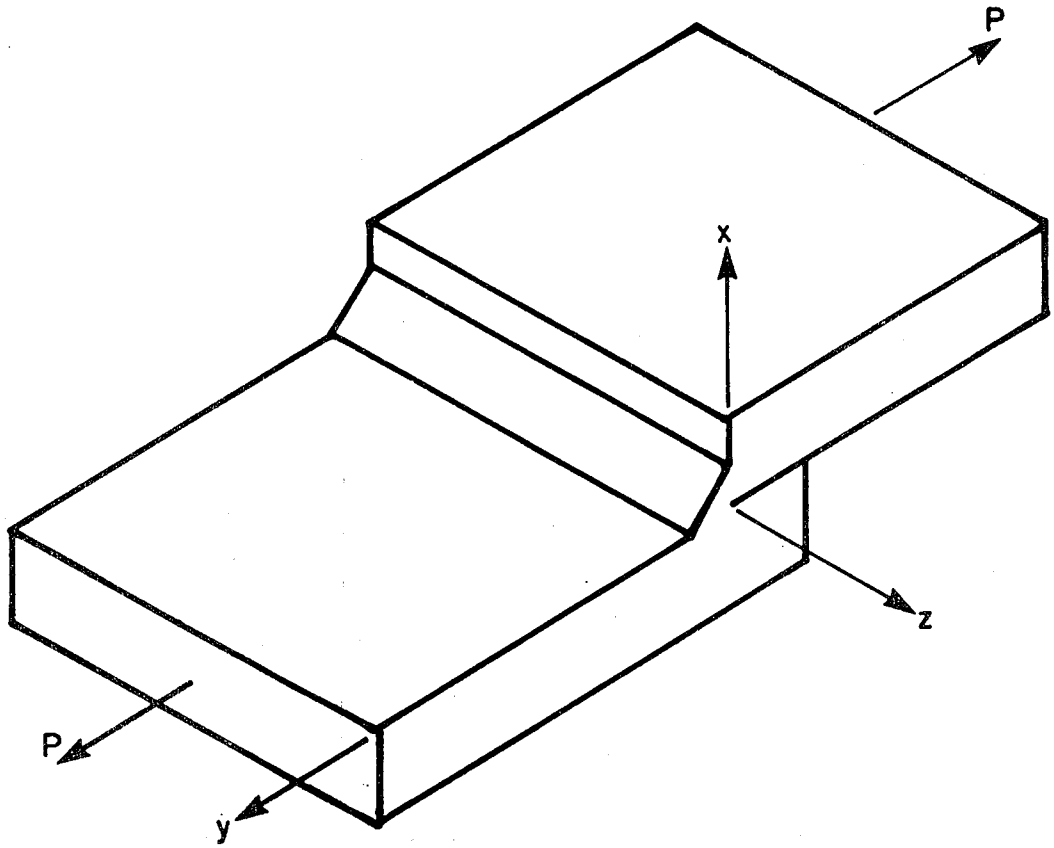

a) Coordinate Axes

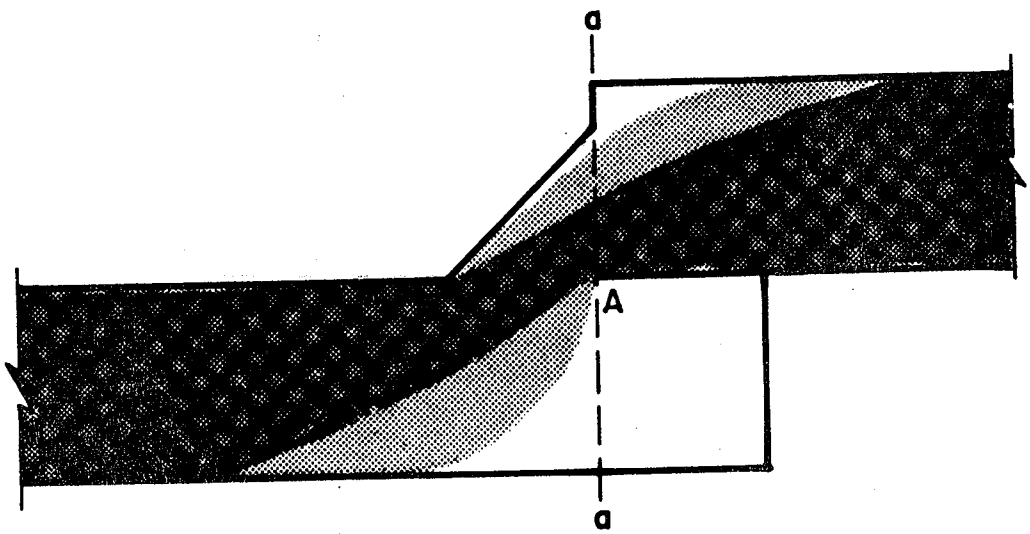

b) Tensile Stress Flow Pattern

Figure 5.13 Transverse Fillet Weld

If the Davis et al strength increase value (restained to unrestrained) of 1.75 is assumed to exist in the weld root region, the distance 2e over which the stress is assumed to be uniform, as shown in Fig 5.10, can be calculated from measured loads, $P\sin\theta$. From the equilibrium of Fig 5.10, the coefficient C can be determined as

$$[5.12] \quad C = \frac{e - [w(\tan\alpha) \,/\, 2(| + (\tan\alpha))]}{[w \,/\, 2(1 + (\tan\alpha))]}$$

where α is given by the relationships shown in Fig 5.8 and 5.9 for the maximum shear stress and von Mises theories, respectively. Average minimum values of C for each loading angle, using the maximum shear stress and von Mises theories, are given in Tables 5.2 and 5.3, respectively. The minimum values of C are about 0.3 and 0.2 for the transverse loading case (θ=90°) for the maximum shear stress and von Mises theories, respectively, and decrease with decreasing loading angles.

5.4 Fracture Angles

Because the restrained weld metal will develop a tensile strength on the vertical weld leg that is consistent with the restraint provided, the resultant tensile force on the vertical weld leg will act at a distance from the weld root consistent with this restrained tensile strength. This

Loading Angle	Minimum C	
	5 mm	9 mm
90	0.27	0.33
75	0.26	0.27
60	0.25	0.11
45	0.0	0.0
30	0.0	0.0
15	0.0	0.0
0	0.0	0.0

Table 5.2 Minimum Values Of C for the Maximum Shear Stress Theory

Loading Angle	Minimum C	
	5 mm	9 mm
90	0.15	0.24
75	0.14	0.16
60	0.14	0.0
45	0.0	0.0
30	0.0	0.0
15	0.0	0.0
0	0.0	0.0

Table 5.3 Minimum Values of C for the von Mises Theory

minimizes the lever arm between the equal and opposite forces P (Figure 5.10) and therefore minimizes the value of the force CP and of the coefficient C. Figure 5.14 shows predicted values of the fracture angle α, based on constant minimum values for C of 0.3 and 0.2 for all loading angles, for the maximum shear stress and von Mises theories, respectively. Strictly speaking, the minimum values of C for each loading angle should be used. These results, averaged for both weld sizes, are shown dashed in Fig 5.14. However, the dashed values are not appreciably different; the greatest variation exists at about θ=45°. Figure 5.14 shows that the maximum shear stress theory, taking into account the balancing stress resultants CPsinθ and using a value of C=0.3, predicts the fracture angles reasonably well and better than does the von Mises failure criterion, using a value of C=0.2. In particular, the predicted fracture angle is in good agreement with the average test results for both the longitudinal and transverse welds. For intermediate angles of loading, the predicted angle of fracture is in good agreement with the test results except for the 9 mm welds with θ=15° and 30° and for the 5 mm welds with θ=30°. This lack of agreement has not been resolved.

5.5 Ultimate Strength

It has been argued that, at the weld root, a highly restrained condition exists in the z and x coordinate directions of Fig 5.13(a). The photomicrograph of Fig

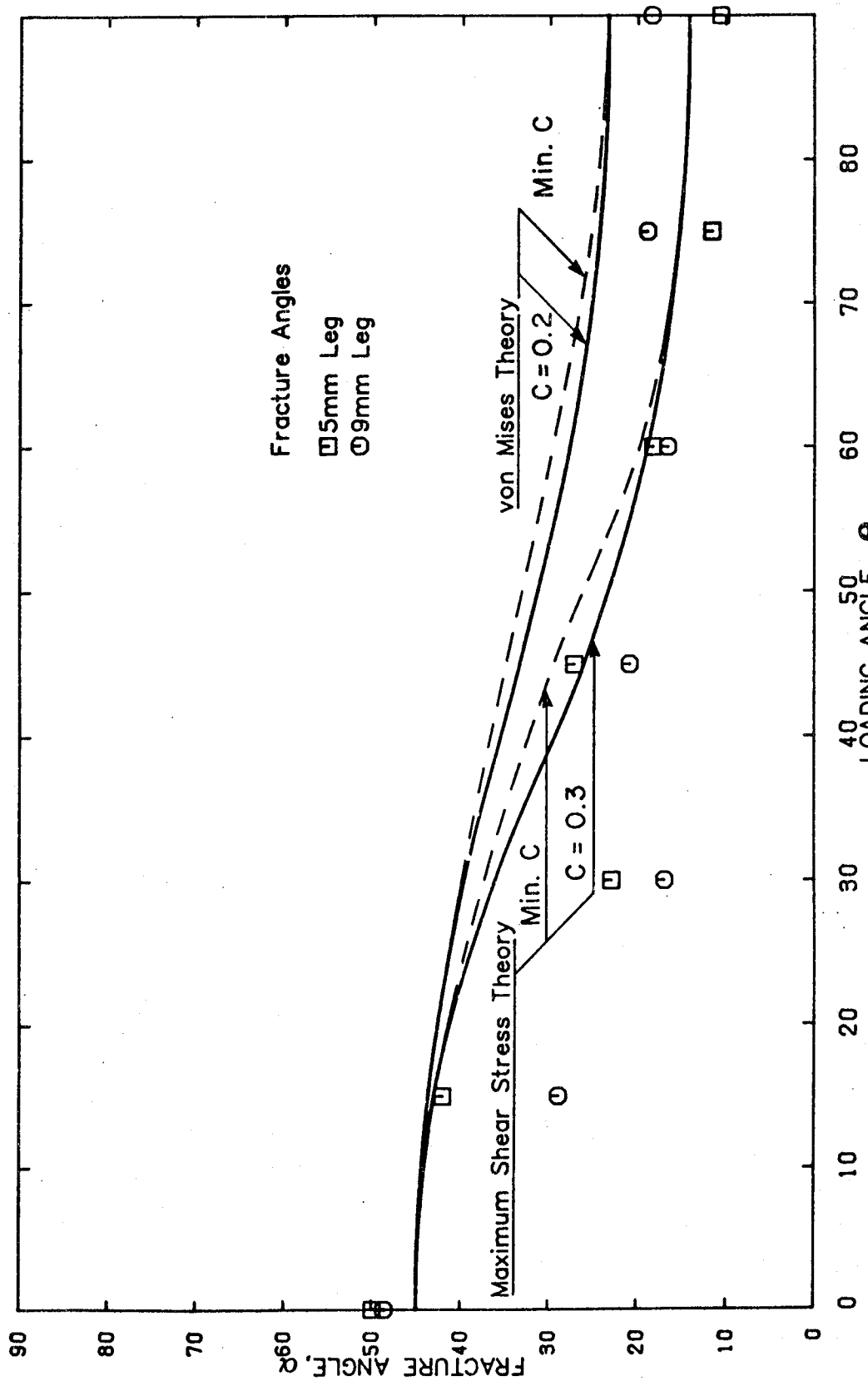

Figure 5.14 Predicted Fracture Angles

4.5(a), indicating an essentially brittle fracture, supports the hypothesis that a condition of biaxial plane strain exists (Lay (1982)). (Biaxial plane strain means full restraint in both directions transverse to the applied load.) Figures 4.5(b) and 4.5(c), on the other hand, indicate, once the fracture has progressed away from the weld root, that the fracture surface is more ductile and that less transverse restraint exists. It is postulated that restraint exists chiefly in the z direction and therefore, a condition of uniaxial plane strain exists in general (Lay (1982)) for the weld metal as a whole. (Uniaxial plane strain means full restraint in a single direction perpendicular to the applied load.)

Using the von Mises maximum energy of distortion theory, under a condition of uniaxial plane strain, yielding occurs at a stress of

$$[5.13] \quad \sigma_{yr} = \sigma_y \; / \; [1 + \nu^2 - \nu]^{1/2}$$

Just subsequent to yielding, the inelastic value for Poissons's ratio of 0.5 (consistent with no volume change) would be appropriate. Extending the von Mises criterion to ultimate conditions, ultimate loads in a transverse weld would be reached at a restrained ultimate strength of the weld metal of

$$[5.14] \quad \sigma_{ur} = \sigma_u / [1 + \nu_p^2 - \nu_p]^{1/2}$$

$$= \sigma_u / [1 + 0.5^2 - 0.5]^{1/2} = 1.155\sigma_u$$

If it is now further assumed that the restraint varies as the sine of the loading angle, ie. from full restraint for transverse welds to zero restraint for longitudinal welds, then, in determining the strength of welds, the ultimate strength from [5.6] and [5.11] is multiplied by (1 + 0.155(sinθ)). Substituting, and using values for C of 0.3 and 0.2 for the maximum shear stress and von Mises theories, respectively, gives

$$[5.15] \quad P_\theta / P_l = (1 + (0.155)(\sin\theta))A_\theta / A_l[((\sin\theta)$$

$$*(\cos\alpha) - 0.3(\sin\theta)(\sin\alpha))^2 + (\cos\theta)^2]^{1/2}$$

and

$$[5.16] \quad P_\theta / P_l = (1 + (0.155)(\sin\theta))A_\theta(3)^{1/2} / A_l[[[(\sin\theta)$$

$$*(\sin\alpha) + 0.2(\sin\theta)(\cos\alpha)]^2$$

$$+ 3[((\sin\theta)(\cos\alpha) - 0.2(\sin\theta)(\sin\alpha))^2$$

$$+ (\cos\theta)^2]]^{1/2}]$$

Curves based on these equations, normalized by dividing by the ultimate shear strength of a longitudinal weld, are shown on Fig 5.15, together with the test results. Curve [5.15], based on the maximum shear stress theory, is seen to fit the test results better than that based on the von Mises criterion. It is recalled that the maximum shear stress theory also predicted fracture angles better than the von Mises criterion (Fig 5.4). Table 5.4 lists the mean value, the standard deviation, σ, and the coefficient of variation, V, for the test-to-predicted ratios for the two sizes of welds and for all the tests taken together, based on the two failure criteria. The maximum shear stress theory shows excellent agreement with test results with a test-to-predicted ratio for all the tests taken together of 1.01 with a standard deviation of 0.076 and a coefficient of variation of 7.6%. For curve [5.15] in Fig 5.15, the maximum and minimum test-to-predicted ratios of 1.12 and 0.83 occur at θ=60° and 90°, respectively for the 5 mm welds. For the 9 mm welds, the maximum and minimum ratios of 1.11 and 0.91 occur at 30° and 45°, respectively. Test-to-predicted ratios exceeding 1.0 for both the 5 and 9 mm welds at θ=30° and 60° are consistent with measured fracture angles smaller than

TEST-TO-PREDICTED RATIOS			
	Maximum Shear Stress Theory		
	5 mm	9 mm	All Welds
Mean	0.99	1.03	1.01
σ	0.086	0.061	0.076
V (%)	8.6	6.0	7.6
n	21	21	42
	von Mises Maximum Energy Of Distortion Theory		
	5 mm	9 mm	All Welds
Mean	1.04	1.08	1.06
σ	0.096	0.082	0.091
V (%)	9.3	7.6	8.6
n	21	21	42

Table 5.3 Test-To-Predicted Ratios For Ultimate Loads

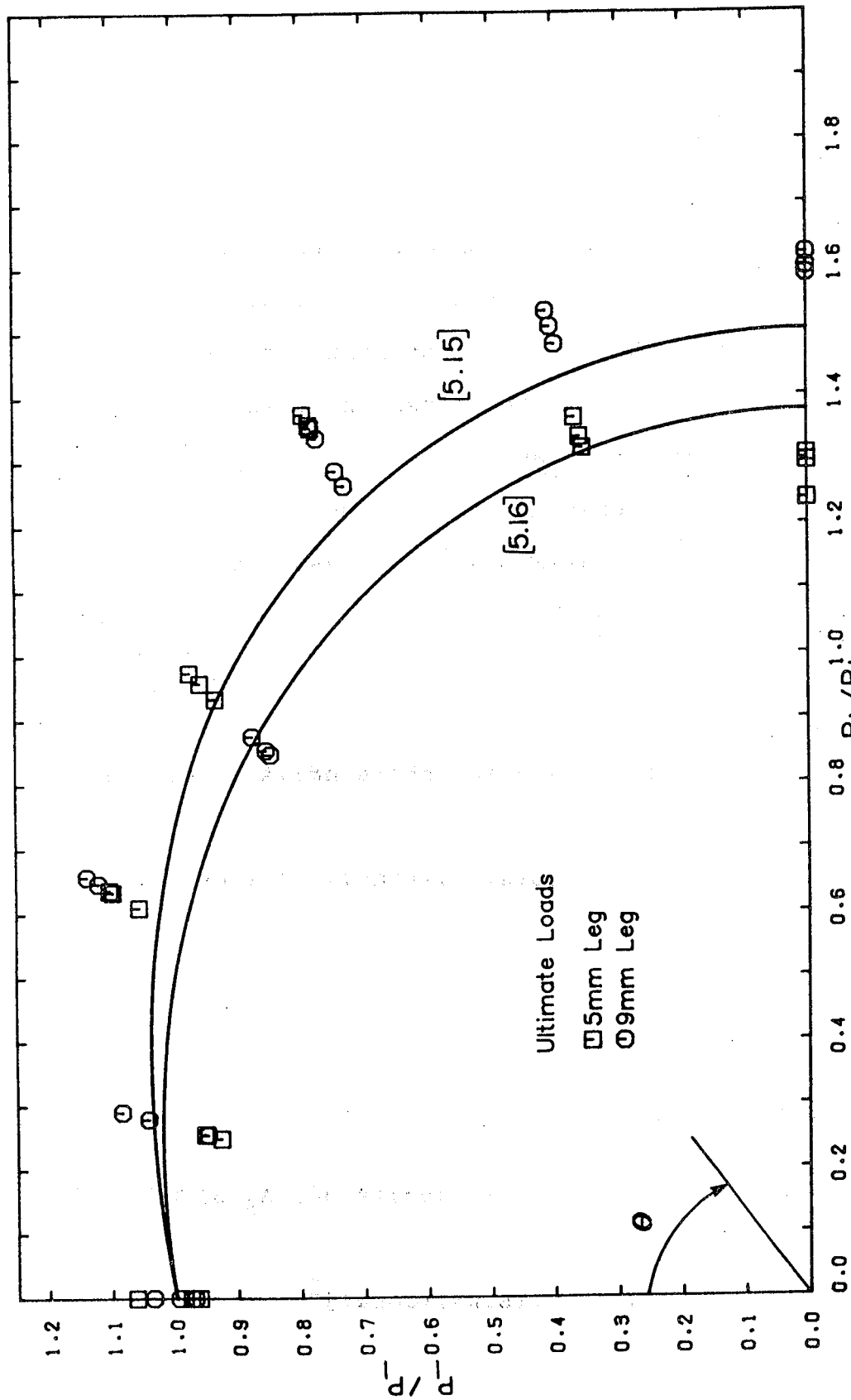

Figure 5.15 Ultimate Load Interaction Diagram

the predicted values; the fracture surface area increases with a decreasing fracture angle, resulting in an increased ultimate load. However, for other loading cases, such as the 5 mm welds with θ=75° and 90° and the 9 mm welds with θ=45°, larger values of C would more accurately predict the fracture angles, but less accurately predict the ultimate loads. Similarly, smaller values of C would more accurately predict fracture angles for 5 mm welds with θ=45° and 9 mm welds with θ=75° and 90°, but less accurately predict ultimate loads. Thus, for the maximum shear stress theory, individual test results may be predicted more accurately with values of C other than 0.3, but for the test series as a whole, a value of 0.3 predicts both the fracture angles and the ultimate strengths reasonably well.

5.5.1 Fillet Welds In Compression

The theoretical method for predicting the ultimate strength of fillet welds loaded at a general angle has been developed assuming the fillet weld joint to be loaded in tension. It is anticipated that the method would also show good agreement with the test results of fillet welds in joints loaded in compression.

For a compressive force P, acting on a fillet weld at a general loading angle, θ, the average shear stress, τ, and the average normal stress, σ, on the fracture surface would have the same magnitude as the corresponding stresses for the tensile loading case, as given by [5.2] and [5.3],

respectively. A parallel to the analysis of restraint in the weld root area of the transverse fillet weld in the joint loaded in tension can be developed for the same area for the transverse fillet weld in the joint loaded in compression. For example, referring to Fig 5.13, lateral expansion in the z direction would be constrained by the relatively unstressed adjoining plate below A. Similarly, expansion in the x direction would be constrained by the less heavily stressed plates adjoining the weld. A condition of triaxial compression in the weld root region would lead to surpressed yielding in this area.

However, the brittle type of fracture which occurred in the weld root area of fillet welds when the joints were loaded in tension, would not be expected to occur, as this is a tensile phenomenon. Thus transverse fillet welds in joints loaded in compression would be anticipated to be even stronger than those in joints loaded in tension.

Few tests have been reported on fillet welds in joints loaded in compression. Spraragen and Claussen (1942) do not provide quantitative information in their review of tests conducted by others. The test results of Swannell and Skewes (1979) are discussed subsequently.

5.5.2 Restraint Using Maximum Principal Strain Theory

Using the maximum principal strain theory, (Lay, 1982) under a condition of uniaxial plane strain, yielding is postulated to occur at a stress of

$$[5.17] \quad \sigma_{yr} = \sigma_y / [1 - \nu^2]$$

This criterion gives a strength only 2% greater than that using the von Mises maximum energy of distortion theory under uniaxial plane strain conditions. However, extending the maximum principal theory to ultimate conditions results in a restrained ultimate strength of

$$[5.18] \quad \sigma_{ur} = \sigma_u / [1 - \nu_p^2]$$

$$= \sigma_u / [1 - 0.5^2] = 1.333$$

which is 15.5% greater than the restrained ultimate strength derived from the von Mises criterion. Using the restrained ultimate strength derived from the maximum principal strain theory, [5.15] and [5.16] become

$$[5.19] \quad P_\theta / P_1 = (1 + (0.333)(\sin\theta))A_\theta / A_1[((\sin\theta)$$

$$*(\cos\alpha) - 0.3(\sin\theta)(\sin\alpha))^2 + (\cos\theta)^2]^{1/2}$$

and

$$[5.20]\quad P_\theta / P_l = (1 + (0.333)(\sin\theta))A_\theta(3)^{1/2} / A_l[[[(\sin\theta)*(\sin\alpha) + 0.2(\sin\theta)(\cos\alpha)]^2 + 3[((\sin\theta)(\cos\alpha) - 0.2(\sin\theta)(\sin\alpha))^2 + (\cos\theta)^2]]^{1/2}]$$

respectively. Curves based on these equations, normalized by dividing by the ultimate shear strength of a longitudinal weld, are shown in Fig 5.16. Listed in Table 5.5 are the mean value, standard deviation and coefficient of variation for the test-to-predicted ratios for the two sizes of welds and for all the tests taken together, based on the two failure criteria. Equation [5.15], based on the maximum shear stress theory with the restraint factor derived from the von Mises maximum energy of distortion theory, is seen to fit the test results better than [5.19] or [5.20].

5.5.3 Ultimate Shear Strength of Longitudinal Fillets

The average ultimate shear strengths for the 5 and 9 mm welds, that is, the maximum loads for the longitudinal welds divided by the throat areas, were found to be 437 MPa and 385 MPa, respectively. Based on the measured ultimate tensile strength for the weld metal (538 MPa), the ratios of the longitudinal fillet weld shear strength to the weld metal tensile strength are 0.81 and 0.72 for the 5 and 9 mm welds, respectively. In a similar manner, based on the

TEST-TO-PREDICTED RATIOS			
	Maximum Shear Stress Theory		
	5 mm	9 mm	All Welds
Mean	0.90	0.94	0.92
σ	0.094	0.063	0.081
V (%)	10.4	6.8	8.8
n	21	21	42
	von Mises Maximum Energy Of Distortion Theory		
	5 mm	9 mm	All Welds
Mean	0.94	0.98	0.96
σ	0.087	0.056	0.075
V (%)	9.3	5.6	7.7
n	21	21	42

Table 5.4 Test-To-Predicted Ratios For Ultimate Loads

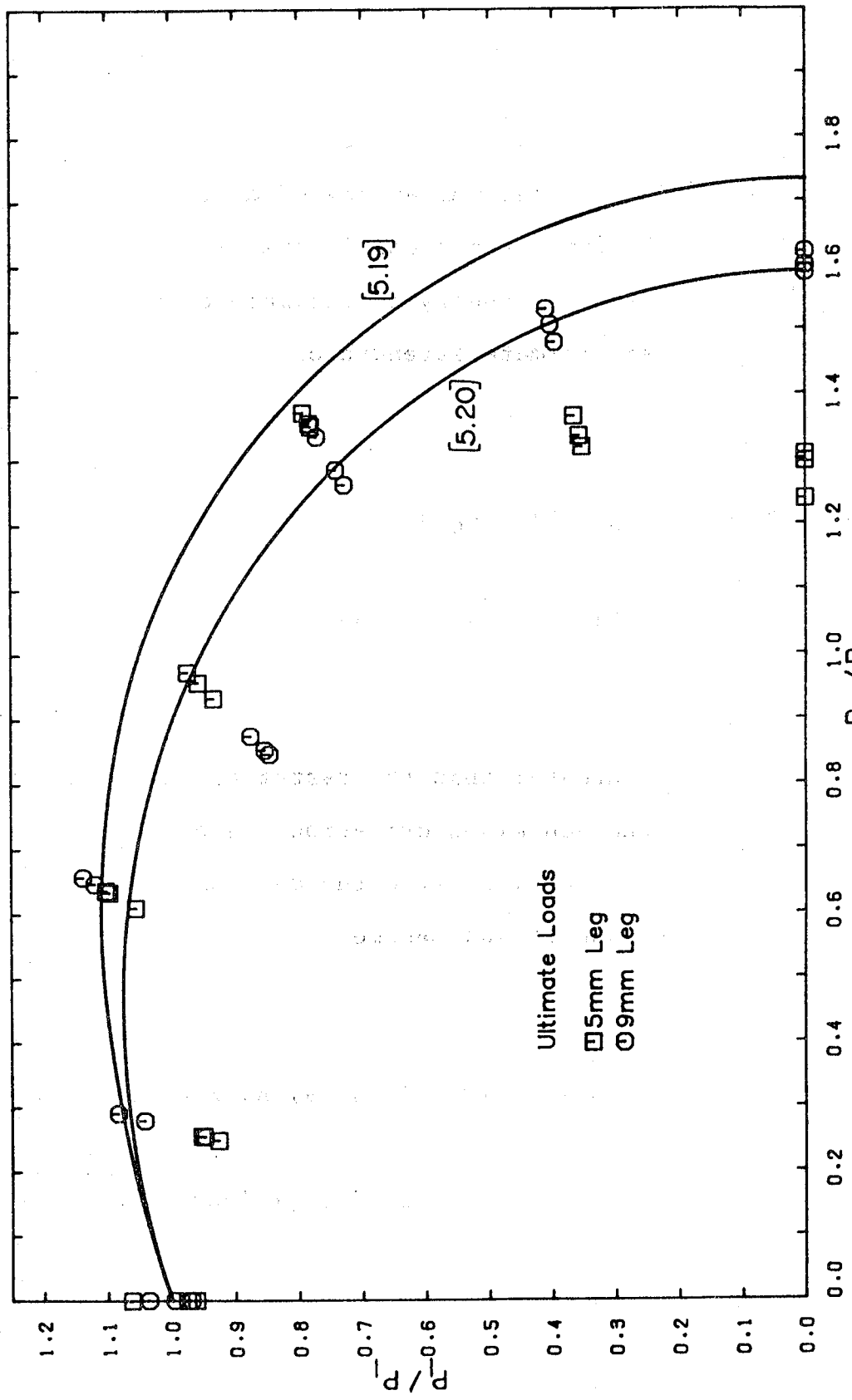

Figure 5.16 Ultimate Load Interaction Diagram

minimum specified tensile strength for an E48014 electrode of 500 MPa, these ratios are 0.87 and 0.77 for the 5 and 9 mm welds, respectively.

For a sample of 133 specimens consisting of a wide range of electrode strengths, Fisher et al (1978) determined a mean shear strength to actual tensile strength ratio of 0.84 with a standard deviation of 0.09 and a coefficient of variation of 0.10. The average shear strength to actual tensile strength ratios for the 5 and 9 mm welds determined herein of 0.81 and 0.72 are 96% and 86% of the Fisher et al ratio. They are therefore considered to be in reasonable agreement with those results.

Krumpen and Jordan (1984) have proposed an equation for the ultimate shear stress of longitudinal fillet welds, τ_l, as a function of the ultimate tensile strength of the weld metal where

$$[5.21] \quad \tau_l = 1.8(\sigma_u)^{0.8}$$

for a range of electode strengths of AWS E60XX to E14018. Substituting the minimum specified tensile strength for E7014 (E48014) electrodes of 72 ksi into [5.21] and dividing by 72 ksi, yields an ultimate shear strength to tensile strength ratio of 0.77. This is in reasonable agreement with values of 0.87 and 0.77 obtained herein for the 5 and 9 mm

welds, respectively.

5.5.4 Comparisons With Other Test Data

The ultimate strength prediction given by [5.15] can be compared with the test data of Butler and Kulak (1971), Clark (1971), Holtz and Harre (1973, unpublished), and Swannell and Skewes (1979). This comparison is shown in Fig 5.17 to 5.21, where all weld strengths have been normalized by dividing by the strengths obtained from the longitudinal loading case.

The test data of Butler and Kulak (1971) shown in Fig 5.17 represent the mean ultimate strengths of a total of 23 tests conducted at loading angles of 0, 30, 60, and 90° (transverse). The welds were 1/4" (6 mm) fillets made using AWS E60XX electrodes with CSA G40.21 steel plate having a specified minimum yield strength of 44 ksi (303 MPa) and a specified minimum tensile strength of 62 ksi (483 MPa). Butler and Kulak developed an empirical relationship for the ultimate strength as a function of the loading angle, θ. This equation, in nondimensional form as given by Kennedy and Kriviak (1985), is

$$[5.22] \quad P_\theta / P_1 = \frac{10 + \theta}{10 + (0.655)(\theta)}$$

where θ is measured in degrees. The curve given by [5.22] is

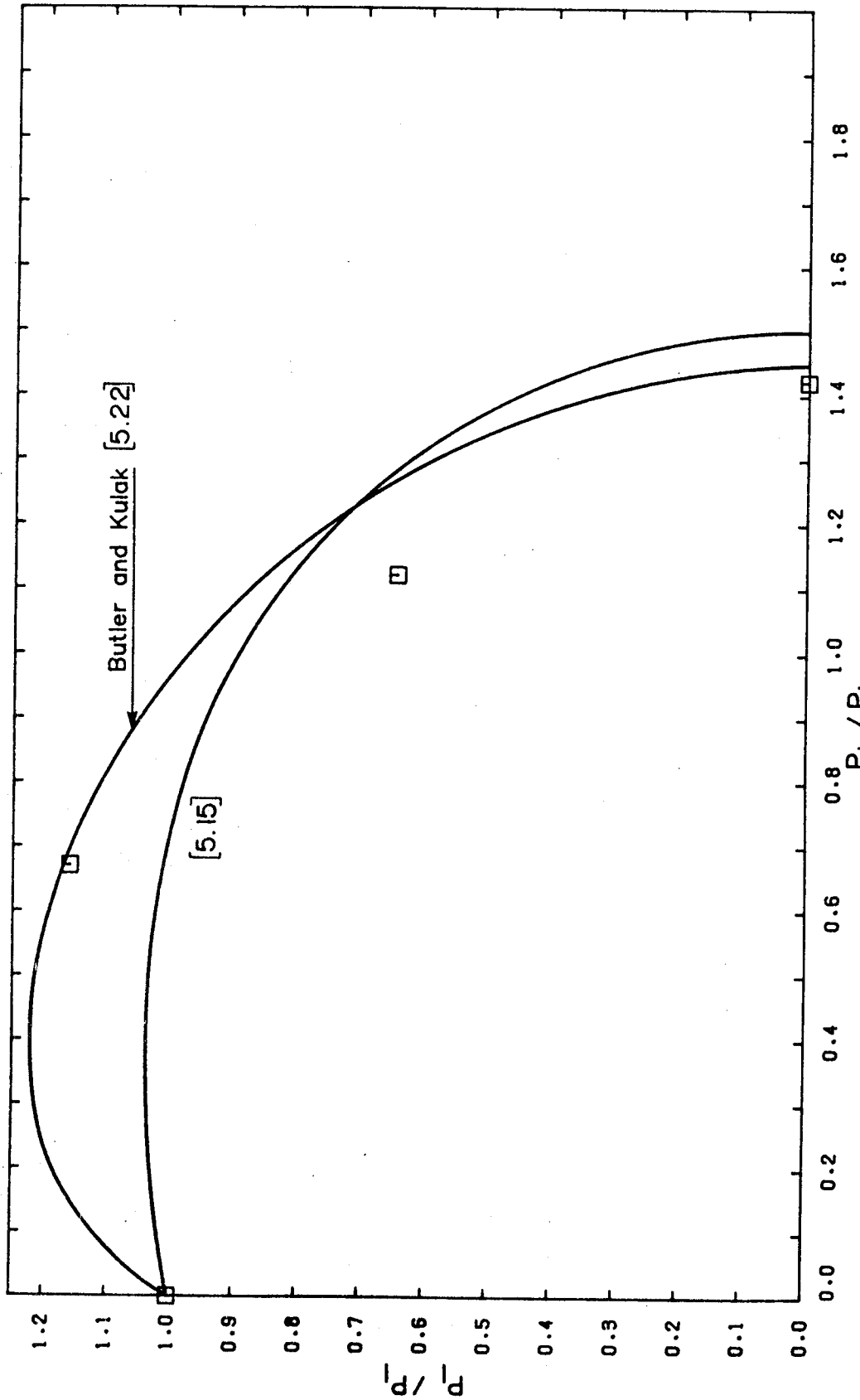

Figure 5.17 Test Results Of Butler And Kulak (1971)

shown in Fig 5.17. The average test-to-predicted ratio using the Butler and Kulak data and [5.15] is 1.00, with minimum and maximum values of 0.91 and 1.13. The range of most significant difference between [5.22] and [5.15] occurs between loading angles of 0° and about 45°, where [5.22] predicts up to 1.2 times the value of [5.15]. However, the ratio of the Butler and Kulak average test value at θ=30° to the test data reported herein is only 1.05, that is, there is good agreement between these two sets of test data.

The test data of Clark (1971) are shown together with [5.15] in Fig 5.18. The tests were conducted on 8 mm fillets; however, the material properties and test arrangement were not reported. Using these data and [5.15], the average test-to-predicted ratio, again normalized using the average ultimate strength of the longitudinal welds, is 1.08 with minimum and maximum values of 0.92 and 1.21. The ultimate strength prediction given by [5.19] can, however, be shown to fit the test data of Clark better than that given by [5.15].

The test data of Holtz and Harre (1973, unpublished) are compared with [5.15] in Fig 5.19. A total of 62 tests were conducted at loading angles of 0, 13, 30, 60, and 90° (transverse). The welds were 1/4" (6 mm) fillets made using AWS E70XX electrodes. Plate material properties were not reported. Using these data and [5.15], the average value of the test-to-predicted ratio is 1.17 with a standard deviation of 0.13 and a coefficient of variation of 11%.

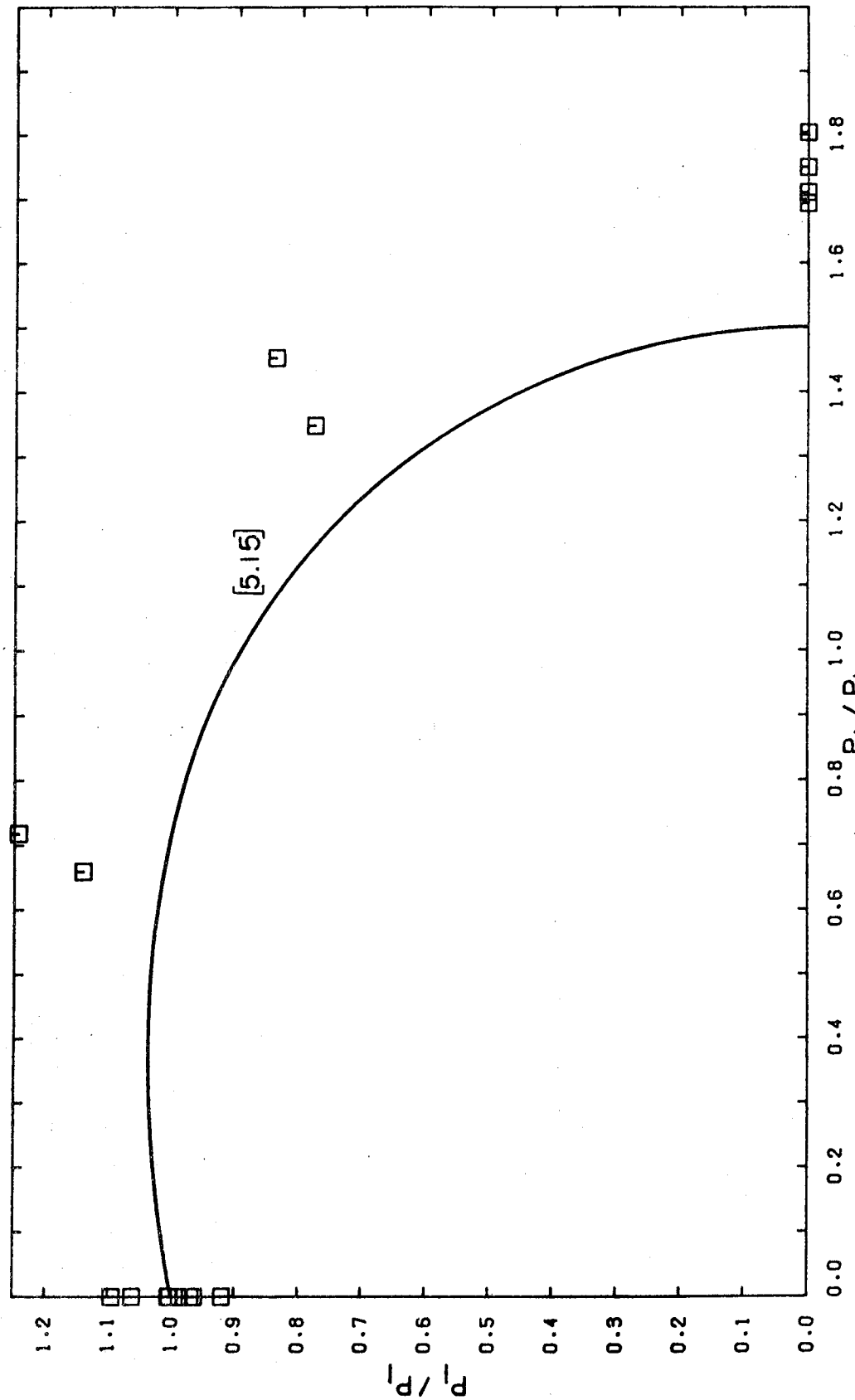

Figure 5.18 Test Results Of Clark (1971)

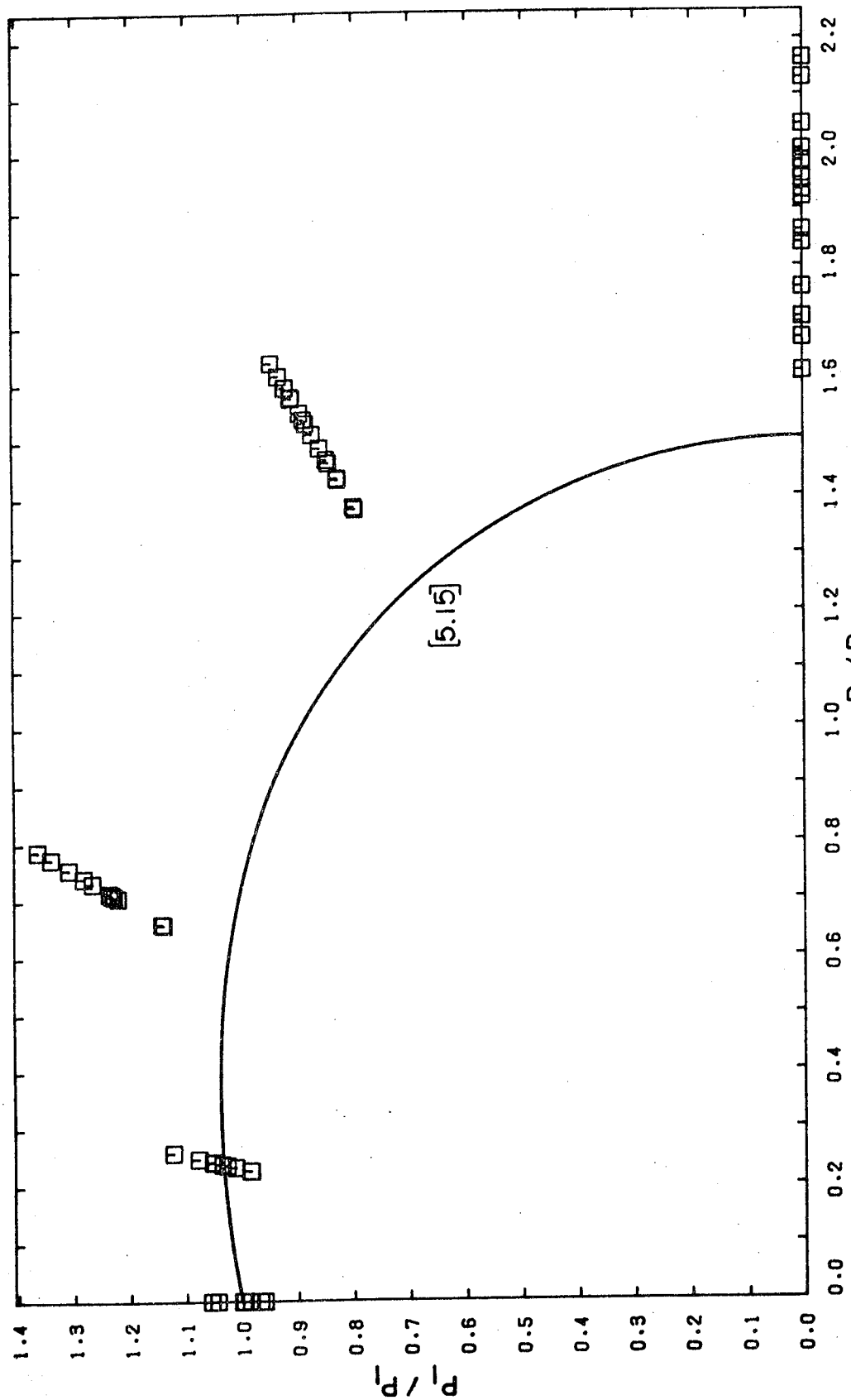

Figure 5.19 Test Results Of Holtz and Harre (1973, unpublished)

Although the test-to-predicted ratios for θ=30, 60, and 90° are significantly greater than 1.0, ie. up to 1.4 times, these high ratios cannot be explained by suggesting that the longitudinal welds were understrength. The ratio of the average ultimate shear strength of longitudinal welds of 59.9 ksi to the weld tensile strength of 70.1 ksi, as determined from all-weld metal tensile tests, is 0.85, which compares closely to the mean value of 0.84 determined by Fisher et al (1978). The ultimate strength prediction given by [5.19] can be shown to fit the test data of Holtz and Harre better than that given by [5.15], but [5.19] still substantially underestimates the test data. Transverse to longitudinal strength ratios exceeding 2.0, as found by Holtz and Harre, have not been recorded by other investigators.

The test data of Swannell and Skewes (1979) are compared with [5.15] in Fig 5.20. In these tests, a mandrel was used to push one block with respect to two neighboring blocks to which it was welded. With this test configuration, the fracture plane was forced to rotate toward the vertical weld leg of the test weld in specimens with fillets other than longitudinal. The authors therefore point out that the specimen configuration could be construed to influence the failure condition. The welds were 6 mm fillets made using AWS E6013 electrodes with steel plate having a specified minimum yield strength of 210 MPa and a specified minimum tensile strength of 410 MPa.

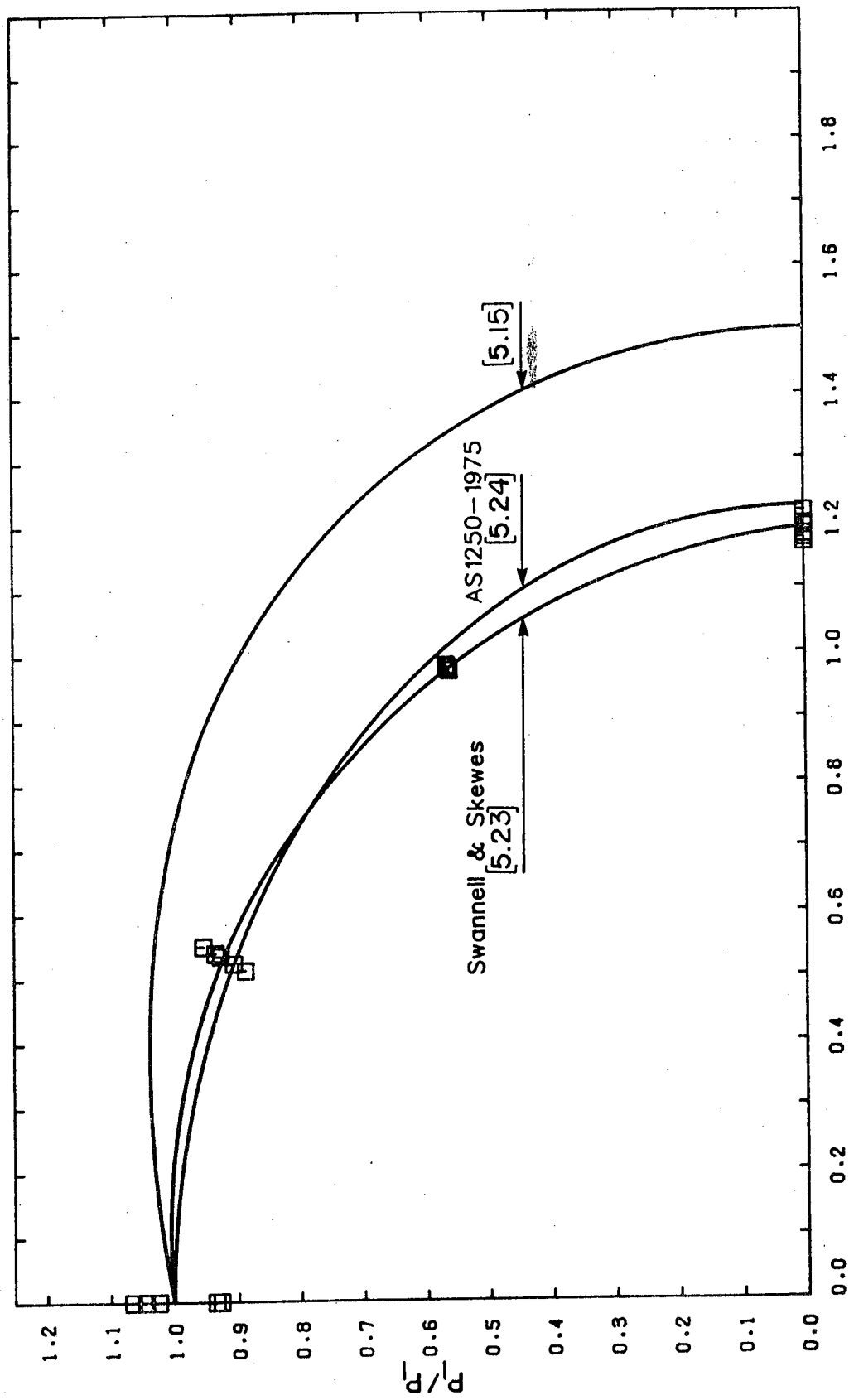

Figure 5.20 Test Results Of Swannell and Skewes (1979)

Comparing Fig 5.20 with Figs 5.17, 5.18 and 5.19, the strength gain for fillet welds loaded at angles other than longitudinal, as reported by Swannell and Skewes, is seen to be less for compression than for tension tests. As discussed previously, the analytical method developed herein predicts at least the same ultimate load for fillets in joints loaded in compression as for the corresponding fillets in joints loaded in tension. Because the test configuration used by Swannell and Skewes forced fracture to occur on planes near the vertical leg of the test weld, thereby providing the maximum fracture area for shear, it would have been anticipated that the weld strength of their transverse fillets would have been greater than that established by the tension tests of others and not less.

Swannell and Skewes (1979) developed an empirical relationship for the ultimate strength as a function of the loading angle, θ (in degrees). This expression, in normalized form, is

$$[5.23] \quad P_\theta / P_1 = \frac{2.2 + 0.004667\theta}{2.2}$$

and is shown in Fig 5.20. Also shown in Fig 5.20 is the design expression specified by AS1250-1975 for fillet welds. This expression, in normalized form, is

$$[5.24] \quad P_\theta / P_1 = [3 / [3(\cos\theta)^2 + 2(\sin\theta)^2]]^{1/2}$$

5.5.5 Friction

The IIW (1980) has stated that transverse to longitudinal strength ratios exceeding 1.22 are primarily due to friction and supporting effects of adjoining plates. However, based on the analysis of test results, friction would not appear to be a significant factor.

Frictional forces, F, arising from the stress resultants $CP\sin\theta$ acting on the middle plate, as shown in Fig 5.21, would be greatest for transverse welds. Baumeister (1967) has shown that the static coefficient of friction for mild steel on mild steel can range from about 0.005 to 0.75, depending on surface conditions. Assuming a value for the static coefficient of friction of 0.2 and a value of C of 0.3, the ultimate transverse weld strength would be underestimated by only about 5% if frictional effects were neglected. Consideration of Poisson's effect would further reduce this estimate as the plates shown in Fig 5.21 reduce in thickness with increasing load P. As well, these frictional forces would not develop for transverse welds loaded in compression.

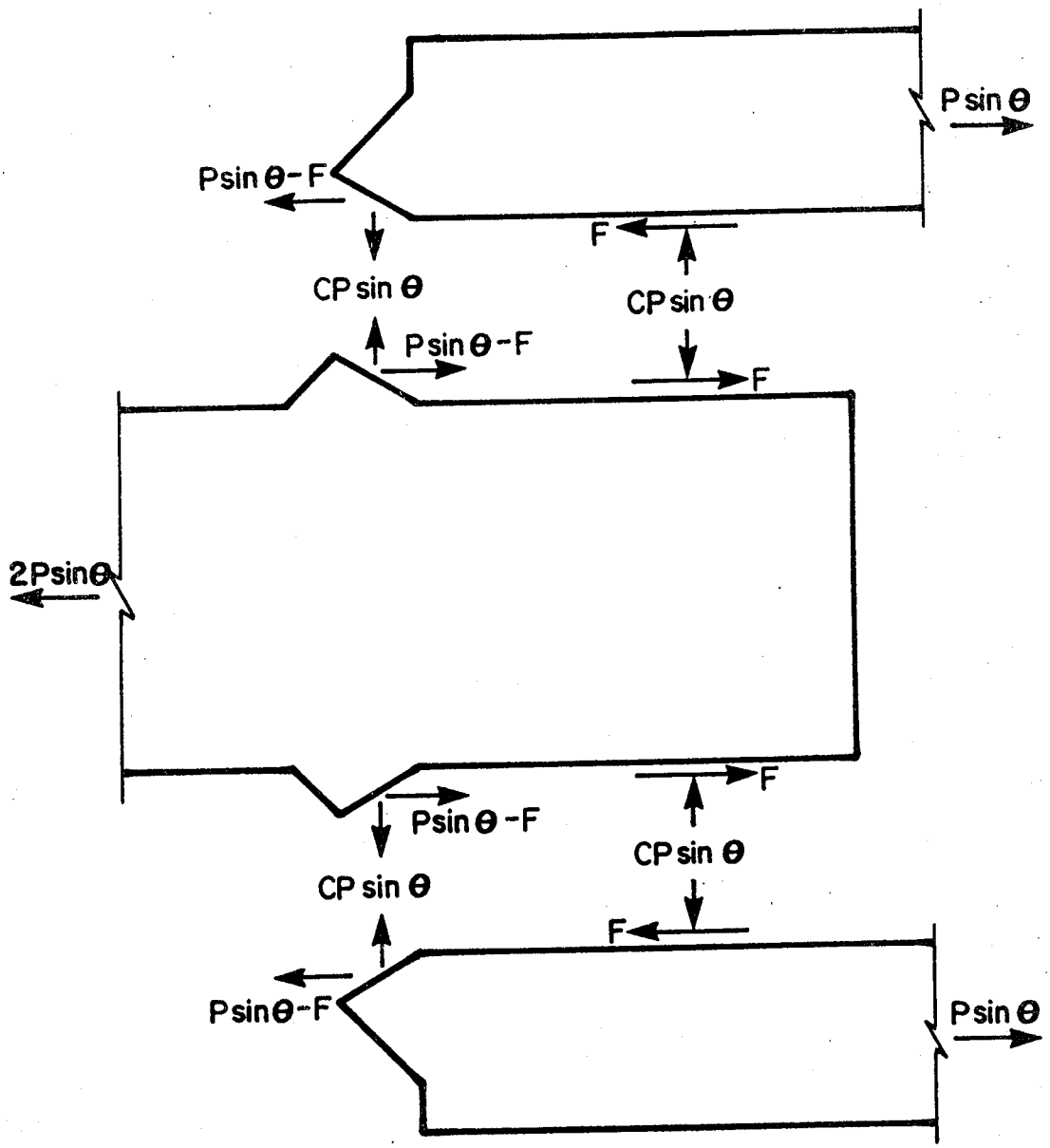

Figure 5.21 Frictional Forces

5.6 Weld Ductility

Butler and Kulak (1971), Clark (1971), and Swannell and Skewes (1979), among others, measured deformations over gauge lengths parallel to the direction of loading. Deformations were not related to actual leg size or gauge length, but were reported for the leg size specified. Reporting total deformations in this way led to the conclusion that longitudinal fillets (θ=0°) are the most ductile and that ductility decreases with an increasing loading angle. It can be noted that the deformation data reported in Section 4.2.5 shows the same trend.

Average weld strains can be calculated by dividing deformations by the gauge lengths used to measure the deformations. For the tests reported herein, weld strains calculated in this way are shown in Fig 5.22 and 5.23. From an examination of these figures, it appears that fillet weld ductility, as reflected by weld strains, is not a function of the loading angle.

A least squares fit to the test results of Fig 5.22 yields

$$[5.25] \quad \epsilon = 0.0474 + (1.429 \times 10^{-4})\theta$$

and

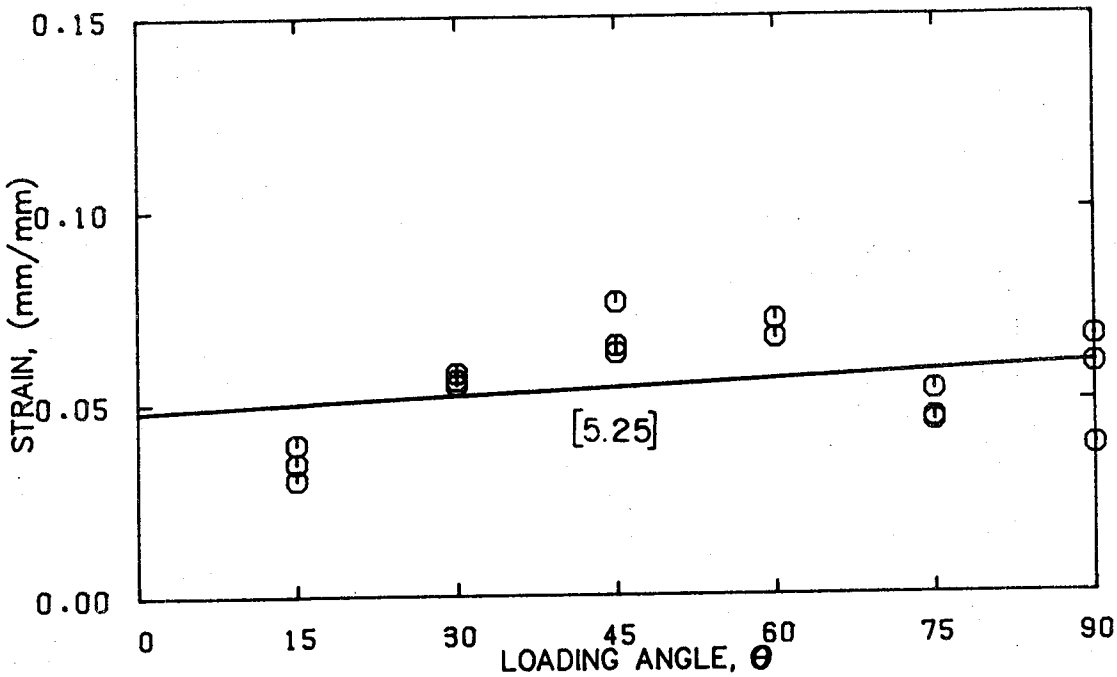

Figure 5.22 5 mm Fillet Weld Strains

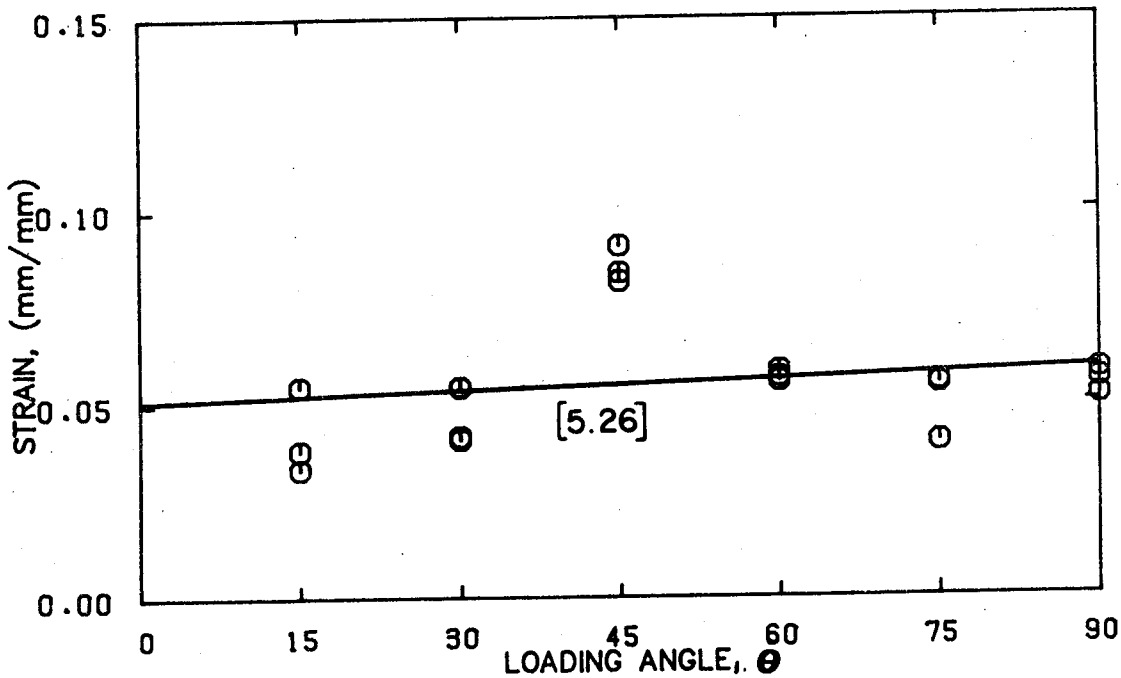

Figure 5.23 9 mm Fillet Weld Strains

$$[5.26] \quad \epsilon = 0.0509 + (9.35 \times 10^{-5})\theta$$

for Fig 5.23. The least squares fits given by [5.25] and [5.26] both approach a horizontal line passing through the average of the 5 mm and 9 mm test data, respectively. The premise that weld metal has a maximum capacity to strain before fracture, regardless of the angle of loading, supports the postulate that the curve fit to Fig 5.22 and 5.23 should be essentially horizontal, provided that fracture occurs in the same or similar manner, ductile or non-ductile, for all loading angles. It can be recalled that once fracture initiated from the weld root of fillet welds loaded at angles approaching the transverse loading case, the fracture propagated essentially in a ductile manner, resulting in a similar fracture surface appearance to that of longitudinal fillets. A horizontal line fitted to the data gives a mean weld strain at fracture for the 5 mm welds of 0.055 with a standard deviation of 0.013 and a coefficient of variation of 24%. Similarly, the mean weld strain at fracture for the 9 mm welds is 0.056 with a standard deviation of 0.014 and a coefficient of variation of 26%.

When the data of Butler and Kulak (1971) are analyzed by the same method, it is found that the strain at ultimate load also did not vary appreciably with the loading angle. For 6 mm fillets made using electrodes of grade E60XX

(E410XX), and loading angles of 90° (transverse), 60°, and 30°, average weld strains at the ultimate load were 0.090, 0.089 and 0.095, respectively, almost twice the value of the mean weld strain for the test results reported here. In addition to the different grade of electrode used, the higher weld strains reported by Butler and Kulak (1971) could also have been due to some yield deformation of the plate within the gauge lengths used to measure deformations. Although the test specimens were proportioned to ensure weld failure prior to rupture of the plates, yielding of the plates may have occurred before weld fracture.

The data of Holtz and Harre (1973, unpublished) do not substantiate that strains are essentially independent of loading angle, as supposed here. Their data indicate an increase in the weld strain, analyzed by the method described, from 0.042 at a loading angle of 13° to 0.117 at a loading angle of 90° (transverse). Again, it is possible that the plate strains within the gauge lengths used to measure the weld deformations could have contributed to the total deformation.

The data of Swannell and Skewes (1979), for fillet welds loaded in compression, do not show a significant variation in the strain at ultimate load with the loading angle. For 1/4" (6 mm) fillets made using electrodes of grade AWS E60XX and loading angles of 90° (transverse), 60°, and 30°, average weld strains, analyzed by the same method, were 0.21, 0.25, and 0.19, respectively. These weld strains

are about 4 times the value of the mean weld strain for the test results reported here, and about twice those of Butler and Kulak (1971). The test configuration used by Swannell and Skewes, as discussed previously, forced weld fracture to occur along the weld leg, and is thought to have caused these large deformations. In addition, welds were machined to the specified leg size prior to testing and it is not known what, if any, effect this had on the weld deformations.

5.7 Design Application

Current design standards in Canada base the strength of fillet welds on the strength of longitudinal fillets, regardless of the loading direction. Experimental data, including the test results reported herein, indicate that this approach is very conservative. Clause 13 of CSA Standard CAN3-S16.1-M84 and Clause 11 of CSA Standard W59-1982 both allow an ultimate strength analysis, although a method for analysis is not given.

It is proposed that the rationale used to develop the ultimate strength formulations herein could be used as a basis for an alternative ultimate strength analysis. By multiplying the strength of longitudinal fillet welds as determined from existing design standards for example, by [5.15] or a simplified form of it, the resistance of fillet welds loaded at angles other than longitudinal would be obtained.

By recognizing the increased strength of fillet welds loaded at angles other than longitudinal, more consistent margins of safety would be established for welded connections.

6. Summary and Conclusions

1. A literature review has shown that the majority of research on fillet welds loaded in shear has been concerned only with transverse and longitudinal fillets. The most significant experimental studies involving welds loaded at intermediate angles have been performed by Butler and Kulak (1971), Clark (1971), Holtz and Harre (1973, unpublished), Swannell and Skewes (1979) and Biggs et al (1981). Neis (1985) and Marsh (1985) have attempted to establish theoretically ultimate fillet weld behaviour as a function of loading angle, but these analyses appear to be based on inaccurate and incorrect force systems, respectively.

2. In all tests reported herein, plates were not strained beyond the yield strain. Therefore, the deformation of the plates was negligible as compared to that of the welds.

3. All test specimens failed in the welds.

4. Weld fractures did not occur on well-defined planes, but rather on uneven surfaces. Therefore, measurements of fracture angles represent average values.

5. Photomicrographs of cross-sections of 9 mm welds, made with 3 passes, revealed that crack extension within the welds tended to follow heat affected zones between weld passes for loading angles of 30° to 90° (transverse). The strength and ductility of these welds do not appear to have been significantly reduced by this fracture phenomenon.

6. The fracture surface of transverse fillets exhibited a transition from brittle fracture at the weld root to ductile fracture where the crack terminated. The fracture surface of longitudinal fillets predominantly consisted of ductile fracture, with 'islands' of brittle fracture randomly dispersed.

7. An analytical method has been developed for predicting the ultimate strength of fillet welds loaded in shear, based on the maximum shear stress failure criterion. This method is in good agreement with the test results with a test-to-predicted ratio for all the tests taken together of 1.01 and it predicts test results better than methods based on the maximum normal stress or von Mises strain energy of distortion failure criteria. The method predicts fracture angles reasonably well and is consistent with the fracture mechanisms observed in the photomicrographs of the fracture surfaces.

8. An examination of the equilibrium of a transverse weld has shown that the force component perpendicular to the weld axis tends to act near the weld root, consistent with the restrained tensile strength of the weld metal, as the transverse loading case is approached. This is in contrast to previous analytical studies on transverse fillets in which stresses perpendicular to the weld axis have been assumed to be uniformly distributed.

9. Photomicrographs of the fracture surface of transverse fillets support the hypothesis that a condition of uniaxial plane strain exists, in general, for the weld metal of transverse fillets. This restrained condition is assumed to vary as the sine of the loading angle, ie. from a condition of full restraint for transverse welds to zero restraint for longitudinal welds. A restraint factor derived from the von Mises maximum energy of distortion theory has been shown to fit the test results better than a factor derived using the maximum principal strain theory.

10. Frictional forces do not appear to be a significant factor in the analysis.

11. Based on the analytical method developed herein, fillet welds in joints loaded in compression appear to be at least as strong as corresponding fillets in joints

loaded in tension.

12. Historically, researchers have not related deformations of fillet welds to the gauge lengths used to measure the deformations. By normalizing the deformations of the welds, measured in the direction of loading, to the gauge lengths used to obtain the deformations, it is concluded that fillet weld ductility is essentially independent of the loading angle, and that deformations are proportional to the gauge length.

6.1 Future Work

1. Further experimental research is needed on fillet welds in joints tested in compression to determine the applicability of the analytical method described herein. The test configuration for these tests should not predetermine the fracture angle.

2. A standardized test specimen should be developed for testing fillet welds loaded at intermediate angles.

3. A more rigorous assessment of frictional forces arising in test specimens should be conducted.

4. A statistical examination of well-documented test

results of fillet welds loaded at various angles, using the analytical method developed herein, would enable a resistance factor for these welds to be determined.

References

AMERICAN SOCIETY FOR TESTING AND MATERIAL. 1980. Standard Practice For Liquid Penetrant Inspection Method. ASTM E165-80, Philadelphia, Penn.

AMERICAN SOCIETY FOR TESTING AND MATERIAL. 1977. Standard Methods And Definitions For Mechanical Testing Of Steel Products. ASTM A370-77 Part(1), Philadelphia, Penn.

AMERICAN SOCIETY FOR TESTING AND MATERIAL. 1961. Standard Test Method For Young's Modulus At Room Temperature. ASTM E111-61 Part (10), Philadelphia, Penn.

ARCHER, F.E., FISCHER, H.K., and KITCHEN, E.M. 1959. "Fillet Welds Subject to Bending and Shear." Civil Engineering and Public Works Review, Vol. 54, No. 634, pp. 455-458.

BAUMEISTER, T. (ed). 1967. "Standard Handbook for Mechanical Engineers." 7th Edition, McGraw-Hill Co., New York.

BIGGS, M.S., CROFTS, M.R., HIGGS, J.D., MARTIN L.H., and TZOGIUS, A. 1981. "Failure of Fillet Weld Connections Subject to Static Loading." Joints in Structural Steelwork, Proc. Of Conf. held at Teeside Polytechnic, Pentech Press, London, England, pp. 1.92-1.109.

BUTLER, L.J., and KULAK, G.L. 1971. "Strength of Fillet Welds as a Function of Direction of Load." Welding Journal, Welding Research Supplement, Vol. 36, No. 5, pp. 231s-234s.

CANADIAN INSTITUTE OF STEEL CONSTRUCTION (CISC). 1984. "Handbook of Steel Construction, 4th Ed." Canadian Institute of Steel Construction, Willowdale, Ontario.

CANADIAN STANDARDS ASSOCIATION (CSA). 1980. "Mild Steel Covered Arc Welding Electodes, W48.1-M1980." Canadian Standards Association, Rexdale, Ontario.

CANADIAN STANDARDS ASSOCIATION (CSA). 1982. "Welded Steel Construction (Metal Arc Welding), W59-1982." Canadian Standards Association, Rexdale, Ontario.

CANADIAN STANDARDS ASSOCIATION (CSA). 1984. "Steel Structures For Buildings - Limit States Design, Standard CAN3-S16.1-M84." Canadian Standards Association, Rexdale, Ontario.

CANADIAN STANDARDS ASSOCIATION (CSA). 1981. "Structural Quality Steels, Standard CAN3-G40.21-M81." The Algoma Steel Corporation Limited, Sault Ste. Marie, Ontario, Canada.

CLARK, P.J. 1971. "Basis of Design For Fillet-Welded Joints Under Static Loading." Proc. Conf. on Improving Welded Product Design, The Welding Institute, Cambridge, England, Vol 1, pp. 85-96.

DAVIS, H.E., TROXELL, G.E., and HAUCK, G.F.W. 1982. "The Testing of Engineering Materials, 4th Ed." McGraw-Hill, New York, pp. 140-143.

FEDER, D. 1979. "Recommended Practice For Testing the Strength of Fillet Welds in Structural Steels and Aluminum Alloys." IIW Doc XV-439-79, International Institute of Welding, pp. 1-16.

FISHER, J.W., GALAMBOS, T.V., KULAK, G.L., and RAVINDRA, M.K. 1978. "Load and Resistance Factor Design Criteria For Connectors." Journal of the Structural Division, ASCE, Vol. 104, No. ST9, pp. 1427-1441.

FREEMAN, F.R. 1932. "Strength of Arc-Welded Joints." Welding Journal, Vol. 11, No. 6, pp. 16-24.

HANKINS, G.A., and ALLAN, G.W. 1934. "Second Report of the Steel Structures Research Committee." His Majesty's Stationary Office, London, pp. 319-332, 360-366.

HIGGINS, T.R. and PREECE, F.R. 1969. "Proposed Working Stresses For Fillet Welds in Building Construction." Engineering Journal, AISC, Vol. 6, No. 1, pp. 16-20.

INTERNATIONAL INSTITUTE OF WELDING (IIW), COMMISSION XV. 1980. "Deformation Curves of Fillet Welds, Doc. No. XV-467-80." International Institute of Welding, London, pp. 1-15.

KAMTEKAR, A.G. 1982. "A New Analysis of the Stength of Some Simple Fillet Welded Connections." Journal of Constructional Steel Research, Vol. 2, No. 2, pp.33-45.

KATO, B., and MORITA, K. 1969. "The Strength of Fillet Welded Joints, IIW Doc XV-267-69." International Institute of Welding.

KATO, B., and MORITA, K. 1974. "Strength of Transverse Fillet Welded Joints." Welding Journal, Welding Research Supplement, pp. 59s-64s.

KENNEDY, D.J.L., and KRIVIAK, G.J. 1985. "The Strength of Fillet Welds Under Longitudinal and Transverse Shear: A Paradox." Canadian Journal of Civil Eng., Vol. 12, pp. 226-231.

KRUMPEN, R.P., and JORDAN, C.R. 1984. "Reduced Fillet Weld Sizes for Naval Ships." Welding Journal, Apr., pp.34-41.

LAY, M.G. 1982. "Structural Steel Fundamentals - An Engineering and Metallurgical Primer." Australian Road Research Board, Australia.

LIGTENBERG, F.L. 1968. "International Test Series, Final Report, IIW Doc XV-242-68." International Institute of Welding.

MARSH, C. 1985. "Strength of Aluminum Fillet Welds." Welding Journal, Welding Research Supplement, Vol. 64, No. 12, pp 335s-338s.

NAKA, T., and KATO, B. 1966. "Deformations and Strength of End Fillets." Journal of the Faculty of Engineering, University of Tokyo, Vol. XXVIII, No. 3.

NEIS, V.V. 1985. "New Constitutive Law for Equal Leg Fillet Welds." Journal of Structural Engineering, ASCE, Vol. 111, No. 8, pp. 1747-1759.

SPRARAGEN, W., and CLAUSSEN, G.E. 1942. "Static Tests of Fillet and Plug Welds - A Review of the Literature From 1932 to Jan 1, 1940." Welding Journal, Vol. 21, No. 4, Research Suppl., pp. 161s-197s.

SWANNELL, P., and SKEWES, I.C. 1979. "The Design of Welded Brackets Loaded In Plane: Elastic and Ultimate Load Techniques - AWRA Report P6-8-77." Australian Welding Research, Jan, pp. 28-59.

SWANNELL, P. 1972. "Primary Stress and Strain Distributions In Longitudinal Fillet Welds, Technical Paper No. 11." Australian Welding Journal, Sept/Oct, pp 117-123.

TIMOSHENKO, S. 1951. "Theory of Elasticity." McGraw-Hill Co., New York.

TIMOSHENKO, S. 1955. "Strength of Materials, Part II, Advanced Theory and Problems." D. Van Nostrand Co., Princeton, New York, 3rd Ed., pp 430-435.

VANDEPERRE, I.J., and JOUKOFF, A. 1939. "Le Calcul des Constructions Soudees." A de Boeck, Brussels, 274 pp.